Crack Width Prediction for Exterior Portion of Inverted "T" Bent Caps

Research Report 0-1854-4

Prepared for
Texas Department of Transportation
Project 0-1854

By

Ronnie Rong-Hua Zhu
Research Associate

Thomas T.C. Hsu
Moores Professor

Department of Civil and Environmental Engineering
University of Houston
Houston, Texas

April 1, 2003

Research Report 0-1854-4
to
Texas Dept. of Transportation
Project 0-1854

Crack Width Prediction for Exterior Portion of Inverted 'T' Bent Caps

By

Ronnie Rong-Hua Zhu

Research Associate

and

Thomas T. C. Hsu

Moores Professor

Department of Civil and Environmental Engineering

University of Houston

Houston, Texas

April 1, 2003

TxDOT Research Report 0-1854-4

Crack Width Prediction for Exterior Portion of Inverted "T" Bent Caps

By Ronnie R. H. Zhu and Thomas T. C. Hsu
Dept. of Civil & Environmental Engineering
University of Houston, Houston, TX 77204

Abstract

Unacceptable diagonal cracks frequently occur at the re-entrant corners between the cantilever ledges and the web of inverted "T" bent caps at service load. In order to control the diagonal cracks, an extensive investigation was carried out. The first phase of this research was to predict the diagonal crack widths at the interior portions of the bent caps. A 2-D analytical model, called Compatibility-Aided Strut-and-Tie Model (CASTM), was developed and calibrated by the test results of seven full-size 2-D specimens. The first phase of research were reported in TxDOT research report 0-1854-3.

This report (0-1854-4) describes the second phase of research to predict the diagonal crack widths at the end faces of the exterior portions of bent caps. In this second-phase research, the CASTM was extended to 3-D analysis. Ten 3-D specimens were then tested and the resulting data were used to calibrate the model. Crack control methods for the exterior end faces were recommended.

Keywords: Bent caps; Bridges; Crack control; Crack width; Inverted-T Beam; Reinforced concrete; Serviceability.

Table of Contents

List of Tables

List of Figures

1. INTRODUCTION

1.1 Project Objectives

Inverted "T" bent caps are used extensively on Texas bridges because they are aesthetically pleasing and offer a practical means to increase vertical clearance. As shown in Fig. 1.1(a), the cross-section of an inverted "T" bent cap consists of a "web" with short cantilever "ledges" at the bottom to support the beams, thus minimizing the structural depth of bridges. The problem is that at service load unacceptable diagonal cracking frequently occurs between the cantilever ledges and the web as shown in Fig. 1.1(b) and (c).

Current design guidelines do not adequately address the problem of crack control at service load. Explicit design provisions for cracking need to be developed. To date no rational behavioral theory has been developed to support serviceability design for such bent caps. This project seeks to do so.

The research is divided into three phases: Phase One deals with two dimensional test specimens, Fig. 1.1(b), that represent interior portions of T-caps and dapped ends of bridge girders. Phase Two deals with three-dimensional test specimens, Fig. 1.1(c), that represent the exterior portion of the cap where cracking is most visible. Phase Three deals with the inverted T bent caps as a whole, Fig. 1.1(d), including both the interior span and the exterior cantilever portion.

Phase One research has been completed with the submission of a research report (Zhu, Wanichakorn and Hsu, 2001), and the publication of a paper in the ACI Journal (Zhu et al, 2003). This research followed a two-step methodology: First, a theoretical model was developed that lead to a simple design method capable of controlling crack widths at service load. Second, experimental tests were conducted on full-sized specimens to calibrate the theoretical model. As a result, simple, accurate equations were derived for predicting the diagonal crack widths at interior locations of inverted "T" bent caps and dapped ends of bridge girders.

Phase Two research, the focus of this report, deals with the diagonal crack widths at the exterior portion of the bent cap. This second phase of research is more difficult because the stresses and strains in this region of the cap are three-dimensional, rather than two-dimensional as in Phase One.

Phase Three research deals with the tests and analyses of whole specimens. The test results will be presented in a separate report TxDOT 0-1854-5.

1.2 Scope of Phase Two Report

This report, which summarizes the Phase Two research, describes the tests and analyses of ten 3-D specimens as listed in Table 1.2. Two primary variables were investigated; (1) the load position from the most exterior load to the end face, and (2) the number of diagonal bars. The proposed design formulas for predicting crack widths at service load are based on these two variables and are reasonably simple and conceptually clear.

2. EXPERIMENTS

2.1 3-D Test Specimens

The ten 3-D specimens as listed in Table 1.2 are designed to study two primary variables as reflected in the labels of the specimens. The first character in the labels is a letter "E" that stands for the "end region." The end regions of inverted T bent caps are the focus of this Phase Two study. The second character is a number (0, 1, 2 or 5), which indicates the number of diagonal bars. The third character is also a number (6, 10, 12, 14, 18 or 20), which signifies the distance L_E, in inches, from the most exterior load to the end face. The spacing of hanger bars, flexural bars and diagonal bars are maintained at a constant of 4 in. center-to-center.

The 3-D test specimens as shown in Fig. 1.1(c) are symmetrical about their centerlines so that each specimen can furnish two tests, one on the west side and one on the east side. Figure 2.1(a) shows the steel cage without diagonal bars and Figure 2.1(b) shows the steel cage with diagonal bars.

There is a third minor variable: the size of the bearing plates. All specimens have bearing plates of 6 in. × 6 in. except specimens E-0-12, E-0-20 and E-5-12, which have bearing plates of 10 in. × 8 in.

The nominal shear resistance V_n for the service limit state is calculated based on Eq. (5.13.2.5.5-1) of AASHTO (2000):

$$V_n = \frac{A_{hr}(0.5f_y)}{S}(W + 3a_v) \tag{2.1}$$

where V_n = the nominal shear resistance, in kips, for single-beam ledges
A_{hr} = area of one leg of hanger reinforcement (in^2)
S = spacing of hangers (in)
f_y = yield strength of reinforcing steel (ksi)
W = width of bearing (in)
a_v = distance from face of wall to the load (in)

Eq. (2.1) does not take into account the cases where $W + 3a_v$ is larger than the spacing of the bearings or is larger than 2 times the distance L_E from the center of bearing to the end face. In the case of exterior pad and $W + 3a_v > 2L_E$, the following equation should apply:

$$V_n = \frac{A_{hr}(0.5f_y)}{s}2L_E \tag{2.2}$$

The nominal shear resistance V_n for the service limit state calculated for the ten 3-D specimens are given in Table 2.1.

2.2 Materials

2.2.1 Concrete

The concrete used in the 3-D specimens of Phase Two study was the same as that used in the 2-D specimens of Phase One study. The Class F, six-sack, ready-mix concrete had a compressive strength of 5000 psi or more. The proportioning of the ready-mix concrete was decided jointly with the supplier based on TxDOT specifications as follows:
Type 1 Portland cement –398 lbs;
Limestone aggregate (1" max.)-1573 lbs;
Sand – 1391 lbs;
Fly ash – 132 lbs;

Water – 250 lbs;
Slump – 6 – 7 in.;
Compressive strength – 5633 psi.

2.2.2 Steel

Grade 60 No. 5 rebar was used for the hanger and flexural bars. The stress-strain curves of steel bars are shown in Fig. 2.2. The average yield stress was 64.0 ksi, and the yield strain was 0.0022.

2.3 Test Facility

2.3.1 Loading System

All specimens were tested in the 2.5-million lbs MTS testing system, located at the Structural Research Laboratory, University of Houston. The test set-up is shown in Fig. 2.3(a) and (b).

As shown in Fig. 2.3(b) the load V was calculated from the applied load P by the following formula:

$$V = \frac{P}{2}\left(\frac{13\text{ in.}}{67\text{ in.} - L_E}\right) \tag{2.3}$$

When L_E = 10 in., V = 0.114 P.

This MTS test system was controlled by a versatile TestStar system, which could provide both load-control and strain-control procedures. The load was first applied by the load-control procedure in the linear stage of load-deformation curve, and was then switched to the strain-control mode when the curve became non-linear. A continuous record of the stresses and strains was obtained during the test.

2.3.2 Instrumentation and Data Acquisition

A total of 35 LVDTs and 40 SR4 electrical strain gauges were available for testing each specimen. They were placed at the most desirable locations to maximize the required information according to the design of each specimen. The exact location of LVDTs and SR4 gauges for each specimen are shown in the appendices. For most of the specimens, the strains of concrete and steel on the end face of a specimen were measured by 16 LVDTs as shown in Fig. 2.3(c). The geometric layout, the labeling, and the gauge length of the LVDTs are shown in Fig. 2.3(d).

In order to study the variation of strains in hanger bars along the span direction, about 14 LVDTs were used to measure the hanger strains as shown in Fig. 2.3(e).

The local strains on the hanger steel, the flexural steel, and the diagonal steel were measured by 6 mm SR4 electrical strain gauges glued to the steel bars, as shown in the Appendices.

A 80-channel HBM Spider 8 data acquisition system is used for the test. The HBM Spider 8 system is a new type of data acquisition system for parallel, dynamic measurement. These characteristics are desirable for cyclic loading tests simulating repeated vehicle loading. This new instrument is also more versatile, because each of the 80 channels can accept both the high-voltage signals from LVDTs and the low-voltage signals from SR4 gauges.

2.3.3 Deflection Measurements

Nine LVDTs were used to measure the deflected shape of each loaded specimen. The vertical deflections of the specimens were measured with respect to a reference frame, made of light-gage steel members and rigidly bolted to the massive bottom crosshead of the MTS machine. The reference frame can be seen in Fig. 2.3(a). The deflection measurements are recorded in the Appendices.

3. TEST RESULTS

3.1 Load –Displacement Curves

The load – displacement curves of the 10 specimens are shown in Fig. 3.1. In this figure, the vertical axis represents the applied load P of the MTS hydraulic actuator (see Fig. 2.3(b)), and the horizontal axis represents the corresponding stroke displacement.

The ultimate capacities and the ductility of the 10 specimens can be compared in Fig. 3.1. The specimen E-2-6 and E-2-10, which have two diagonal bars, are much more ductile than the specimens with only one diagonal bar or without diagonal bars. The specimen E-5-12 did not show the expected ductility, perhaps because of low concrete strength.

3.2 Crack Patterns

There are basically two kinds of cracks on the end face, originating from the re-entrant corners of a specimen: diagonal cracks and horizontal cracks.

3.2.1 Crack Pattern for Specimens without Diagonal Bars

For specimens E-0-6, E-0-10, E-0-12, E-0-14, horizontal cracks appeared first, as shown in Fig. 3.2.1(a). Then, diagonal cracks appeared as shown in Fig. 3.2.1(b). For specimens E-0-18 and E-0-20, diagonal cracks appeared before the horizontal cracks as shown in Fig. 3.2.1(c) and (d).

The observed trend for specimens without diagonal bars seemed to be as follows: horizontal cracks appeared first when the end distance L_E was small, and diagonal cracks appeared first, when L_E was large.

3.2.2 Crack Pattern for Specimens with Diagonal Bars

For specimens E-2-6 and E-2-10, diagonal cracks appeared first, as shown in Fig. 3.2.2(a) and (c). Then, horizontal cracks appeared as shown in Fig. 3.2.2 (b) and (d). For specimens E-1-10 and E-5-12, horizontal cracks appeared before the diagonal cracks as shown in Fig. 3.2.2 (e), (f), (g) and (h).

In short, no obvious trend could be observed for specimens with diagonal bars.

3.3 Modes of Failure

Two modes of failures were observed for all specimens: punching shear failure and web shear failure. All specimens without diagonal bars failed due to punching shear as shown in Fig. 3.3 (a) and (b). All specimens with diagonal bars failed due to web shear as shown in Fig. 3.3 (c) and (d). It was obvious that diagonal bars increased the punching shear strength, thus forcing the

specimens to fail by web shear. Web shear failure had a failure surface that avoided intersecting the diagonal bars as sketched by the heavy line in Fig. 3.3 (e). Fig. 3.3(f) shows a perspective view of the failure surface (cross hatched).

3.4 Crack Width

Figure 3.4(a) shows the crack widths obtained by LVDT C2 as a function of load V. The load V is the force applied on one bearing pad located closest to the end face and is defined in Fig. 2.3(b) and Eq. (2.3). Fig. 3.4(a)(1) shows crack width vs. load V curve in full range. Fig. 3.4(a)(2) shows crack width vs. load V curve in the expanded range where crack widths are less than 0.02 in. Fig. 3.4(a)(2) shows three important observations: (1) crack widths increase rapidly after reaching 0.004 in., (2) At a certain crack width (say 0.004 in) the load V is effected strongly by the distance L_E. Controlling the edge distance L_E is the most effective way to control the crack widths, and (3) Specimens with diagonal bars are more effective than specimens without diagonal bars. At least two diagonal bars are recommended.

Figure 3.4(b) shows the crack width measured by LVDTs on the west side and by microscopes on the east side. Although the specimens and the test set-ups are designed to be symmetrical for the west and east sides, some specimens, such as E-0-20, E-0-14 and E-2-10, exhibited obvious differences in the crack widths of the two sides. The installation of SR4 strain gauges may have weakened the west side.

In order to verify the validity of crack widths measured by LVDTs, the crack widths measured by LVDTs were compared with the results measured by microscopes on the same side, as shown in Fig. 3.4(c). Since it is difficult to measure the crack widths on the west side crowded with LVDTs, only one point, C3 or C2, on a diagonal crack on the west side was measured by microscopes. Fig. 3.4(c) shows that the crack width measured by the two methods match well in general. The small differences may be caused by the following: (1) the loads corresponding to the crack width measured by microscopes were not exact because several minutes were required to complete all the measurements. (2) the measurement locations for the crack width may be different for the two methods. (3) The measurement by LVDTs may cover more than two cracks, while the measurement by microscope covers only one crack. For the three specimens E-1-10, E-0-18 and E-2-6 that were tested last, the results match much better because more experience and attention were paid to the measurements on the west side. It can be concluded from these observations that the crack widths measurement by LVDTs can be used to develop a design method for checking the crack widths at service loads.

3.5 Variation of Hanger Bar Strains along the Longitudinal Axis

Figure 3.5 (a) to (g) show the variation of hanger bar strains along the length of seven specimens. The vertical line indicates the location of the exterior load V. These graphs show that the strain variation is largely affected by the location of load V. When the ratio of end distance to the ledge depth, L_E / h, is small, such as 6/13 or 10/13, the strains increased rapidly toward the end face. When the ratio L_E / h increased to 18/13, the strains actually decreased toward the end face.

4. CALCULATION OF CRACK WIDTH BY COMPATIBILITY-AIDED STRUT-AND-TIE MODEL (CASTM)

4.1 Introduction

The CASTM model has been proposed for predicting the diagonal crack widths at re-entrant corners of 2-D specimens (Fig. 1.1(b)) *with* or *without* diagonal steel bars (Zhu, Wanichakorn and Hsu, 2001). 2-D specimens represent the interior portion of inverted 'T' bent caps. This 2-D CASTM is substantiated by the tests of seven 2-D specimens. The diagonal crack width w can be predicted by CASTM as follows:

$$w = L_{HF}\varepsilon_{HF} \tag{4.1}$$

where

w = predicted diagonal crack width (in.)

L_{HF} = CASTM gauge length for calculated hanger and flexural steel strains
$= 9500\,\varepsilon_{HF} - 3.0$ (in.)

ε_{HF} = diagonal crack strain calculated by hanger and flexural strains $= \sqrt{\varepsilon_H^2 + \varepsilon_F^2}$

ε_H = hanger strain or strain in the vertical direction $= \dfrac{(1-B)V}{E_S A_{SH} + E_C A_{CH}}$

ε_F = flexural strain or strain in the horizontal direction $= \dfrac{(1-B)V\cot\theta_V}{E_S A_{SF} + E_C A_{CF}}$

V = applied service load at each ledge (kips)

θ_V = Angle between flexural steel bars and the diagonal strut at the point of load V

B = distribution factor for diagonal bars $= \dfrac{A_{SD}}{A_{SH} + 0.5A_{SF} + A_{SD}}$

A_{SD} = total cross-sectional area of diagonal reinforcement at each ledge of 2-D specimen (in.^{2})

A_{SH} = total cross-sectional area of hangar reinforcement at each ledge of 2-D specimen (in.^{2})

A_{SF} = total cross-sectional area of flexural reinforcement at each ledge of 2-D specimen (in.^{2})

A_{CH} = total effective concrete area surrounding hanger reinforcement (in.^{2})

A_{CF} = total effective concrete area surrounding flexural reinforcement (in.^{2})

E_S = 29,000 ksi

E_C = $57\sqrt{f'_C}$ (ksi) for compression and $1.87\sqrt{f'_C}$ (ksi) for tension

f'_C = concrete cylinder compressive strength (psi)

The design criteria of CASTM *with* diagonal bars is identical to those *without* diagonal bars, except that the former involves the distribution factor B. When B is taken as zero, the CASTM *with* diagonal bars simplifies to the CASTM *without* diagonal bars.

The model for predicting of crack widths at re-entrant corners of 3-D specimens is developed from the CASTM for 2-D specimens. The first curtain of exterior hanger bars, flexural bars and diagonal bars are treated as a 2-D truss and the crack width is calculated by the above-mentioned CASTM equation (4.1). The relationship between the CASTM calculated crack width and the measured crack width of 3-D specimens can be calibrated as a function of two parameters (1) the distance L_V of the applied exterior load V to the most exterior steel bar, and (2) the distribution factor B. These two parameters were found to be the main factors affecting the crack widths.

4.2 Calibration of 3-D Specimens without Diagonal Bars

Fig. 3.4(a) shows that the load V vs. crack width curves can each be divided into two parts. When crack widths are less than about 0.004, they increase slowly, and the slightly non-linear curves exhibit a small slope. However, when crack width is larger than 0.004, they increase rapidly and the curves exhibit a large slope. In other words, when the crack width reaches about 0.004 inch, cracks opened up very rapidly even with a very small increase of load.

To control diagonal crack widths at the end faces, it is very important to limit the service load to a "critical load" where crack widths exceed 0.004 inch, instead of the flexural crack width limits of 0.013 and 0.016 inch. The calculation results based on Eq.(4.1) corresponding to the point with measured crack width C2 equal to 0.004 are shown in Table 4.2(a) and (b).

The ratio of 0.004/w in Table 4.2(b) is plotted against the distance L_V in Fig. 4.2(a). It is obvious that this ratio, 0.004/w, is a function of the distance L_V. Based on the trend curve in Fig. 4.2(a), the crack width of 3-D specimens without diagonal bars can be obtained by the following equation:

$$w = \frac{L_{HF}\varepsilon_{HF}}{(1+L_v)^{1.9}} \le 0.004 \text{ in.} \qquad (4.2)$$

The only point that deviates significantly from the trend curve is that of specimen E-0-14. This specimen had a strongly unsymmetrical crack development as shown in Fig. 4.2(b). At P = 500 kips, after the nominal shear resistance V_n = 413 kips for the service limit state, there was still no diagonal crack on the east side.

When w is larger than 0.004 in., the crack width increases dramatically and is hard to control. It can be illustrated by the two photos of specimen E-0-18 in Fig. 4.2(c) and Fig. 4.2(d) for a small increase of load P from 600 kips to 625 kips. Fig. 4.2(c) shows the crack pattern at P = 600 kips when w is less than 0.004 in. and Fig. 4.2 (d) shows the crack pattern at P = 625 kips when w is larger than 0.004 in. When w reaches about 0.004 in., the two horizontal cracks become connected and open up rapidly. In this new post-0.004 in. mechanism of resistance, the concrete stiffness reduces dramatically to a very small value and the steel bars began to resist a much larger proportion of force. To avoid such a rapid increase of crack width, the service load should be limited to a load $V_{0.004}$ that corresponds to a crack width of 0.004 in.

The slope of the w vs. V curve when w is larger than 0.004 in. can be calibrated as a function of the distance L_V as shown in Fig. 4.2(e). Based on the trend line in Fig. 4.2(e), the crack width larger than 0.004 in. can be calculated by the following equation:

$$w = 0.004 \text{ in.} + \frac{0.1(V - V_{0.004})}{(1+L_v)^{1.9}} \le 0.015 \text{ in.} \qquad (4.3)$$

where $V_{0.004}$ is defined as the applied service load V at exterior bearing pad when the calculated crack width is equal to 0.004 in.

4.3 Calibration of 3-D Specimens with Diagonal Bars

For specimens with diagonal bars, crack widths also increase slowly when they are less than about 0.004 in. The ratios 0.004 in./w for the 4 specimens with diagonal bars in Table 4.3(b) are added to Fig. 4.2(a) as shown in Fig. 4.3(a). It can be seen that the ratios 0.004 in./w for specimens with diagonal bars would be much larger than those for specimens without diagonal bars. This difference appears to indicate that the distribution factors B for 3-D specimens are different from those of 2-D specimens. Based on the test results in Fig. 4.3(a), a modified equation for the B factors of 3-D specimens is suggested as follows:

$$B = \frac{A_{SD}}{A_{SH} + 0.5A_{SF} + A_{SD}} \frac{\left[1 + (N-1)S_D\right]^{0.7}}{1 + L_V} \tag{4.4}$$

Where L_V = the distance from the most exterior bar to the load V applied on the exterior bearing, inch.

N = number of diagonal bars from the end face to the center of first bearing = 1, 2, 3 and so on. When N = 0, A_{SD} = 0 and B = 0.

S_D = center-to-center spacing of diagonal bars, same as spacing of hangar bars.

Fig. 4.3(a) is replotted using Eq. (4.4) as shown in Fig. 4.3(b). Fig. 4.3(b) shows that the trend curve is only a function of distance L_V, when the modified distribution B in Eq. (4.4) is used.

Beyond a value of 0.004 in., crack width increases rapidly and the curve exhibits a large slope. This difference of behavior before 0.004 in. and after 0.004 in. can be explained by the two photos of specimen E-1-10 in Fig. 4.3(c) and Fig. 4.3(d). Fig. 4.3(c) shows the crack pattern at P = 425 kips when w is less than 0.004 in. and Fig. 4.3 (d) shows the crack pattern at P = 435 kips (a 10 kips increase) when w is larger than 0.004. When w reaches about 0.004 in., the horizontal cracks became connected and a new mechanism of resistance arises. In this post-0.004 in. stage, the concrete stiffness reduces dramatically and the stresses in the steel bars increase rapidly.

For specimens with diagonal bars in the post-0.004 in. stage, the slope of w vs. V curve is not only a function of distance L_v but also a function of distribution factor B. The distribution factor B can be calibrated using specimens with diagonal bars (E-2-6, E-1-10, E-2-10 and E-5-12) as shown in Table 4.3(c). The slope ratio vs. factor B curve is plotted in Fig. 4.3(e) using the data from the Table 4.3(c). Based on the trend lines in Fig. 4.3(e), crack width larger than 0.004 in. can be calculated by the following equation:

$$w = 0.004 \text{ in.} + \frac{0.1(1-B)^5 (V - V_{0.004})}{(1 + L_v)^{1.9}} \le 0.015 \text{ in.} \tag{4.5}$$

4.4 Comparison of Predicted Results with Test Results

The predicted results are compared to the test results in Fig. 4.4. The test results are obtained from the LVDT C2 on the west side. Recalling from Fig. 3.4(b) that the crack widths measured by LVDTs on the west side are close to or larger than those measured by microscopes

on the east side. This difference was likely to be the result of placing more strain gauges in the west side, where gluing of the strain gauges reduced the cross sections and the bond capacity of steel bars. Since the prediction is calibrated to match the larger crack width, the predicted results are on the conservative side.

Fig. 4.4 shows that the predicted results match the test results quite well, except for specimen E-0-14. As discussed in section 4.2 following Eq. (4.2), the unusually large crack on the west side in specimen E-0-14 was caused by the severe unsymmetrical crack development as shown in Fig. 4.2(b). Fig. 4.4 also shows that the predicted results are usually larger than the test results when the crack width w is less than 0.004 inch. This is because a constant concrete stiffness for cracked concrete is used for the whole process. If a varied concrete stiffness is used, the prediction should be much better. However, using a varied concrete stiffness would be too complicated in practical design.

A maximum crack width of 0.007 has been recommended by ACI Committee 224 (2001) for exposure to deicing chemicals. For the purpose of controlling crack width, the prediction of the crack widths between 0.004 in. and 0.007 in. is very important. Table 4.4 compares the loads $V_{0.004}$ and $V_{0.007}$, corresponding to crack widths of 0.004 in. and 0.007 in. For most specimens, the force difference between the test results and predicted results are about 5%. In short, as long as the service loads are limited to $V_{0.004}$, the crack widths should be comfortably less than 0.007 in.

Table 4.5 compares the loads $V_{0.004}$ and $V_{0.015}$, corresponding to crack widths of 0.004 in. and 0.015 in., respectively. For most specimens, the force difference between the test results and the predicted results for crack width of 0.015 in. are less than or about 10%. The force differences between the test results and the predicted results for specimens E-0-6, E-0-14 and E-0-18 are over 10 % , demonstrating the large scatter of crack width measurements.

4.5 Prediction of Diagonal Cracks by CASTM

The diagonal crack widths for 3-D specimens can be predicted by the CASTM as follows:

$$w = \frac{L_{HF}\varepsilon_{HF}}{(1+L_v)^{1.9}} \le 0.004 \text{ in.} \tag{4.6}$$

$$w = 0.004 \text{ in.} + \frac{0.1(1-B)^5(V-V_{0.004})}{(1+L_v)^{1.9}} \le 0.015 \text{ in.} \tag{4.7}$$

where

w = predicted diagonal crack width (in.)

L_{HF} = CASTM gauge length for calculated hanger and flexural steel strains
$= 9500\,\varepsilon_{HF} - 3.0$ (in.)

ε_{HF} = diagonal crack strain calculated by hanger and flexural strains $= \sqrt{\varepsilon_H^2 + \varepsilon_F^2}$

ε_H = hanger strain or strain in the vertical direction $= \dfrac{(1-B)V}{E_S A_{SH} + E_C A_{CH}}$

ε_F = flexural strain or strain in the horizontal direction $= \dfrac{(1-B)V\cot\theta_V}{E_S A_{SF} + E_C A_{CF}}$

V = applied service load at an exterior loading pad (kips)

θ_V = Angle between flexural steel bars and the diagonal strut at the point of load V

B = distribution factor for diagonal bars $= \dfrac{A_{SD}}{A_{SH} + 0.5A_{SF} + A_{SD}} \dfrac{\left[1 + (N-1)S_D\right]^{0.7}}{1 + L_V}$, when $(N-1)S_D > L_V$, $(N-1)S_D = L_V$

A_{SD} = cross-sectional area of a diagonal steel bar at end face of inverted 'T' bent cap (in.^{2})

A_{SH} = cross-sectional area of a hangar steel bar at end face of inverted 'T' bent cap (in.^{2})

A_{SF} = cross-sectional area of a flexural steel bar at end face of inverted 'T' bent cap (in.^{2})

A_{CH} = effective concrete area surrounding the hanger steel bar at end face of inverted 'T' bent cap(in.^{2})

A_{CF} = effective concrete area surrounding flexural steel bar at end face of inverted 'T' bent cap(in.^{2})

L_V = the distance from the most exterior bar to the service load V applied on the exterior bearing pad, inch.

N = number of diagonal bars = 1, 2, 3 and so on. When N = 0, A_{SD} = 0 and B = 0.

S_D = center-to-center spacing of diagonal bars, same as spacing of hangar bars.

E_S = 29,000 ksi

E_C = $57\sqrt{f_C'}$ (ksi) for compression and $1.87\sqrt{f_C'}$ (ksi) for tension

f_C' = concrete cylinder compressive strength (psi)

$V_{0.004}$ = applied service load V at exterior bearing pad corresponding to cracking width 0.004, which can be obtained from Eq. (4.6) using a successive approximation method. This successive approximation calculation can easily be performed using a spreadsheet.

5. DESIGN RECOMMENDATIONS

When the load V exceeds $V_{0.004}$ in a 3-D specimen, the two horizontal cracks or the two diagonal cracks become connected near the middle of the web, resulting in a weak resistance mechanism. A small increment of load beyond $V_{0.004}$ tends to cause a sudden, large increment of crack width that may exceed 0.015 inch. Therefore, it is recommended that the design service load should not exceed $V_{0.004}$. The load $V_{0.004}$ can be calculated from Eq. (4-6) by means of a successive approximation method using a spread sheet as illustrated by an example in Table 5.

6. SUMMARY

1. Diagonal cracks at the re-entrant corners of 3-D specimens open up very fast after reaching a width of 0.004 inch. It is proposed that the design service load be limited to a value of $V_{0.004}$ which induces such a crack width.

2. The proposed design service load $V_{0.004}$ can be obtained by solving Eq. (4.6) derived from CASTM (Compatibility-Aided Strut-and-Tie Model). Equation (4.6) is applicable to 3-D specimens with and without diagonal bars. Predicted values of $V_{0.004}$ for ten 3-D specimens compare very well with the test results.
3. Analytical equation is also proposed to predict crack widths up to 0.015 inch.

ACKNOWLEDGMENTS

This research is supported by Grant 0-1854 from the Texas Department of Transportation. The project supervisory committee consists of: J. C. Liu (Project Coordinator), John P. Vogel (Project Director), Kenneth Ozuna (Project Advisor), Timothy Bradberry (Project Advisor) and Tom Rummel (Project Advisor).

REFERENCE

AASHTO (2000). Standard Specifications for Highway Bridges, 16th Ed., American Association of State Highway Transportation Officials, Washington D.C.

ACI Committee 224 (2001). "Control of Cracking in Concrete Structures," ACI Committee Report ACI 224R-01.

Zhu, R. H., Wanichakorn, W. and Hsu, T. T. C. (2001) "Crack Width Prediction for Interior Portion of Inverted 'T' Bent Caps," TxDOT Report 0-1854-3, Department of Civil and Environmental Engineering, University of Houston, Houston, Texas.

Zhu, R. H., Wanichakorn, W., Hsu, T. T. C. and Vogel, J. (2003) "Crack Width Prediction Using Compatibility-Aided Strut-and-Tie Model," Structural Journal of the American Concrete Institute, Vol. 100, No. 4, July-August, 2003, pp.413-421.

Table 1.2 Test Programs (Specimens and Variables)

Specimen	Edge Distance L_E of Load V (in.)	Number of Diagonal Bar
E-0-6	6	0
E-0-10	10	0
E-0-12*	12	0
E-0-14	14	0
E-0-18	18	0
E-0-20*	20	0
E-1-10	10	1
E-2-6	6	2
E-2-10	10	2
E-5-12*	12	5

* with 8 in. × 10 in. bearing pad instead of 6 in. × 6 in. bearing pad

Table 2.1 Loads and Crack Widths in Test Specimens

Specimen	f'_c (psi)	Crack Width at Nominal Shear Resistance V_n for Service Limit State (in.)		Nominal Shear Resistance V_n for Service Limit State (kips) Eqs.(2.1) & (2.2)	Ultimate Test Load V (kips)	Ultimate Test Load P (kips)
		C2	C3			
E-0-6	5024	0.0031	0.0034	27.9	75.8	711.1
E-0-10	6182	0.0039	0.0053	46.5	98.1	860.5
E-0-12	5876	0.0024	0.0039	55.8	130.7	1106
E-0-14	5801	0.0049	0.0063	50.6	117.8	960
E-0-18	5748	0.0002	0.0007	50.6	135.1	1018.1
E-0-20	6056	0	0.0005	56.4	151.7*	1096.6*
E-1-10	5065	0.002	0.003	46.5	97.6	855.7
E-2-6	5204	0.0013	0.0018	27.9	77.3	725.1
E-2-10	6764	0.0025	0.0028	46.5	113.7	997.1
E-5-12	4611	0.0011	0.0022	55.8	115.6	979.5

Load V and load P are defined in Fig. 2.3(b) and Eq. (2.3).
* Premature failure at the other end of specimen.

Table 4.2(a) Steel Bar Arrangement and Material Properties
for 3-D Specimens without Diagonal Bars

	E-0-6	E-0-10	E-0-12	E-0-14	E-0-18	E-0-20
A_{SD} (in.^{2})	0	0	0	0	0	0
A_{SH} (in.^{2})	.31	.31	.31	.31	.31	.31
A_{SF} (in.^{2})	.31	.31	.31	.31	.31	.31
A_{CH} (in.^{2})	15.5	15.5	15.5	15.5	15.5	15.5
A_{CF} (in.^{2})	15.5	15.5	15.5	15.5	15.5	15.5
E_S (ksi)	29000	29000	29000	29000	29000	29000
E_C (ksi)	132	147	143	142	142	145
f'_c (psi)	5024	6182	5876	5801	5748	6056

Table 4.2(b) Calibration of 3-D Specimens without Diagonal Bars

	E-0-6	E-0-10	E-0-12	E-0-14	E-0-18	E-0-20
L_V (in.)	4	8	10	12	16	18
$V_{0.004}$ (kips)	29.0	46.9	61.0	49.4	82.2	98.4
θ_V ($^\circ$)	51.1	51.1	51.1	51.1	51.1	51.1
B	0	0	0	0	0	0
ε_F	.0021	.0034	.0044	.0036	.0059	.0071
ε_H	.0026	.0042	.0055	.0044	.0074	.0088
ε_{HF}	.0034	.0053	.0070	.0057	.0094	.0112
L_{HF} (in.)	28.70	48.24	64.00	50.47	87.15	104.30
w (in.)	.0976	.2557	.4483	.2877	.8192	1.1676
$\frac{0.004}{w}$	.0410	.0156	.0089	.0139	.0049	.0034

Table 4.3(a) Steel Bar Arrangement and Material Properties
for Specimens with Diagonal Bars

	E-1-10	E-2-6	E-2-10	E-5-12
A_{SD} (in.^{2})	.31	.31	.31	.31
A_{SH} (in.^{2})	.31	.31	.31	.31
A_{SF} (in.^{2})	.31	.31	.31	.31
A_{CH} (in.^{2})	15.5	15.5	15.5	15.5
A_{CF} (in.^{2})	15.5	15.5	15.5	15.5
E_S (ksi)	29000	29000	29000	29000
E_C (ksi)	133	135	154	127
f'_c (psi)	5065	5204	6764	4611

Table 4.3(b) Calibration of 3-D Specimens with Diagonal Bars

	E-2-6	E-1-10	E-2-10	E-5-12
L_V (in.)	4	8	8	10
V (kips)	38.1	49.88	53.86	65.21
θ_V ($^\circ$)	51.1	51.1	51.1	51.1
B	0.4	0.4	0.4	0.4
ε_F	.0017	.0022	.0023	.0029
ε_H	.0021	.0027	.0028	.0036
ε_{HF}	.0027	.0035	.0037	.0046
L_{HF} (in.)	22.11	30.04	31.67	40.46
w (in.)	.0586	.1045	.1156	.1861
$\frac{0.004}{w}$	.0688	.0390	.0348	.0215

Table 4.3(c) Slope Calibration for Distribution Factor B

Specimen	B	$\frac{\text{slope}_{E-1-10}}{\text{slope}_{E-0-10}}$	$\frac{\text{slope}_{E-2-10}}{\text{slope}_{E-0-10}}$	$\frac{\text{slope}_{E-5-12}}{\text{slope}_{E-0-12}}$	$\frac{\text{slope}_{E-2-6}}{\text{slope}_{E-0-6}}$
E-1-10	0.044	0.977			
E-2-10	0.137		0.419		
E-5-12	0.169			0.349	
E-2-6	0.250				0.209

Table 4.4 Loads $V_{0.004}$ and $V_{0.007}$ Corresponding to Crack Widths of 0.004 in. and 0.007 in.

Specimen	Test (kips)			Prediction (kips)			$V_{0.004}$	$V_{0.007}$
	$V_{0.004}$	$V_{0.007}$	ΔV	$V_{0.004}$	$V_{0.007}$	ΔV	$\frac{V_{test} - V_{pred.}}{V_{test}} \times 100$	$\frac{V_{test} - V_{pred.}}{V_{test}} \times 100$
E-0-6	29.0	32.0	3.0	27.2	27.8	0.6	6.2	13.1
E-0-10	46.9	48.2	1.3	47.4	49.4	2.0	-1.1	-2.5
E-0-12	61.0	61.7	0.7	56.7	59.6	2.9	7.0	3.4
E-0-14	49.4	51.7	2.3	66.1	70.0	3.9	-33.8	-35.4
E-0-18	82.2	87.9	5.7	84.8	91.3	6.5	-3.2	-3.9
E-0-20	98.4	101.3	2.9	94.6	102.6	8.0	3.9	-1.3
E-1-10	49.9	51.0	1.1	48.6	51.0	2.4	2.6	0.0
E-2-6	38.1	40.3	2.2	36.1	38.8	2.7	5.2	3.7
E-2-10	53.9	60.5	6.6	55.4	59.4	4.0	-2.8	1.8
E-5-12	65.0	69.5	4.5	66.8	74	7.2	-2.8	-6.5

Table 4.5 Loads $V_{0.004}$ and $V_{0.015}$ Corresponding to Crack Widths of 0.004 in. and 0.015 in.

Specimen	Test (kips)			Prediction (kips)			$V_{0.004}$	$V_{0.015}$
	$V_{0.004}$	$V_{0.015}$	ΔV	$V_{0.004}$	$V_{0.015}$	ΔV	$\frac{V_{test} - V_{pred.}}{V_{test}} \times 100$	$\frac{V_{test} - V_{pred.}}{V_{test}} \times 100$
E-0-6	29	33.5	4.5	27.2	29.5	2.3	6.2	11.9
E-0-10	46.9	55.1	8.2	47.4	54.6	7.2	-1.1	0.9
E-0-12	61	67.5	6.5	56.7	67.2	10.5	7.0	0.4
E-0-14	49.4	66.5	17.1	66.1	80.5	14.4	-33.8	-21.1
E-0-18	82.2	96.7	14.5	84.8	108.7	23.9	-3.2	-12.4
E-0-20	98.4	120.1	21.7	94.6	124.1	29.5	3.9	-3.3
E-1-10	49.9	57.7	7.8	48.6	57.6	9	2.6	0.2
E-2-6	38.1	49.1	11	36.1	45.8	9.7	5.2	6.7
E-2-10	53.9	75.6	21.7	55.4	70.3	14.9	-2.8	7.0
E-5-12	65	88.3	23.3	66.8	93.3	26.5	-2.8	-5.7

Table 5 Calculation of $V_{0.004}$ by a Trial-and-error Method Using Spread Sheet for E-2-10

V (kips)	40	50	53	55.4
θ_V ($^\circ$)	51.1	51.1	51.1	51.1
N	2	2	2	2
L_V (in.)	8	8	8	8
S_D (in.)	4	4	4	4
$B = \frac{A_{SD}}{A_{SH} + 0.5A_{SF} + A_{SD}} \frac{[1 + (N-1)S_D]^{0.7}}{1 + L_V}$	0.137	0.137	0.137	0.137
$\varepsilon_H = \frac{(1-B)V}{E_S A_{SH} + E_C A_{CH}}$	0.003036	0.003795	0.004023	0.004202
$\varepsilon_F = \frac{(1-B)V \cot\theta_V}{E_S A_{SF} + E_C A_{CF}}$	0.002446	0.003057	0.00324	0.003385
$\varepsilon_{HF} = \sqrt{\varepsilon_H^2 + \varepsilon_F^2}$	0.003899	0.004873	0.005166	0.005396
$L_{HF} = 9500\varepsilon_{HF} - 3.0$ (in.)	34.04	43.29	46.07	48.26
$w = \frac{L_{HF}\varepsilon_{HF}}{(1 + L_v)^{1.9}}$ (in.)	0.0020	0.0032	0.0037	0.0040

Steel area and material properties for specimen E-2-10 are listed in Table 4.3(a)

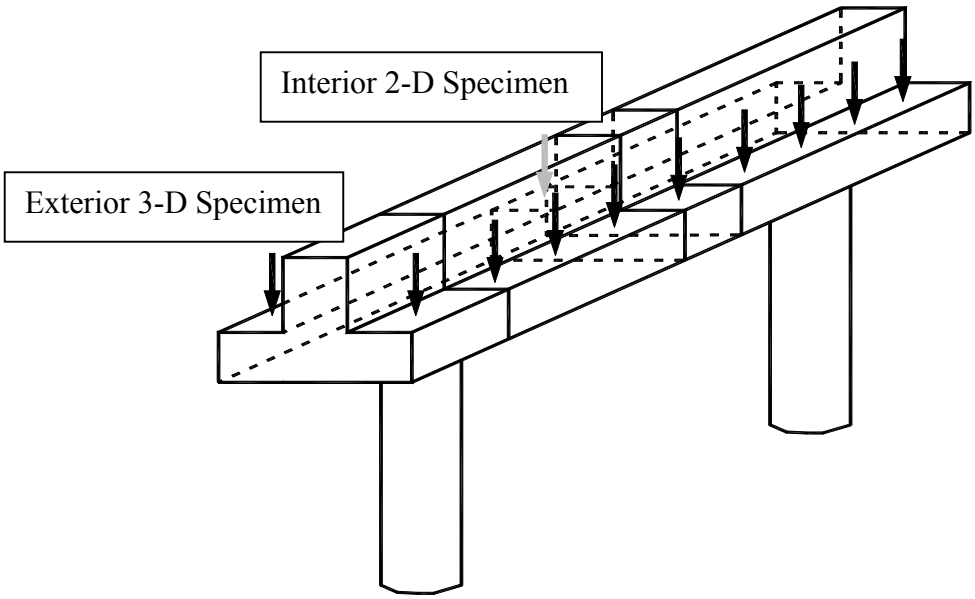

Fig. 1.1(a) An inverted 'T' bent cap showing an exterior 3-D specimen and an interior 2-D specimen

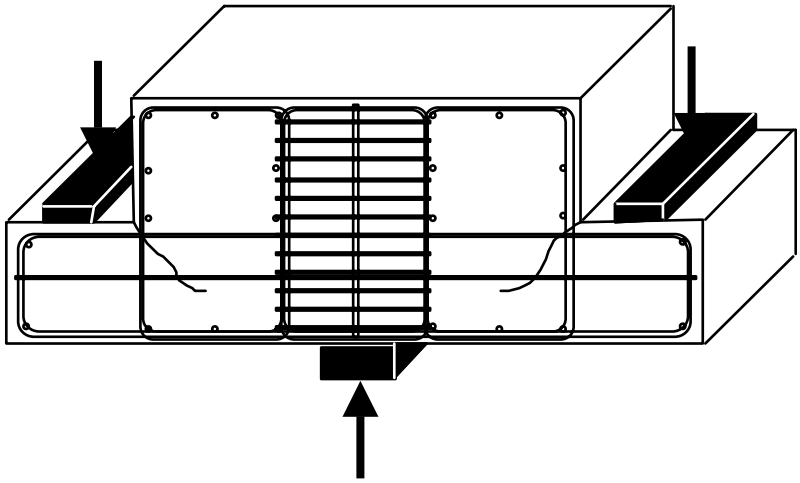

Fig. 1.1(b) 2-D test specimen

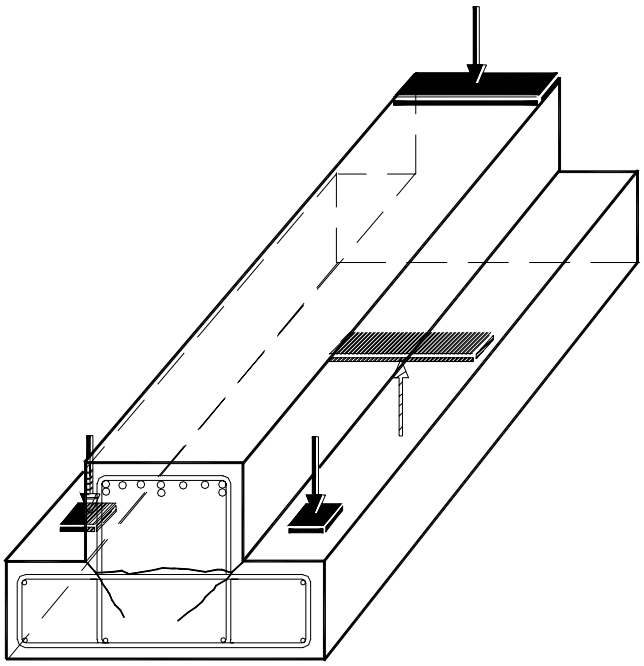

Fig. 1.1(c) 3-D test specimen

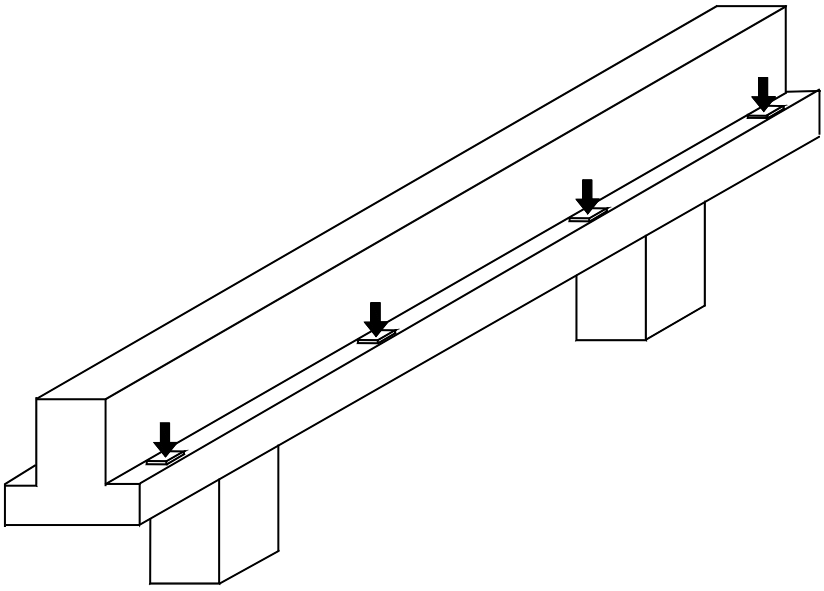

Fig. 1.1(d) Tests of whole inverted T bent caps

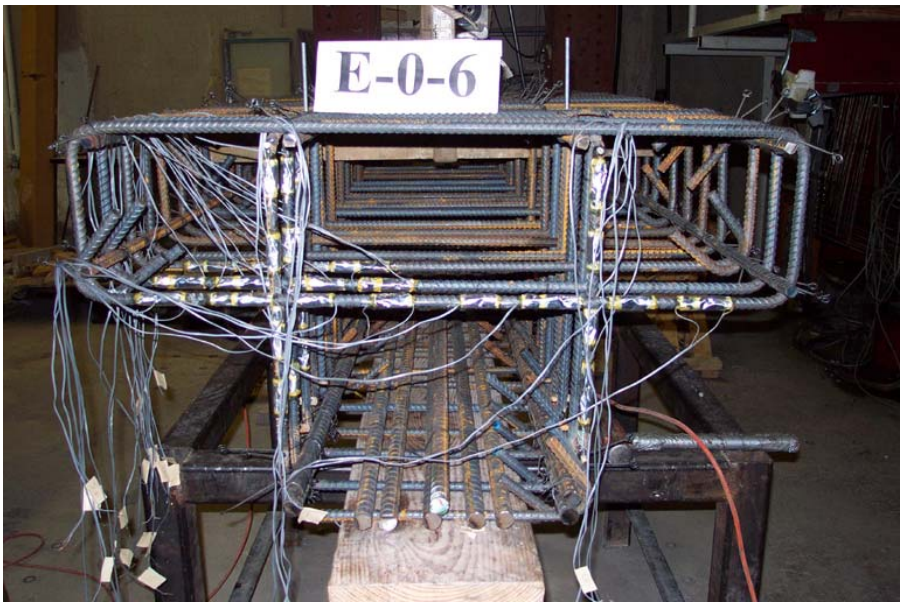

Fig. 2.1(a) Steel cage without diagonal bars (Specimen E-0-6)

Fig. 2.1(b) Steel cage with two diagonal bars (Specimen E-2-6)

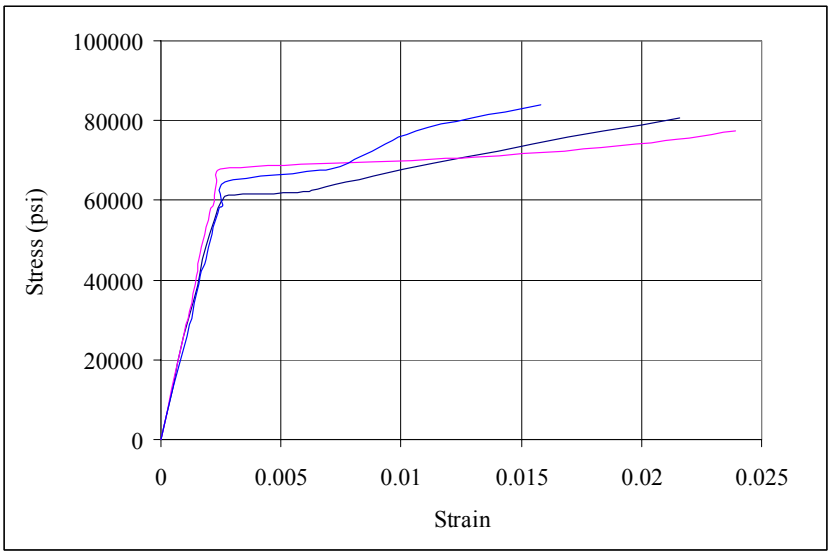

Fig. 2.2 Steel stress vs. strain curves

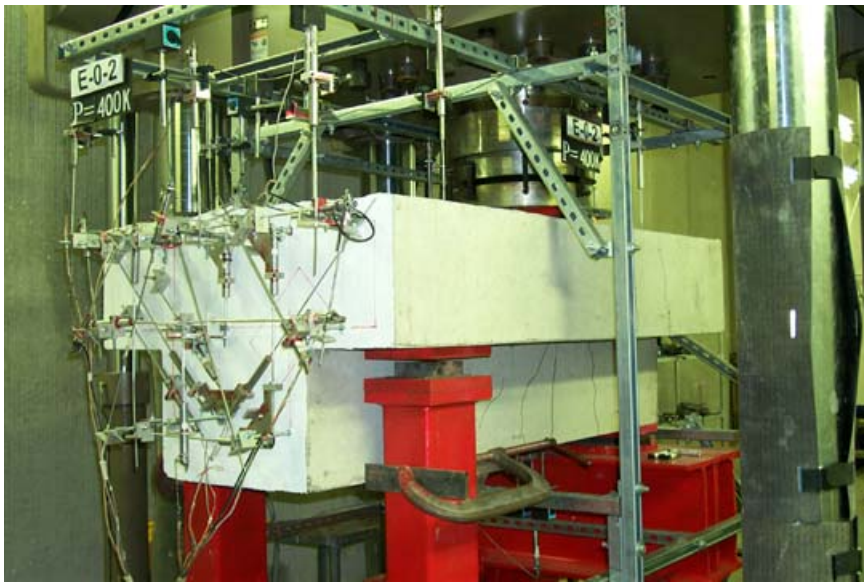

Fig. 2.3(a) General view of test set-up

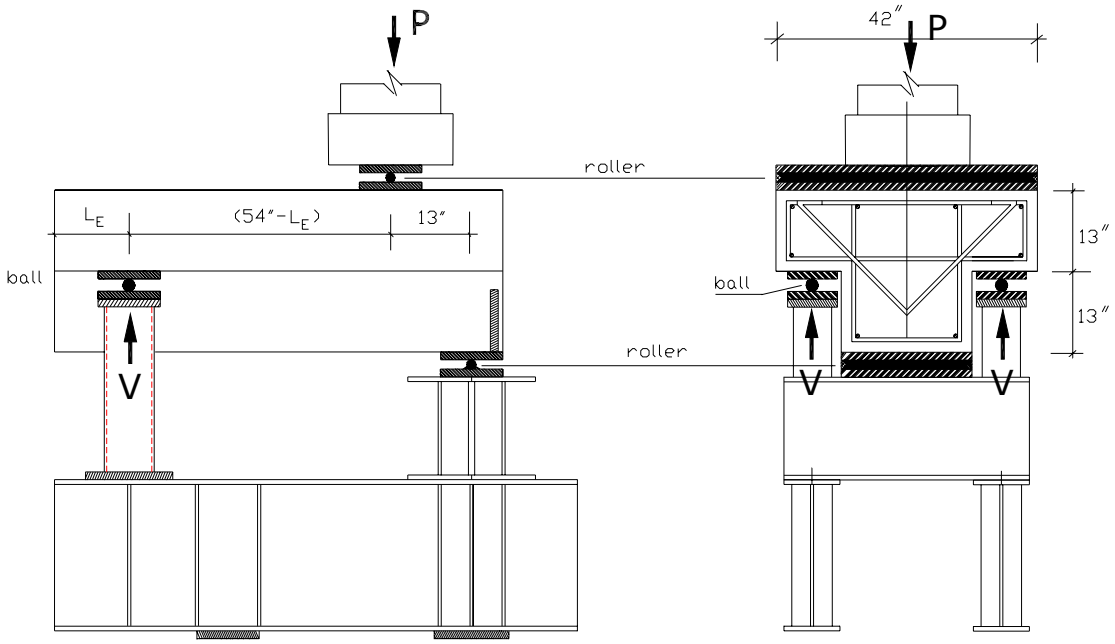

Fig. 2.3(b) Arrangement and dimension of test set-up

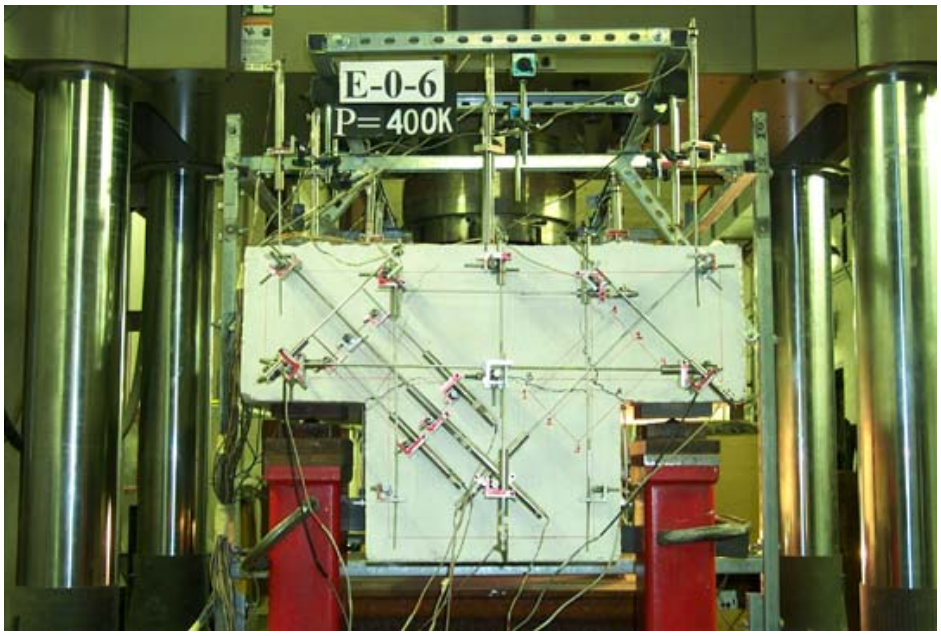

Fig. 2.3(c) Arrangement of LVDTs on end face

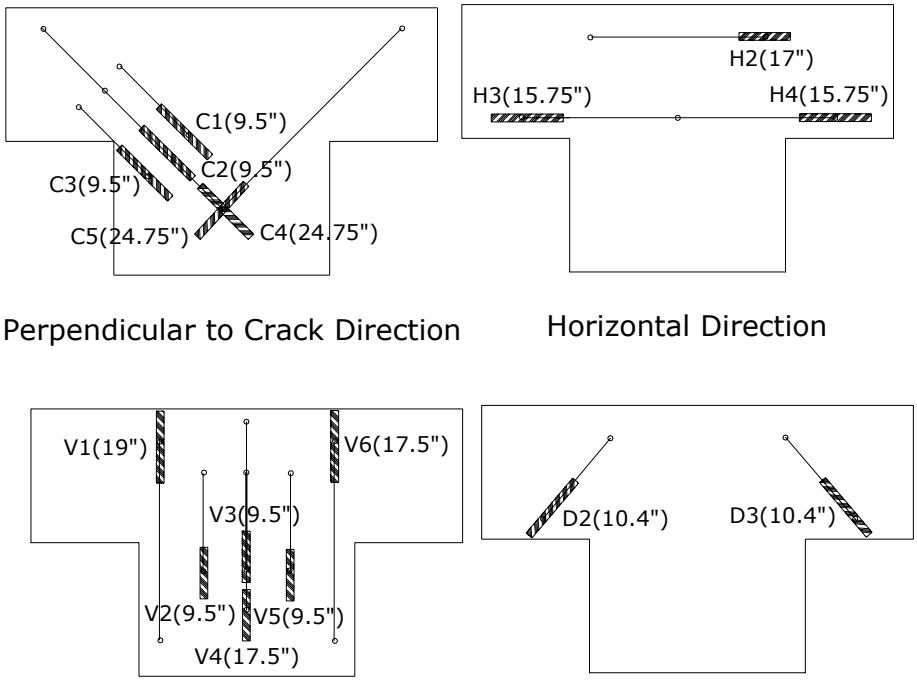

Fig. 2.3(d) Labeling of LVDTs on the end face

Fig. 2.3(e) LVDTs to study the variation of hanger steel strains along the span

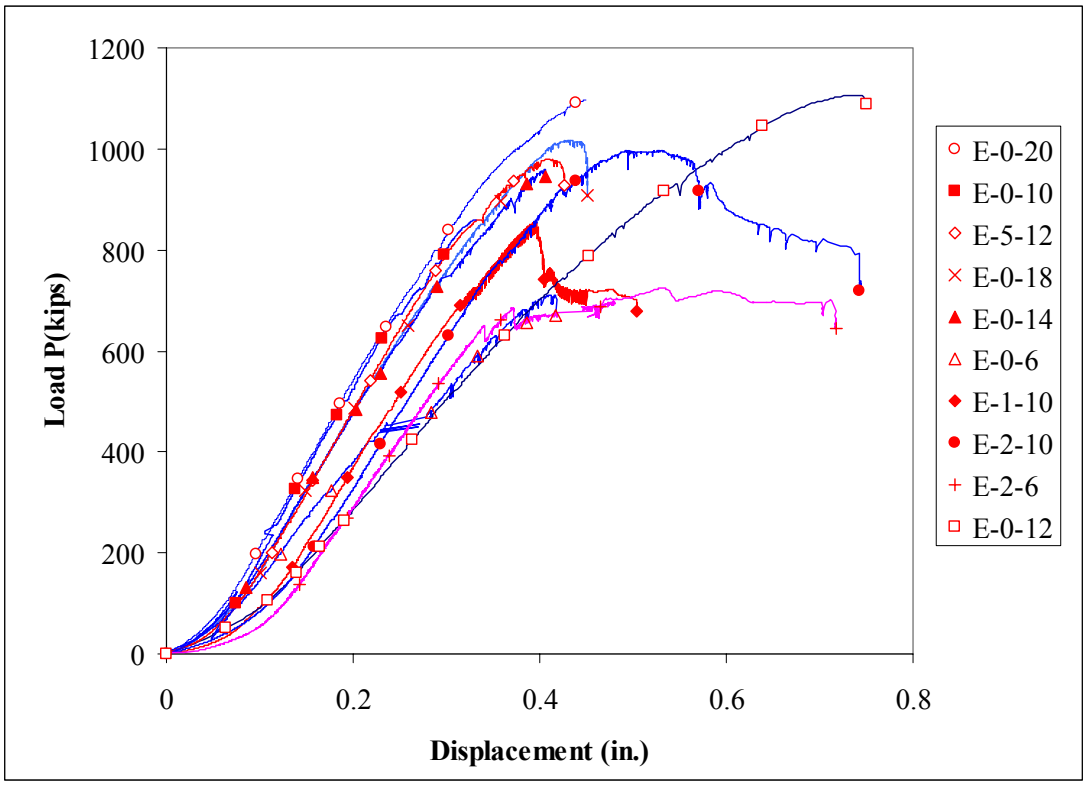

Fig 3.1 Load-displacement curves of 10 3-D specimens

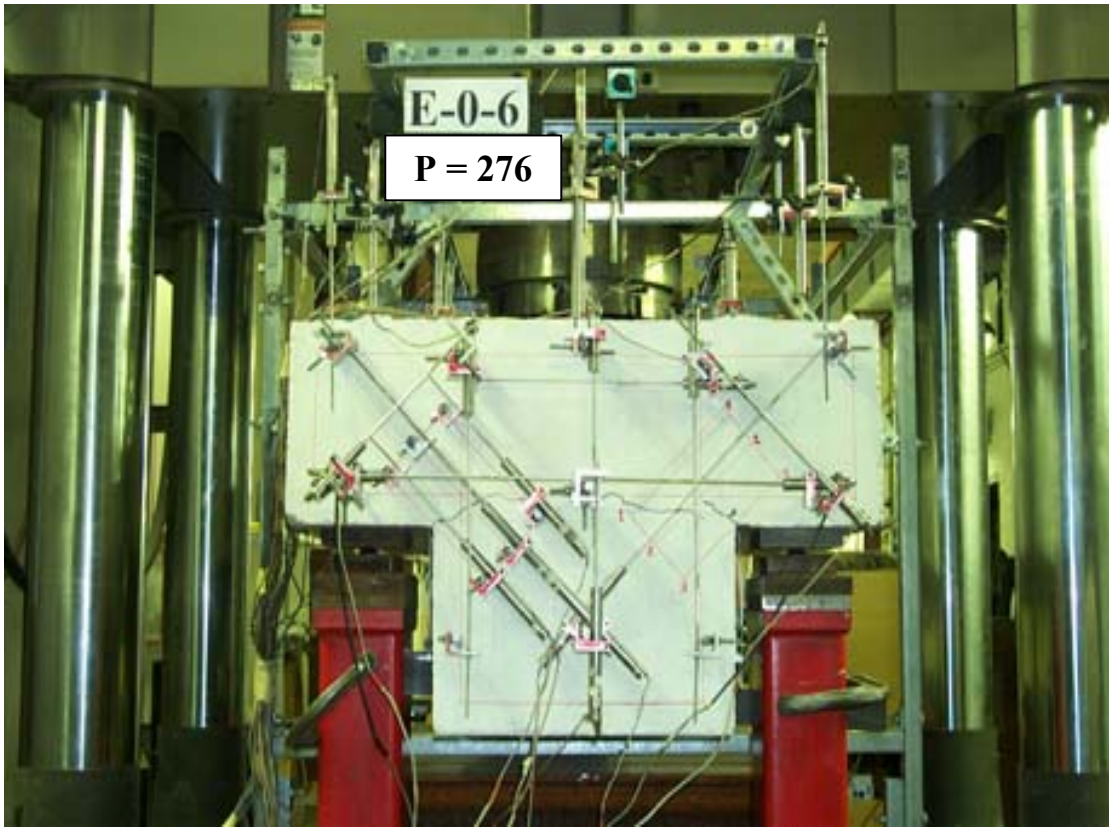

Fig. 3.2.1(a) Horizontal cracks in Specimen E-0-6

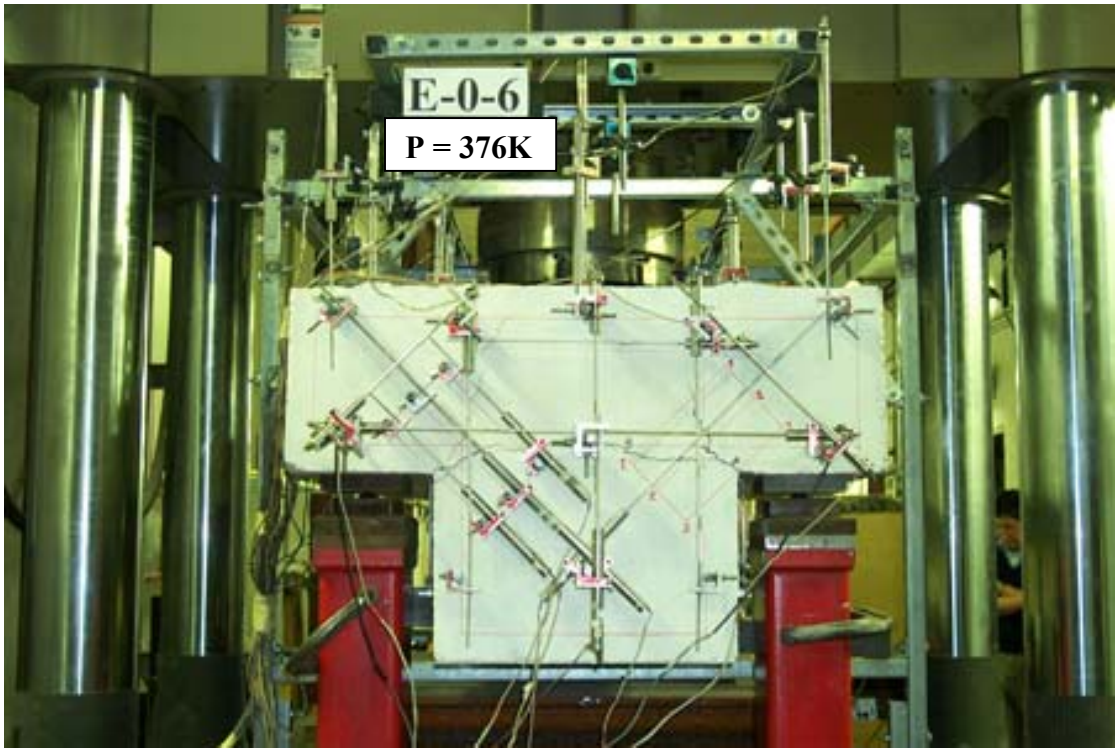

Fig. 3.2.1(b) Horizontal and diagonal cracks in Specimen E-0-6

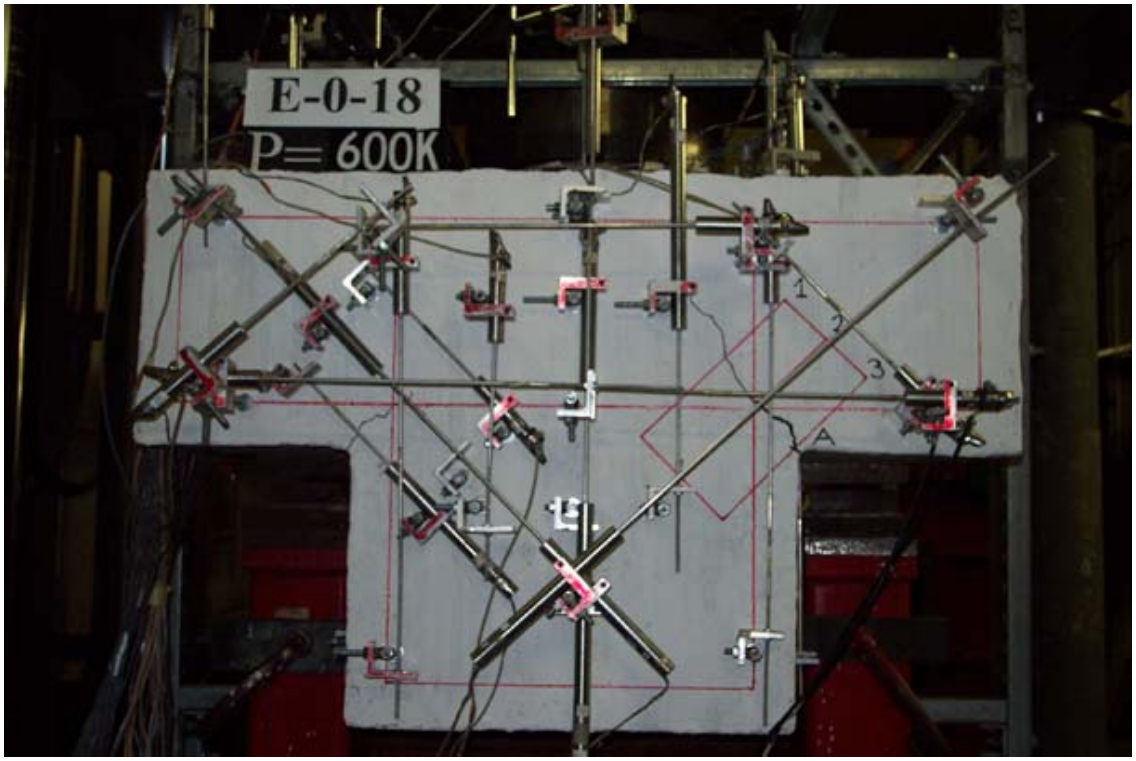

Fig. 3.2.1(c) Diagonal cracks in Specimen E-0-18

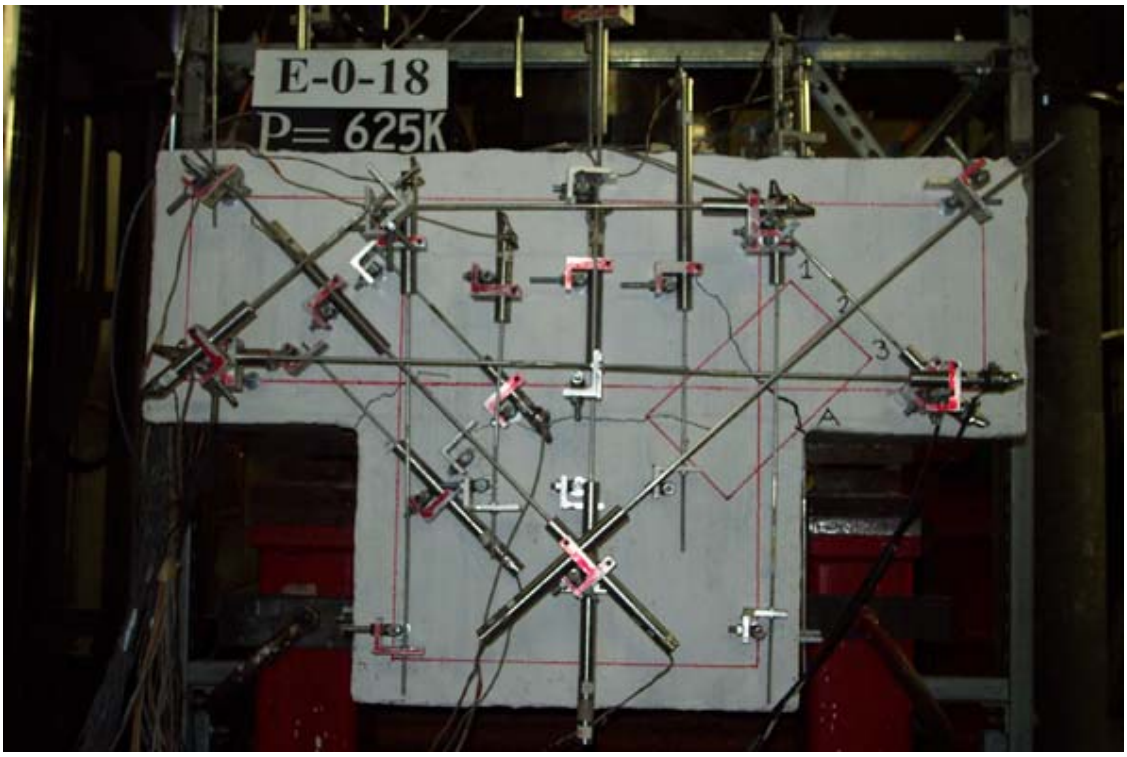

Fig. 3.2.1(d) Diagonal and horizontal cracks in Specimen E-0-18

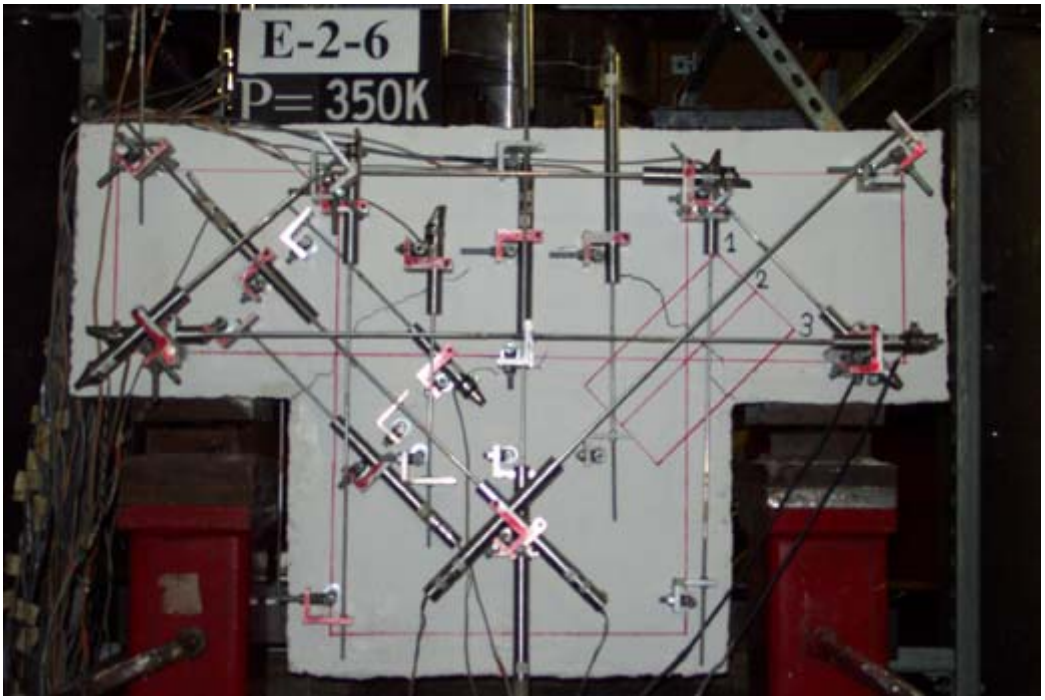

Fig. 3.2.2(a) Diagonal cracks in Specimen E-2-6

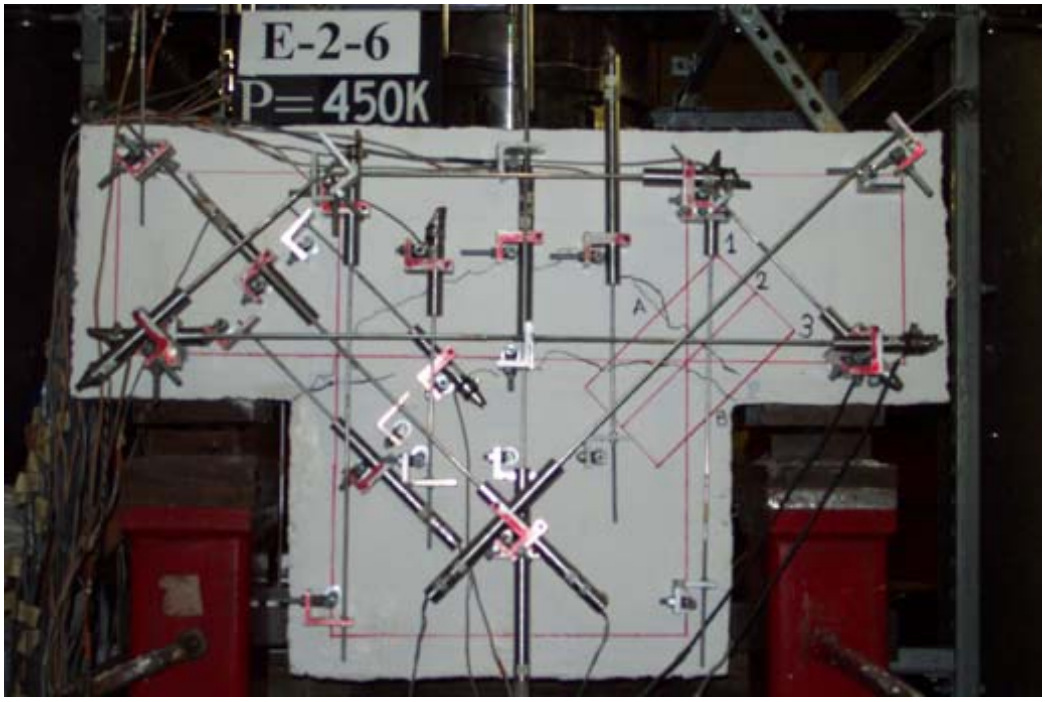

Fig. 3.2.2(b) Diagonal and horizontal cracks in Specimen E-2-6

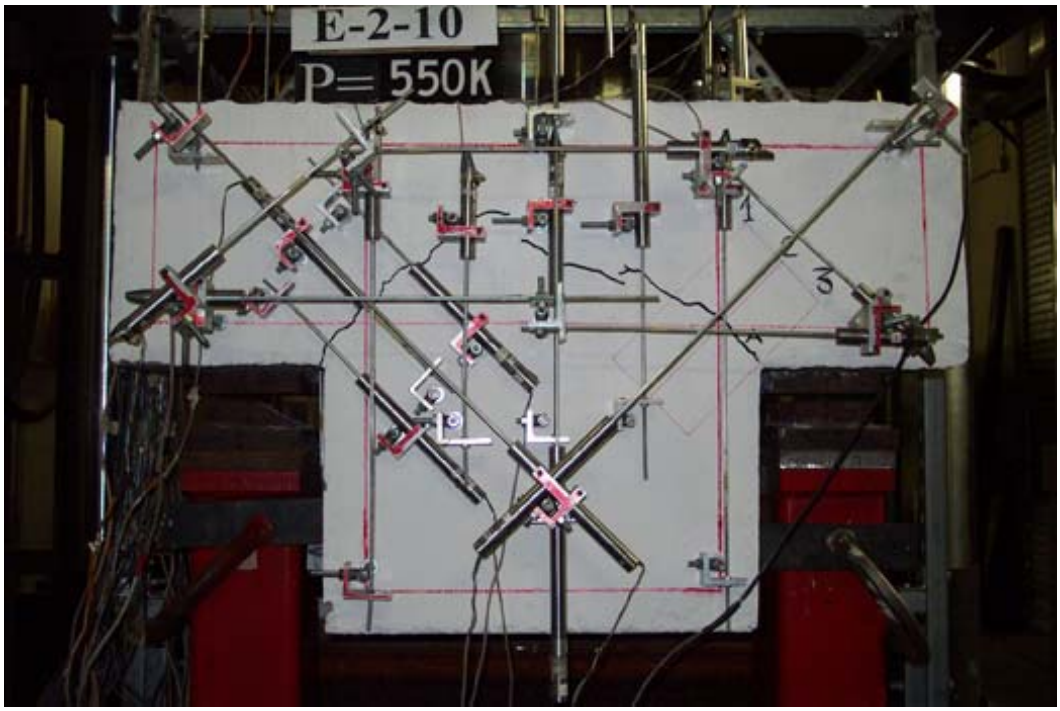

Fig. 3.2.2(c) Diagonal cracks in Specimen E-2-10

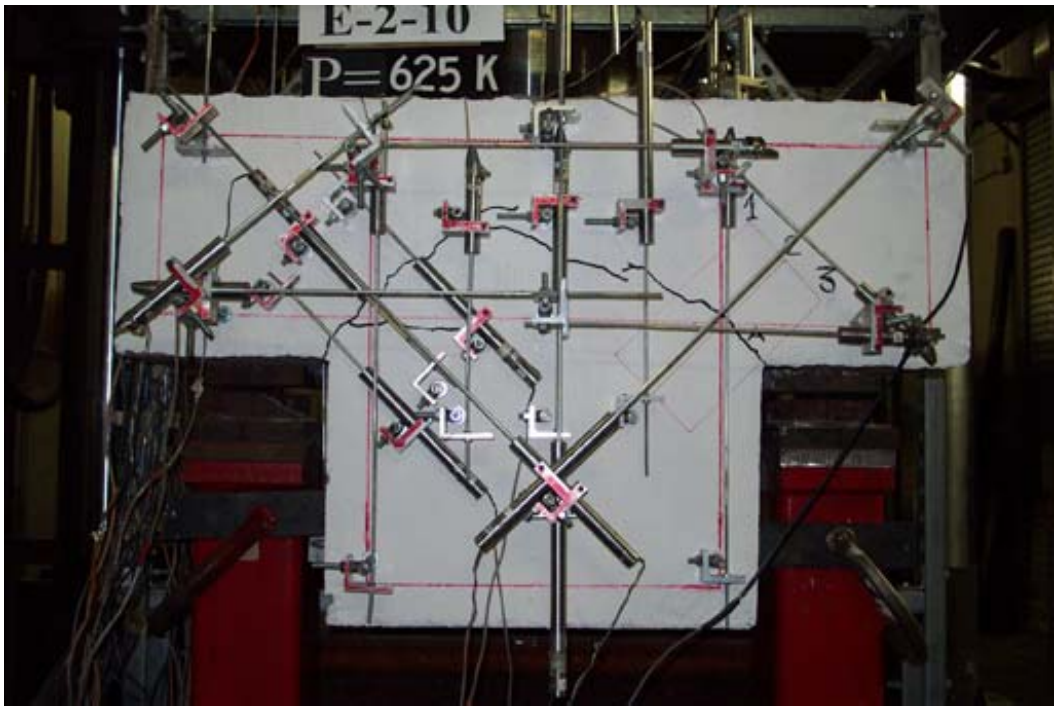

Fig. 3.2.2(d) Diagonal and horizontal cracks in Specimen E-2-10

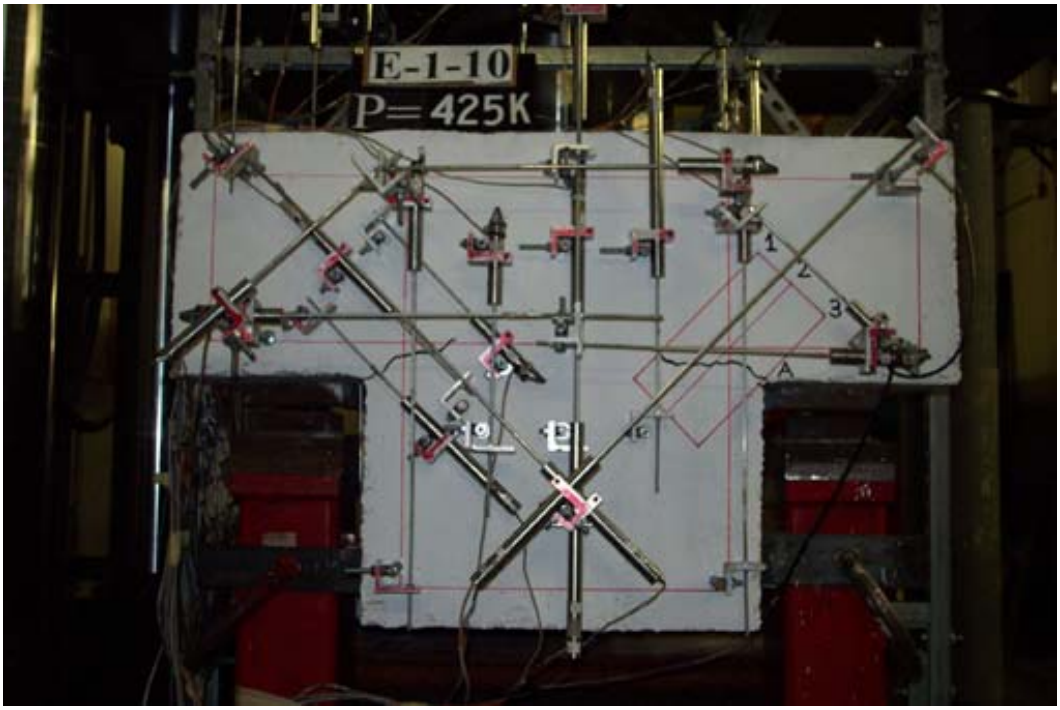

Fig. 3.2.2(e) Horizontal cracks in Specimen E-1-10

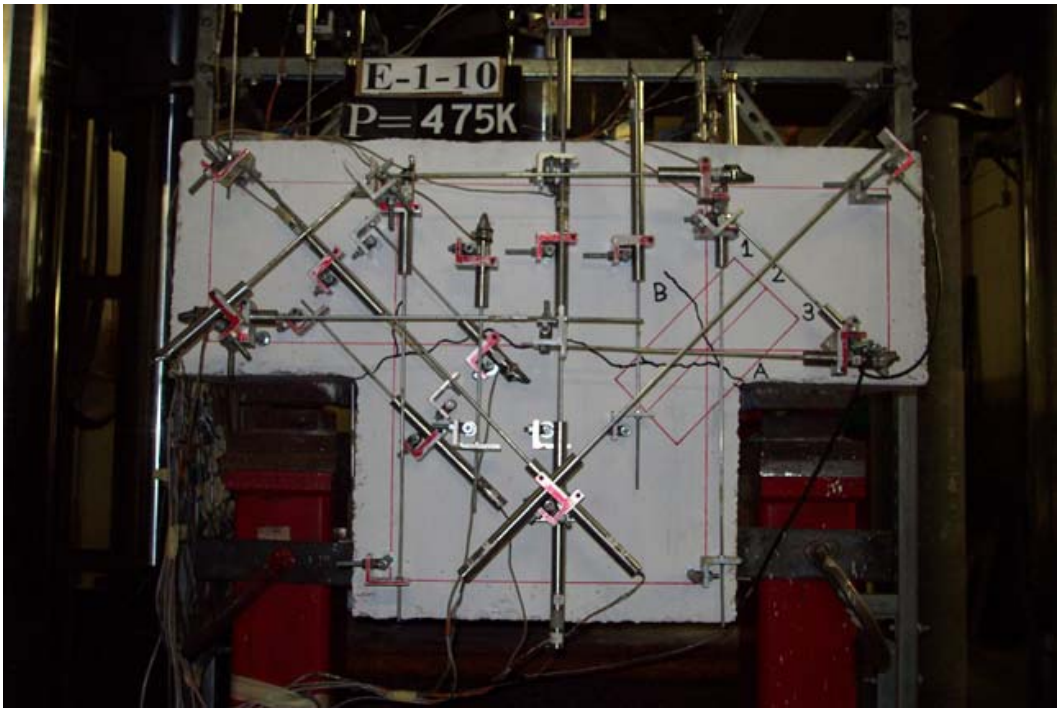

Fig. 3.2.2(f) Horizontal and diagonal cracks in Specimen E-1-10

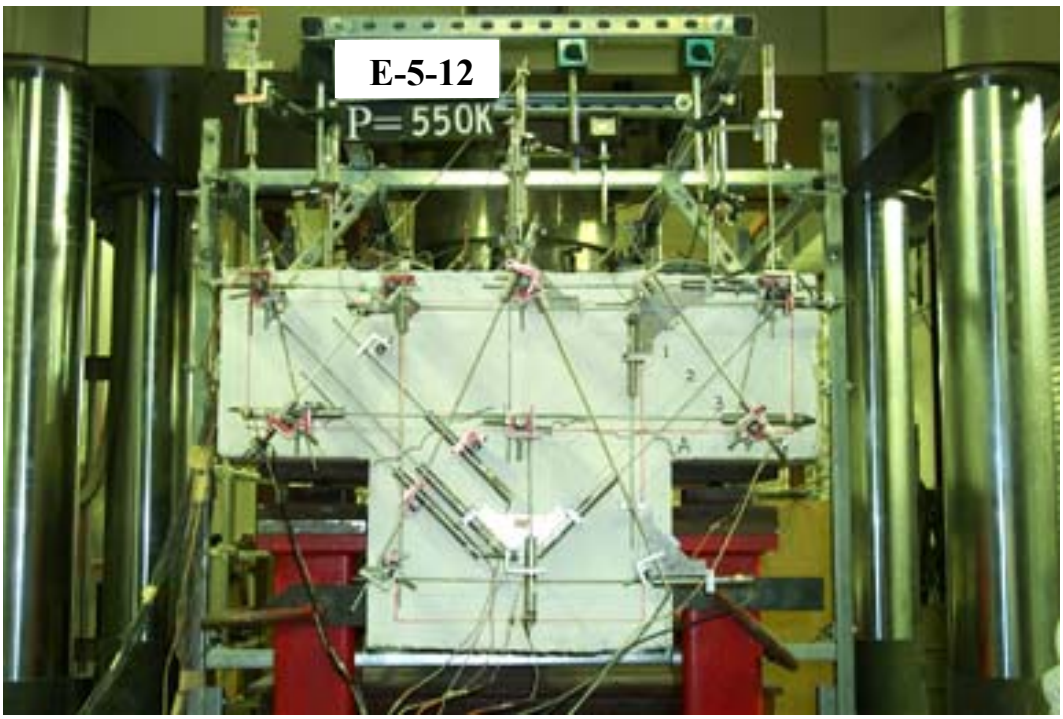

Fig. 3.2.2(g) Horizontal cracks in Specimen E-5-12

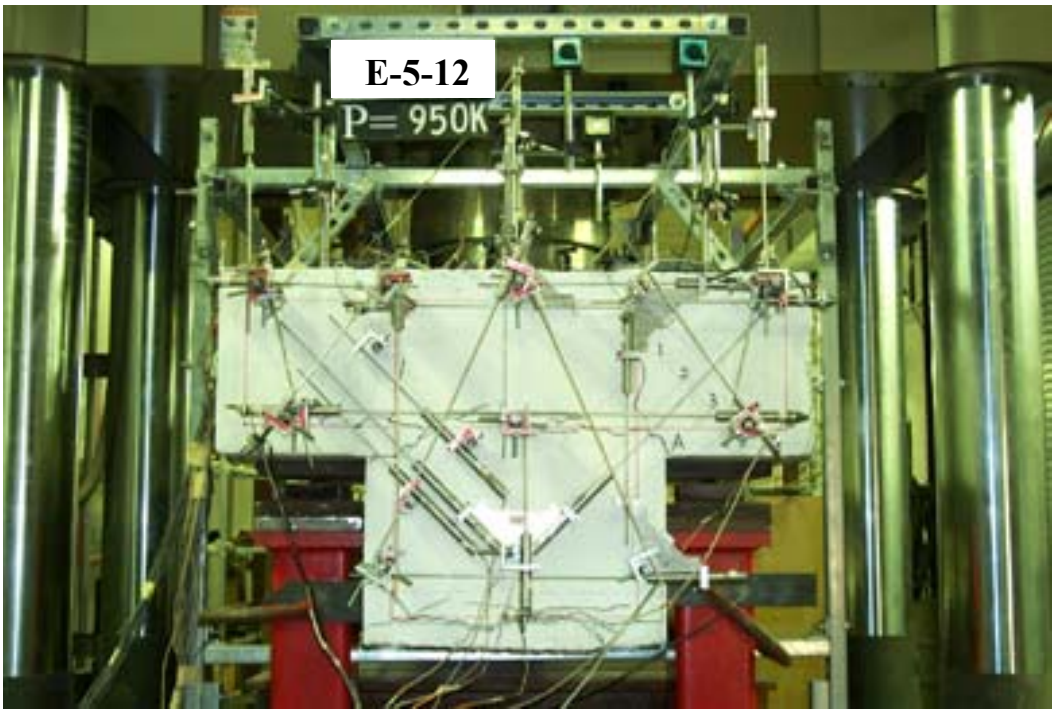

Fig. 3.2.2(h) Horizontal and diagonal cracks in Specimen E-5-12

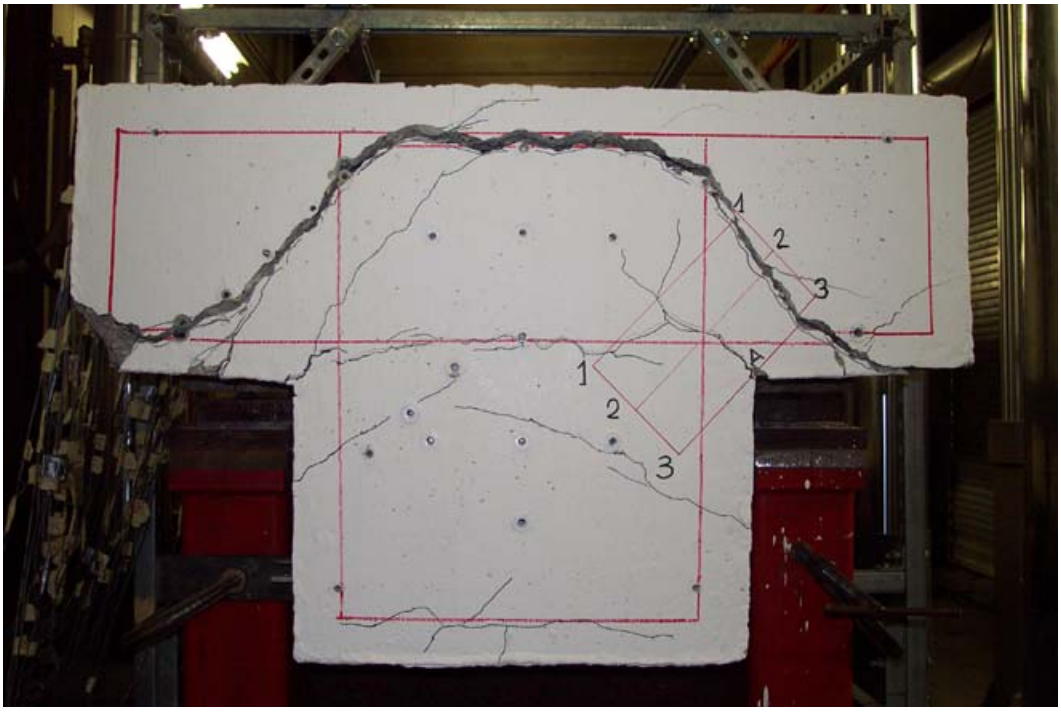

Fig. 3.3(a) Punching shear failure in Specimen E-0-14

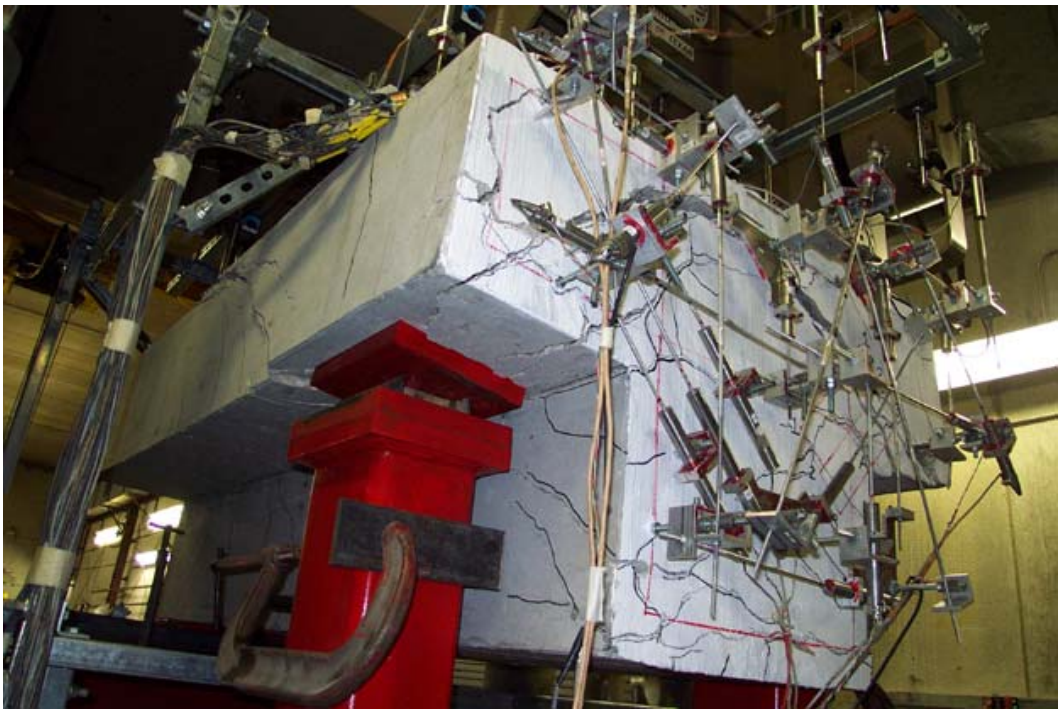

Fig. 3.3(b) Punching shear failure in Specimen E-0-12

Fig. 3.3(c) Web shear failure in Specimen E-2-6

Fig. 3.3(d) Web shear failure in Specimen E-2-10

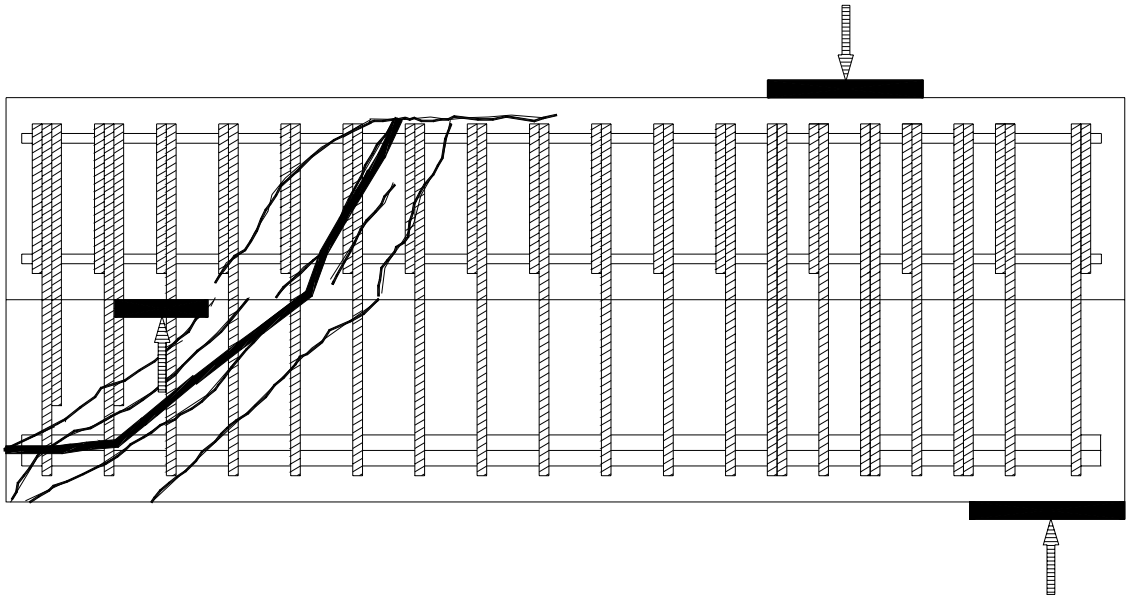

Fig. 3.3(e) Failure surface of specimen E-2-10 from a side view
(Notice how the surface avoids intersecting the diagonal bars)

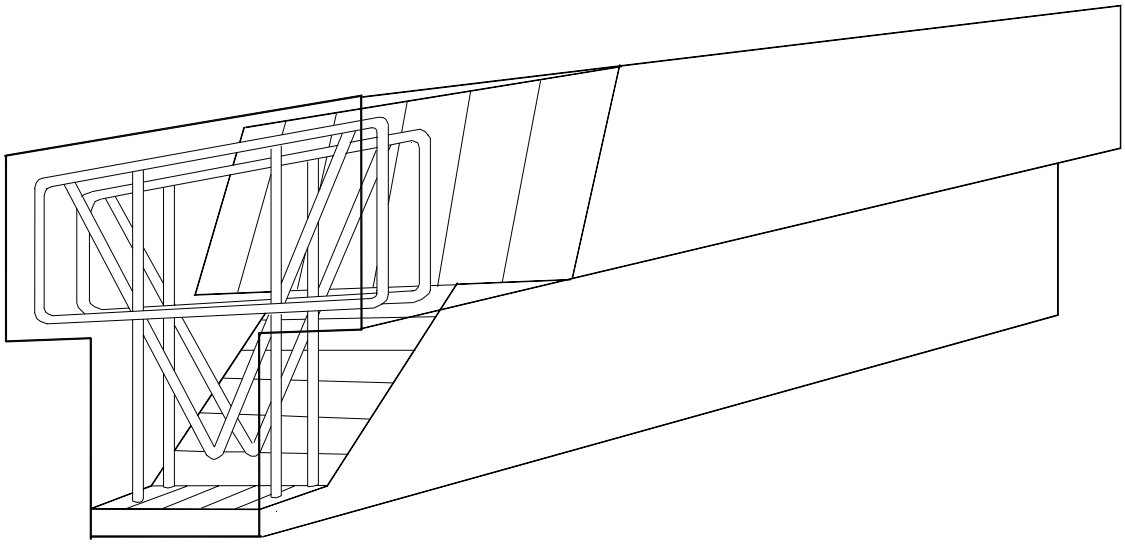

Fig. 3.3(f) Failure surface of Specimen E-2-10 in perspective

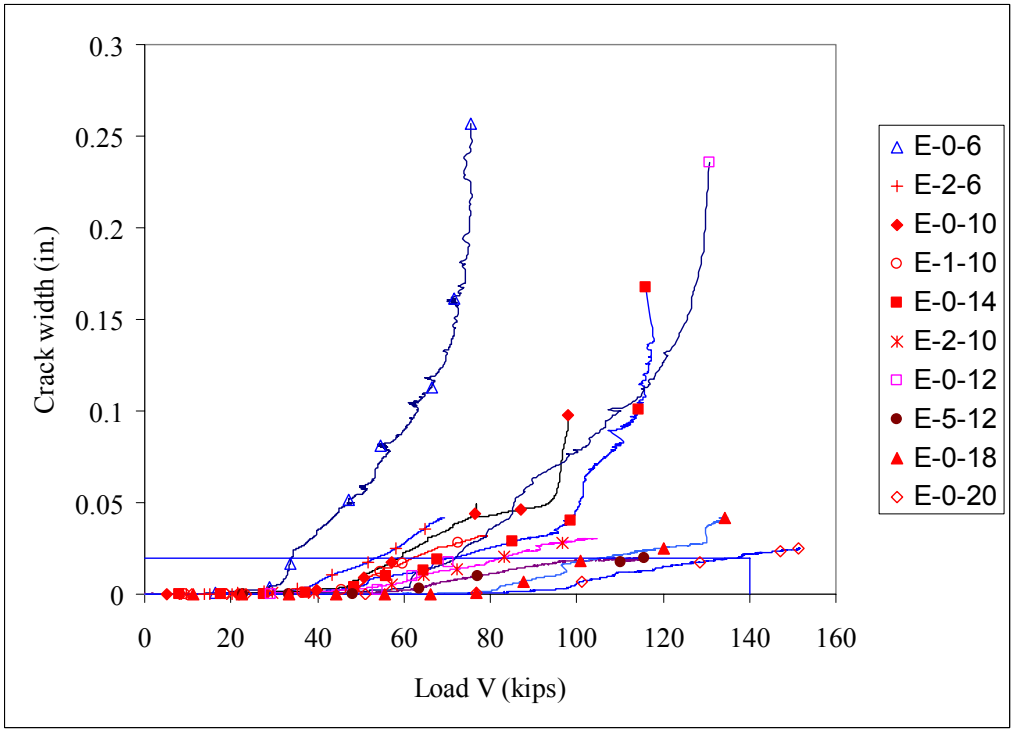

(1) Full range

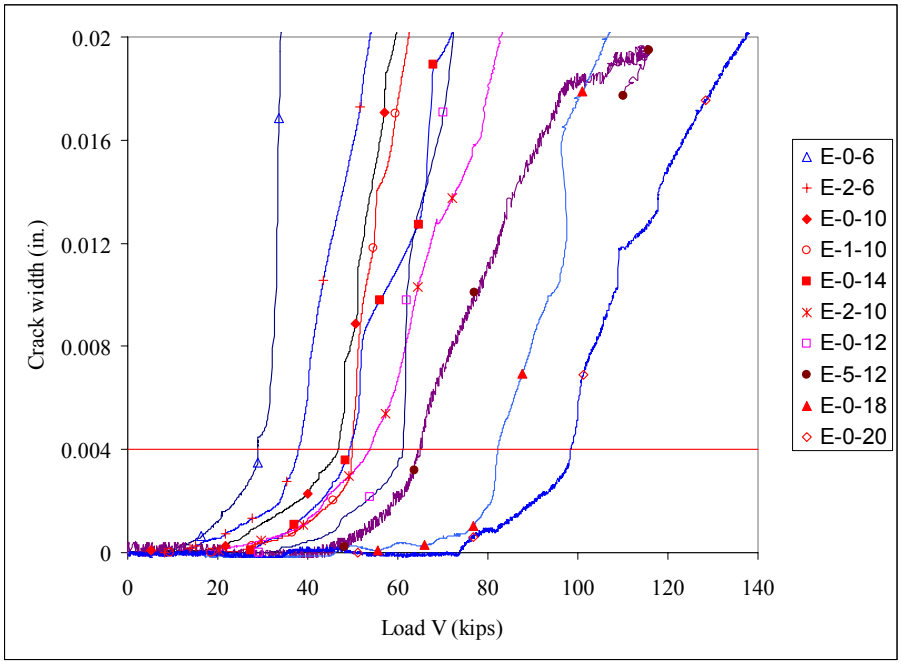

(2) Expanded view

Fig. 3.4(a) Crack width vs. load V curve

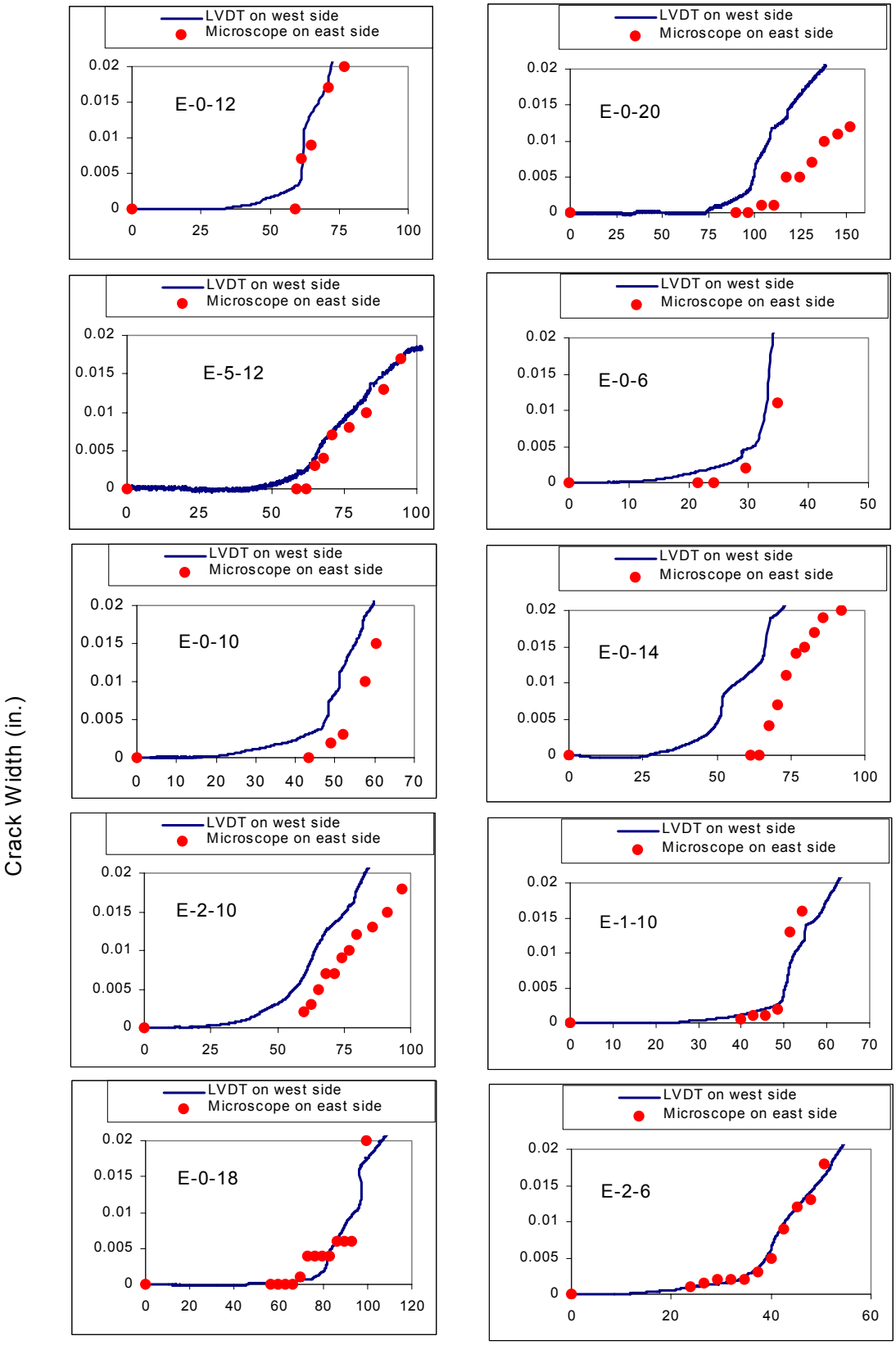

Fig. 3.4 (b) Crack widths measured by LVDT and microscope

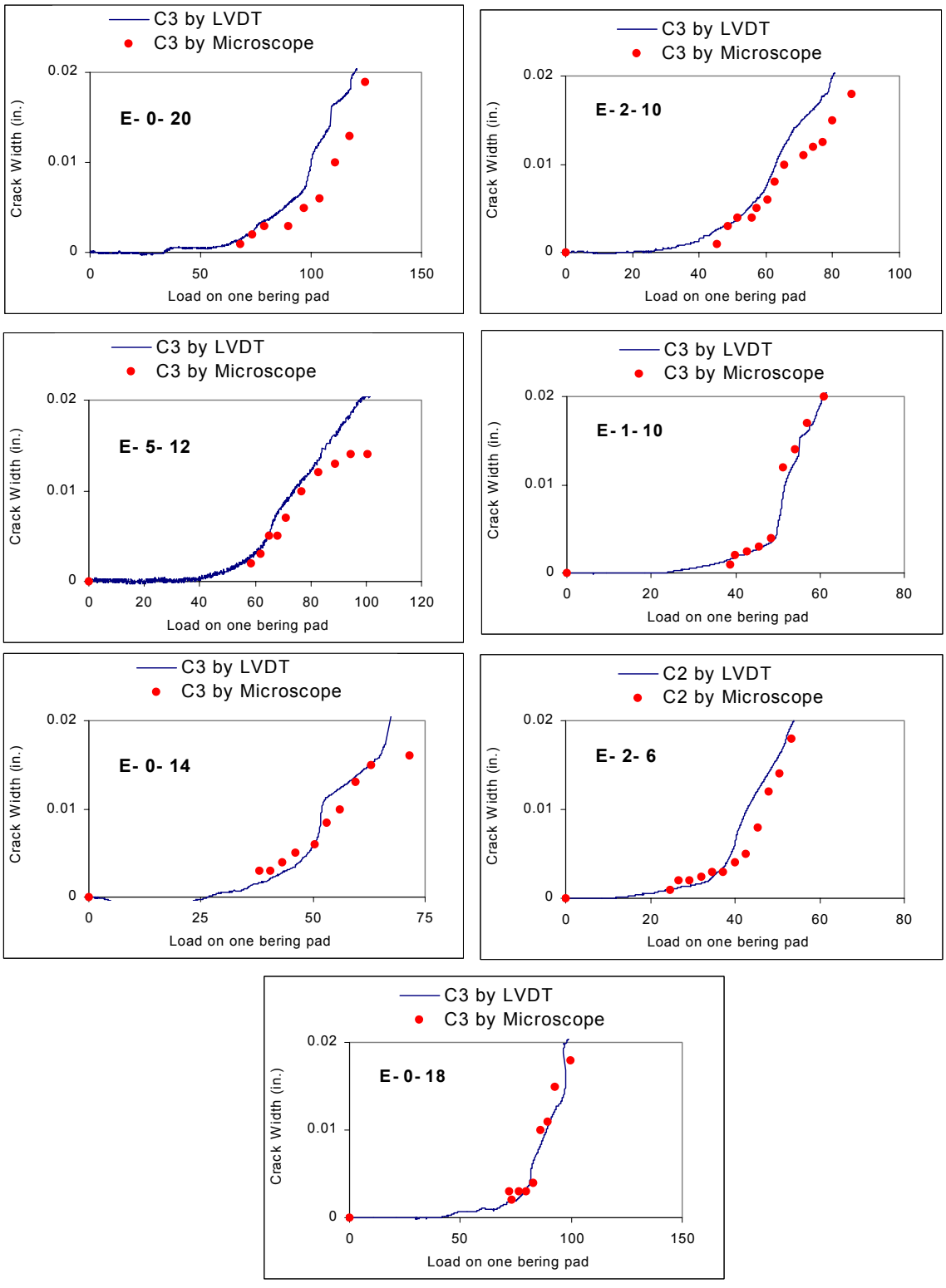

Fig. 3.4 (c) Comparison of crack width measured by LVDT and microscope on the same side

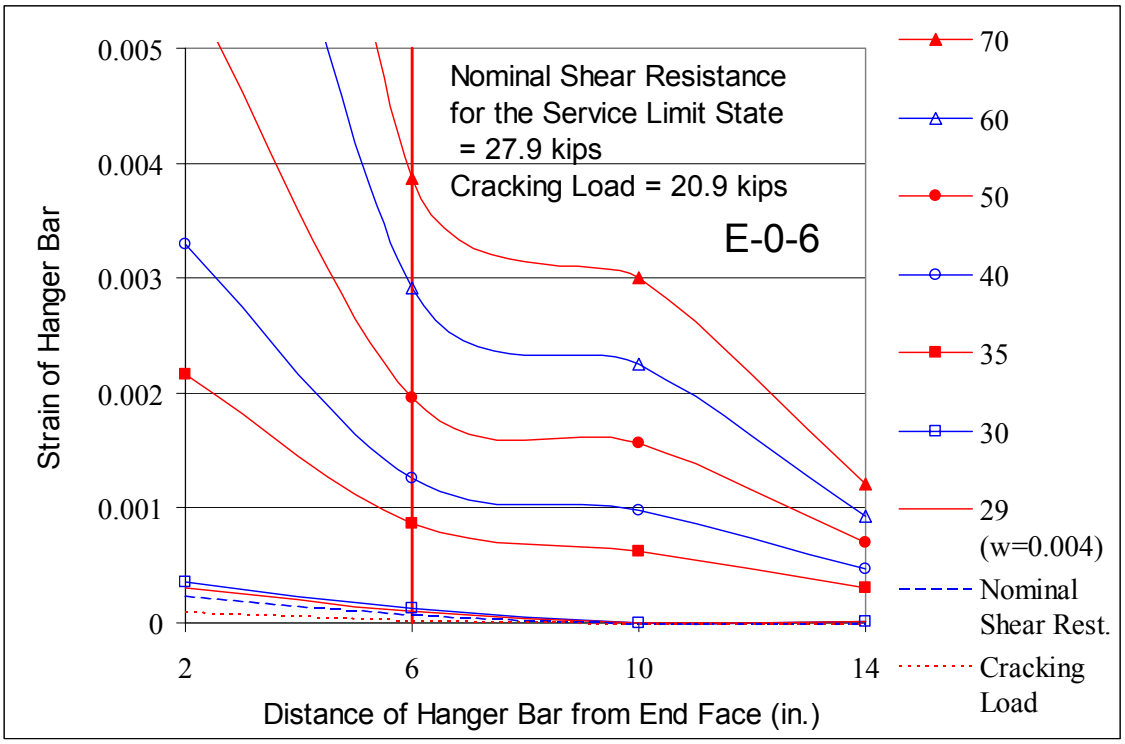

Fig. 3.5 (a) Strain distribution on hanger bars of E-0-6

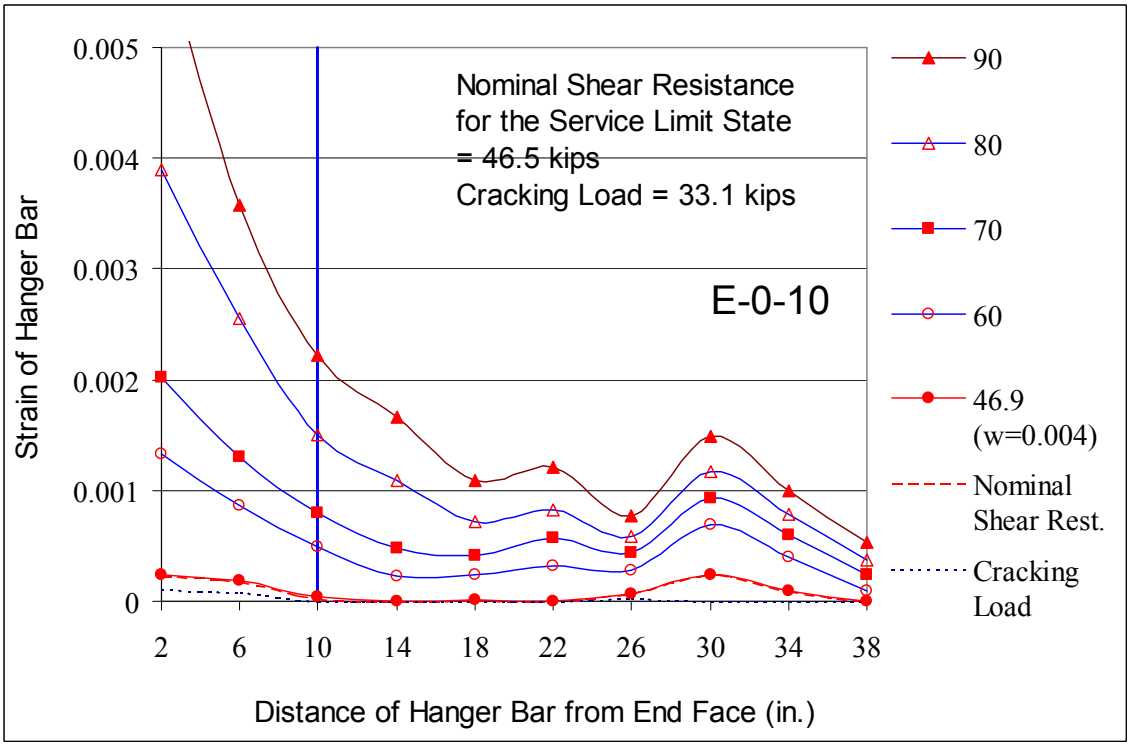

Fig. 3.5 (b) Strain distribution on hanger bars of E-0-10

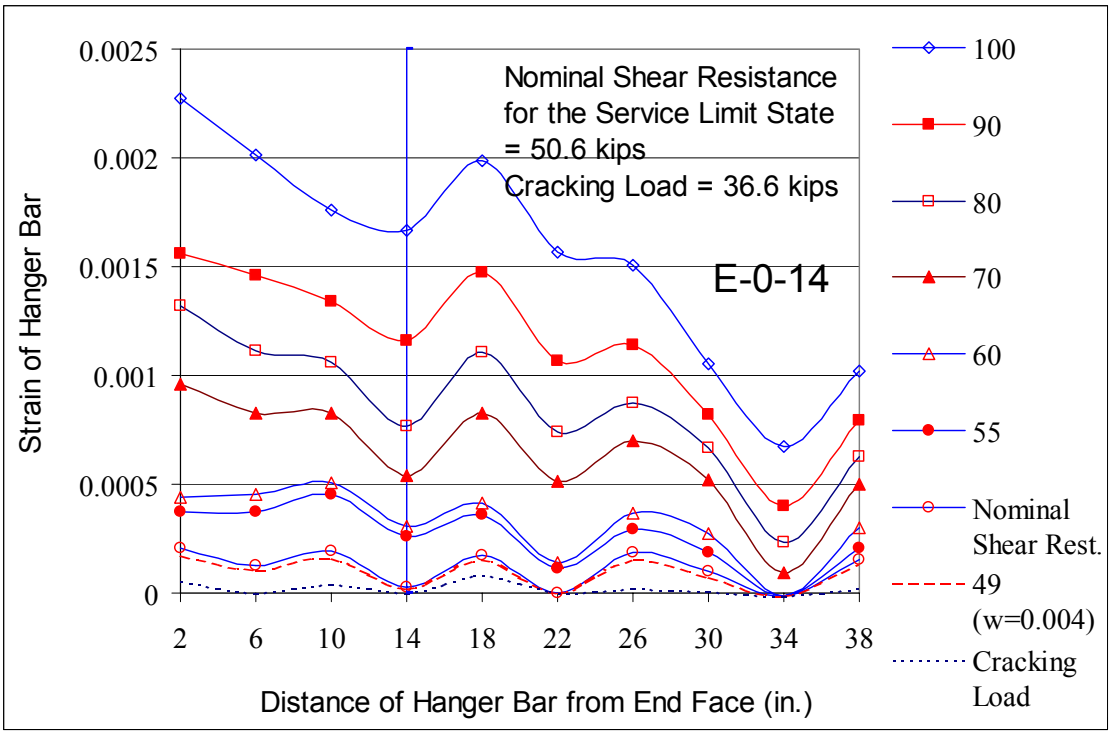

Fig. 3.5 (c) Strain distribution on hanger bars of E-0-14

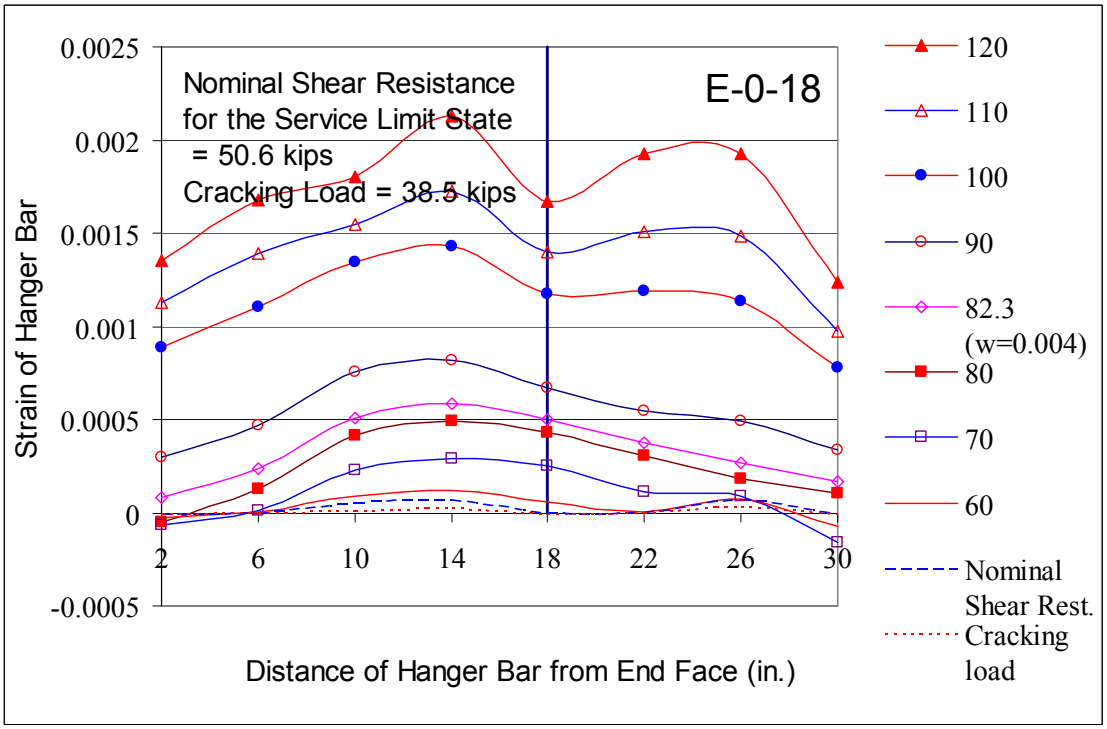

Fig. 3.5 (d) Strain distribution on hanger bars of E-0-18

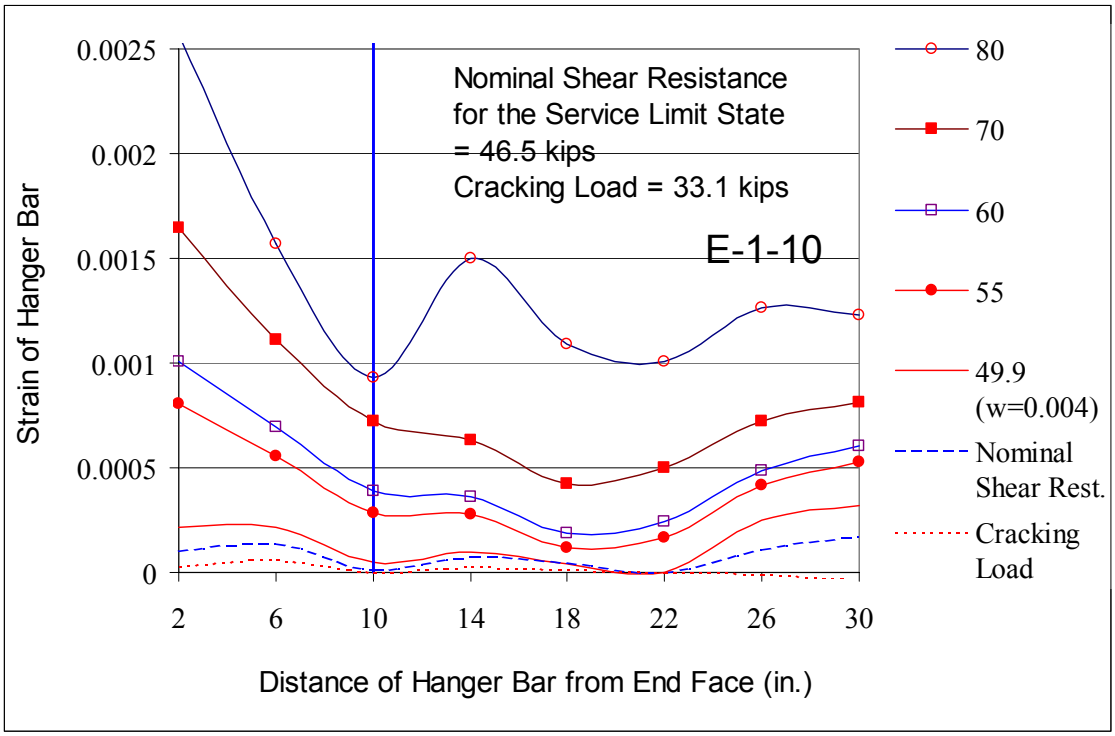

Fig. 3.5 (e) Strain distribution on hanger bars of E-1-10

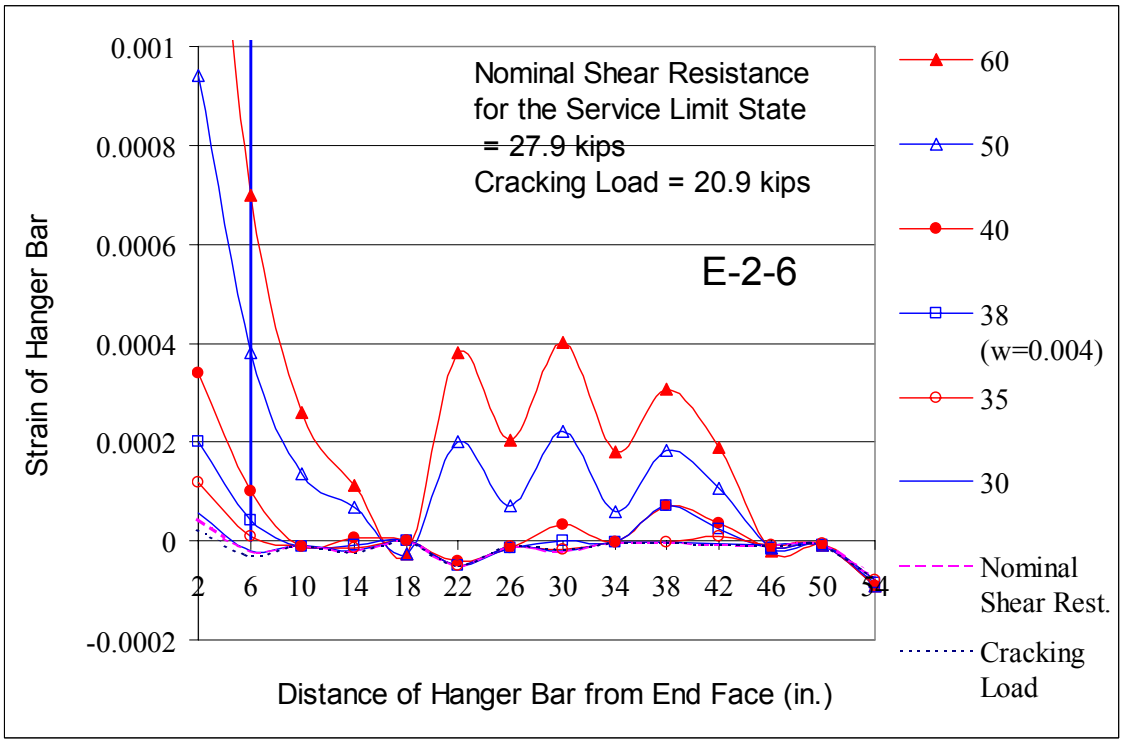

Fig. 3.5 (f) Strain distribution on hanger bars of E-2-6

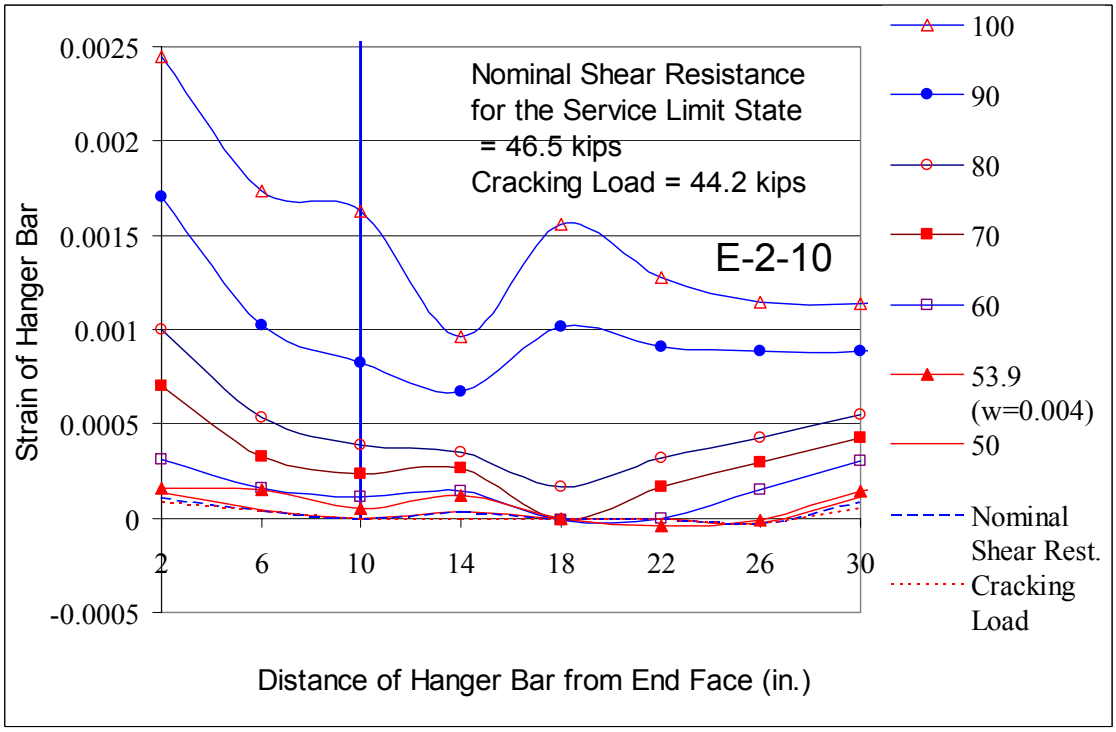

Fig. 3.5 (g) Strain distribution on hanger bars of E-2-10

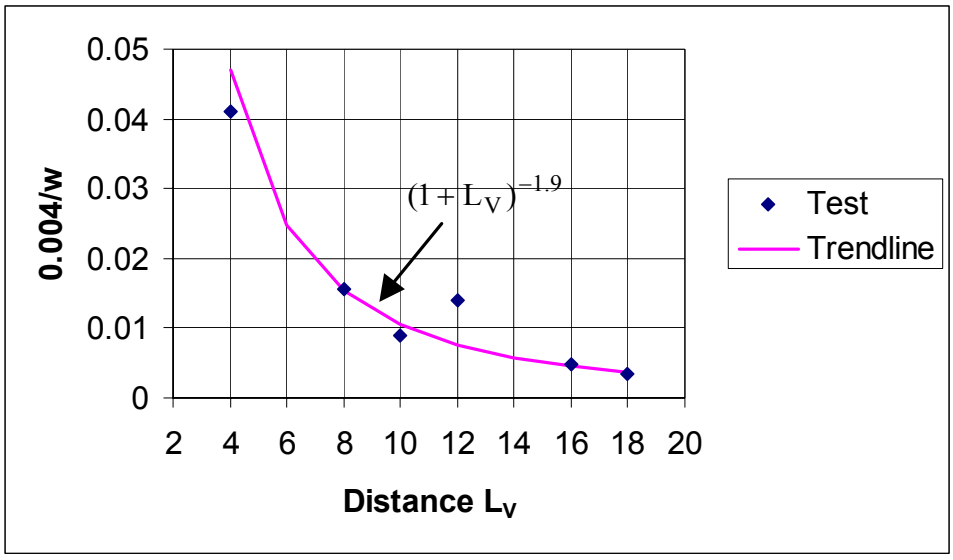

Fig. 4.2(a) Calibration curve

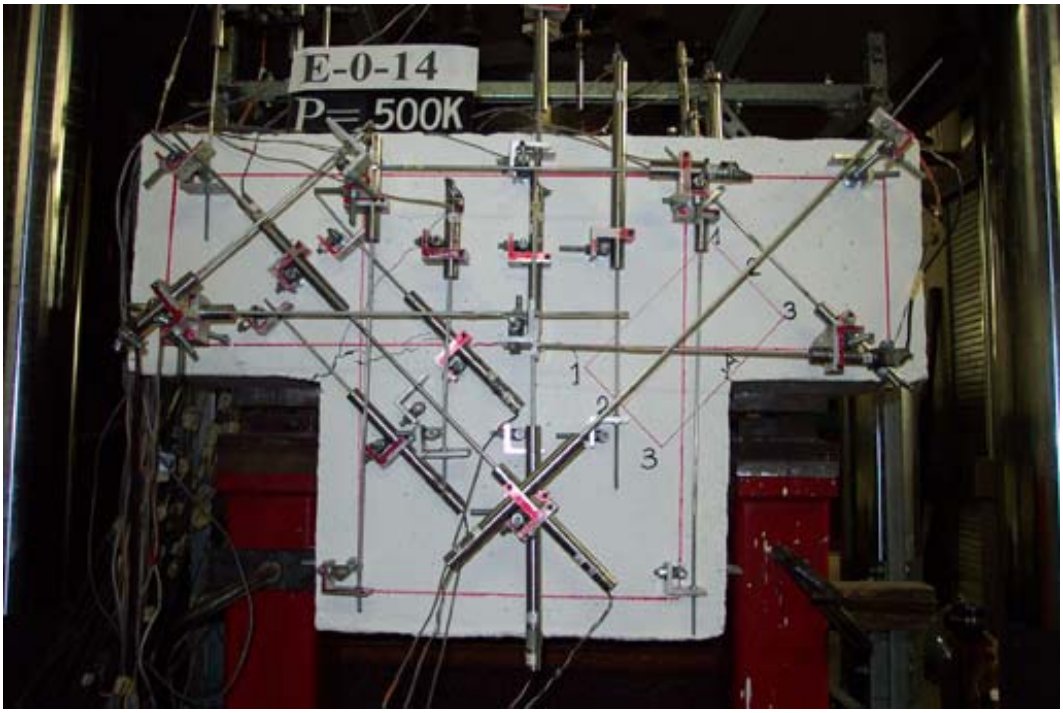

Fig. 4.2(b) Unsymmetrical crack

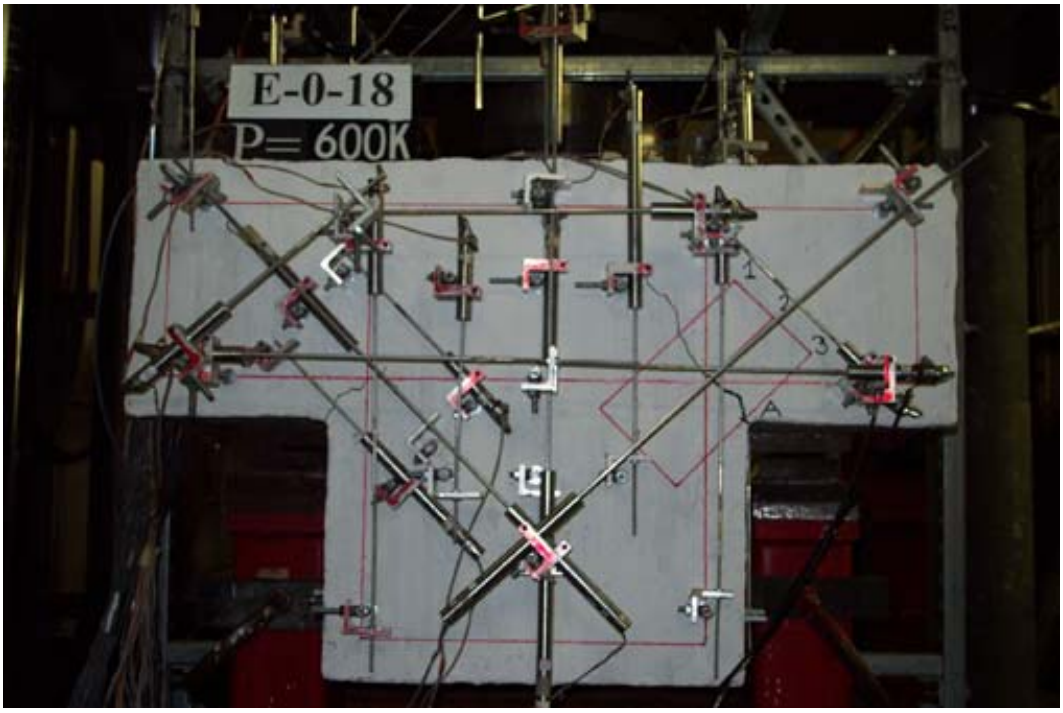

Fig. 4.2(c) Crack pattern of E-0-18 when w is less than 0.004 inch

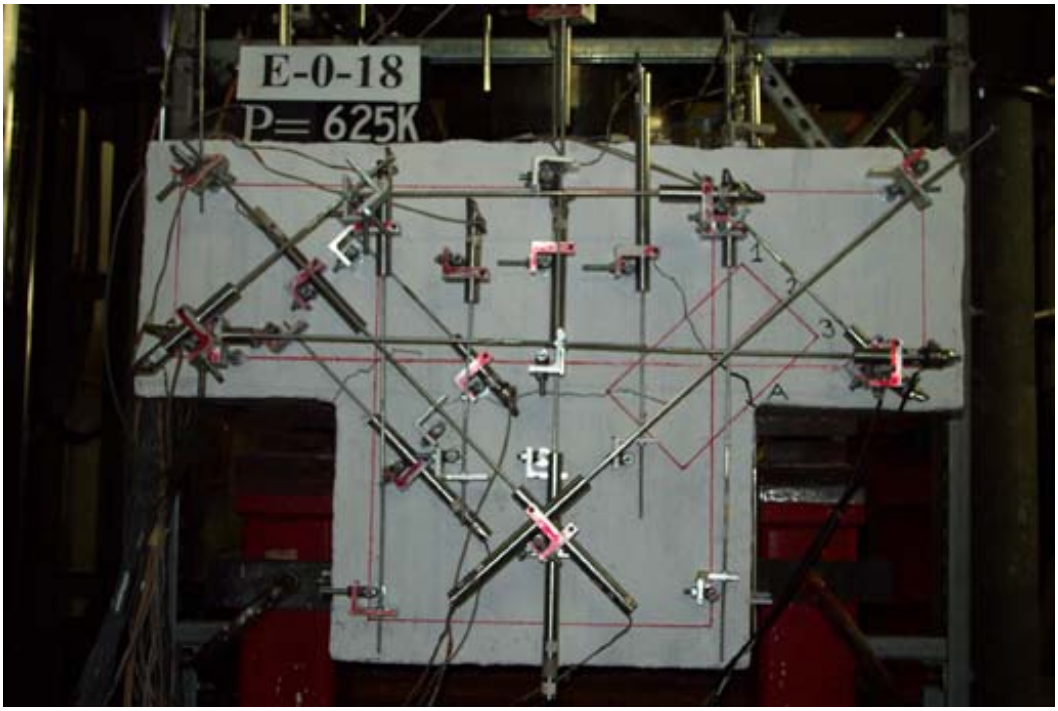

Fig. 4.2(d) Crack pattern of E-0-18 when w is larger than 0.004 inch

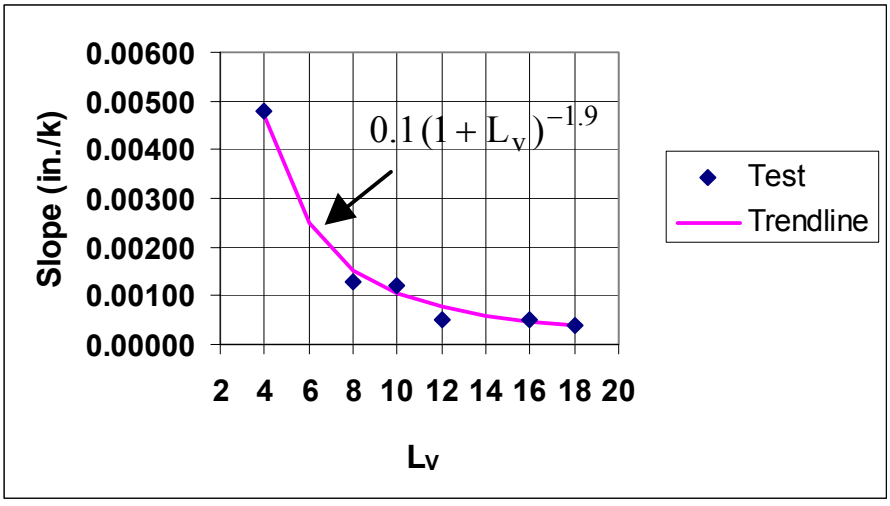

Fig. 4.2(e) Slope calibration for L_V

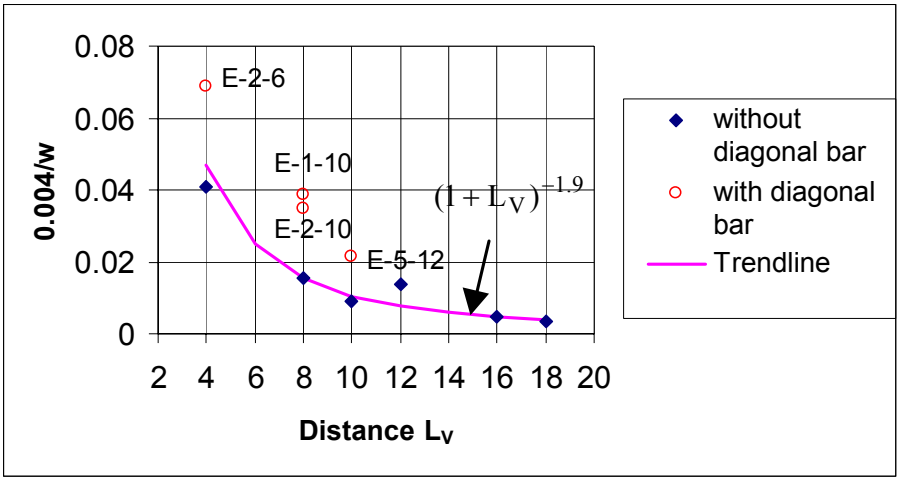

Fig. 4.3(a) Trend curve without modification of distribution factor B

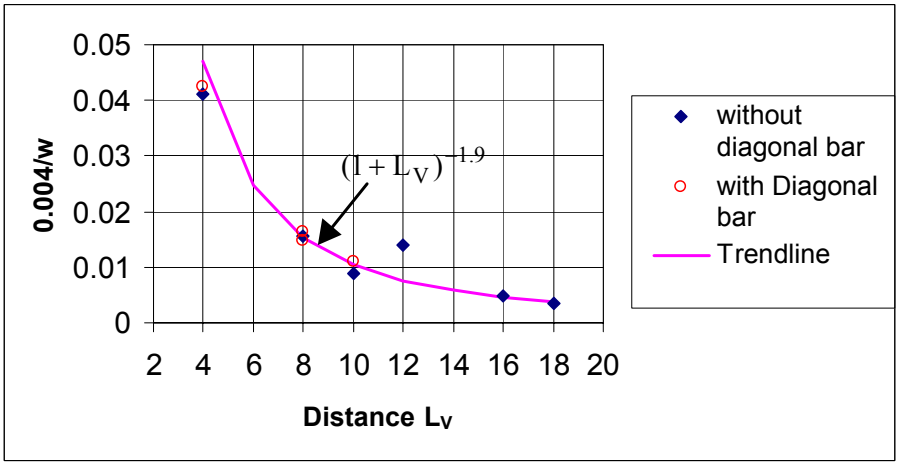

Fig. 4.3(b) Trend curve with modification of distribution factor B

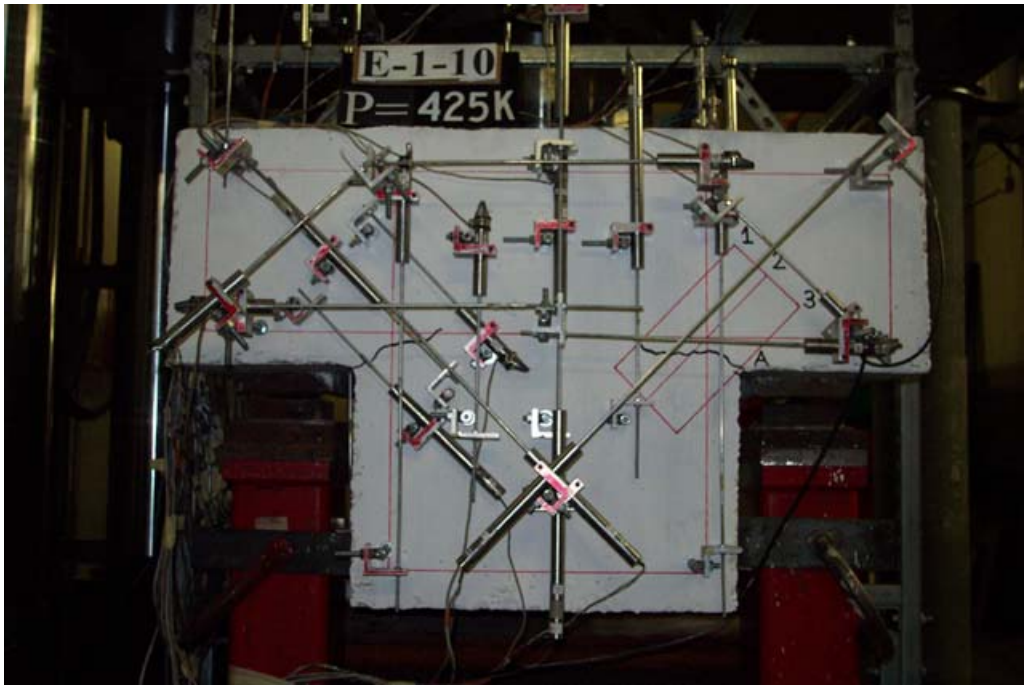

Fig. 4.3(c) Crack pattern when w is less than 0.004 inch

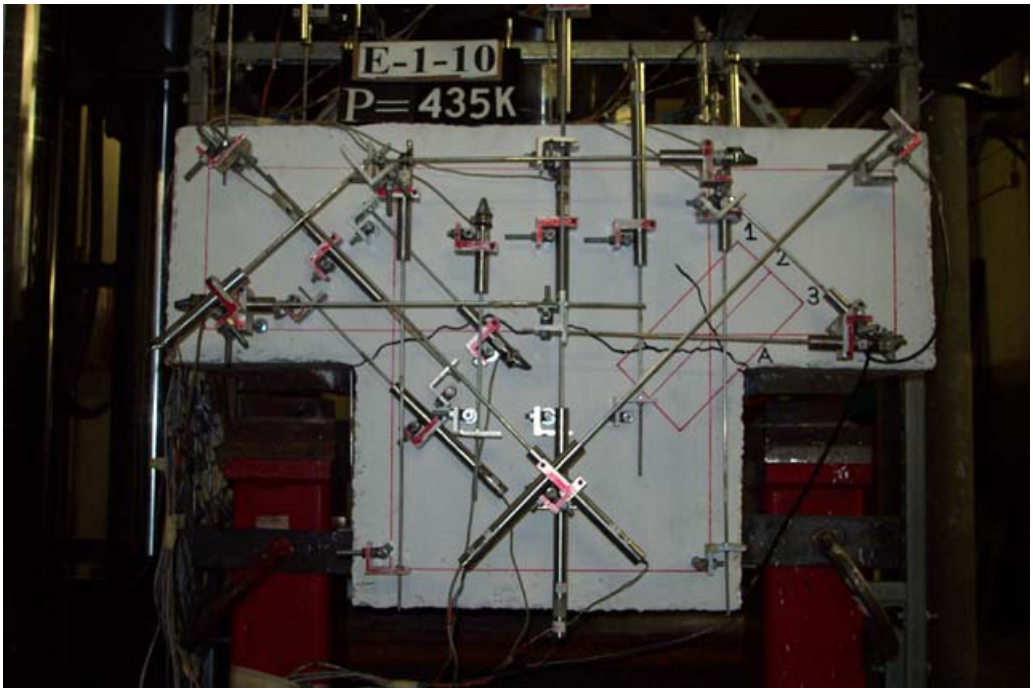

Fig. 4.3(d) Crack pattern when w is larger than 0.004 inch

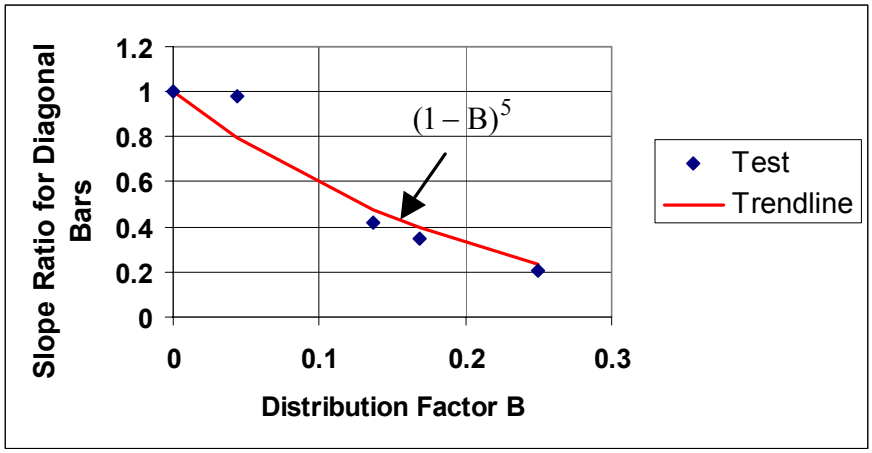

Fig. 4.3(e) Slope calibration for B

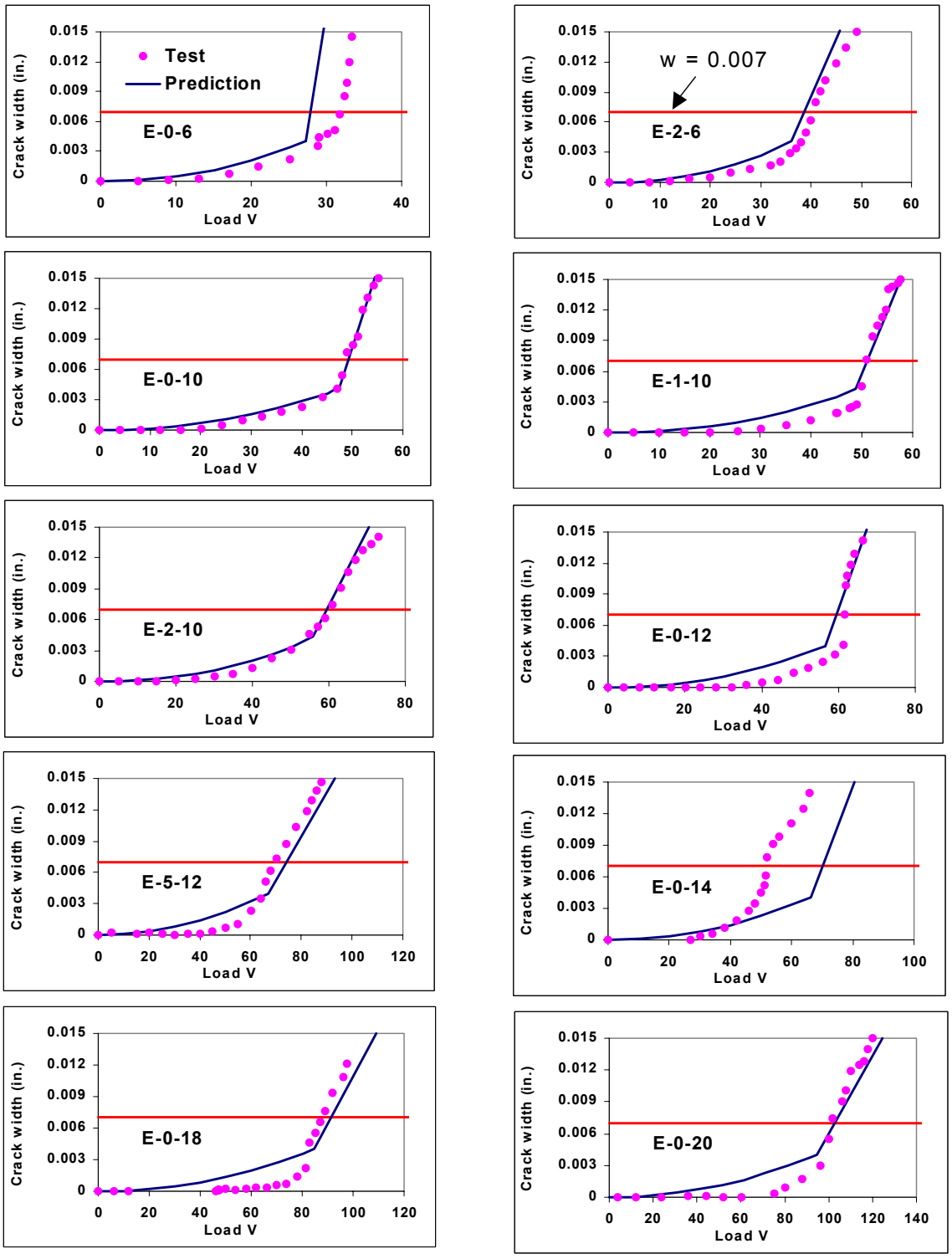

Fig. 4.4 Comparison of tests and predictions

APPENDICES

List of Figures

List of Tables

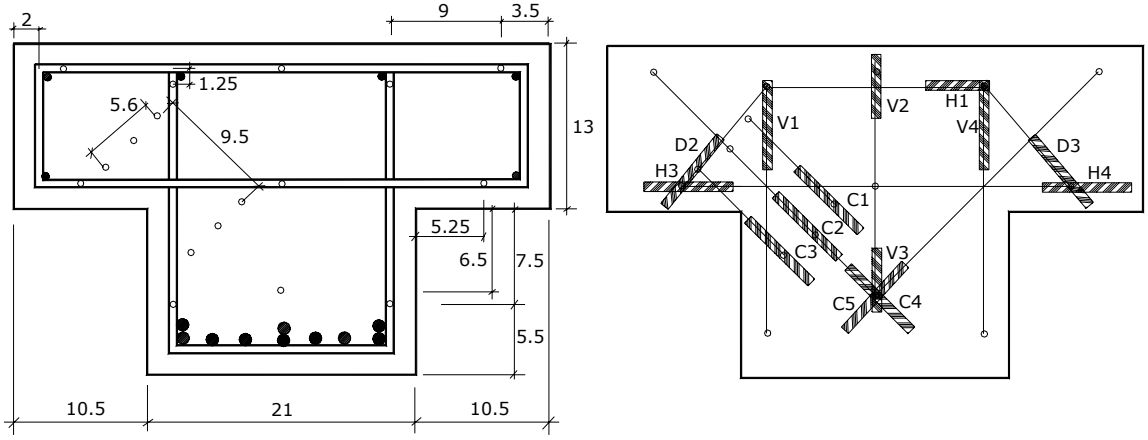

End view of LVDT arrangement

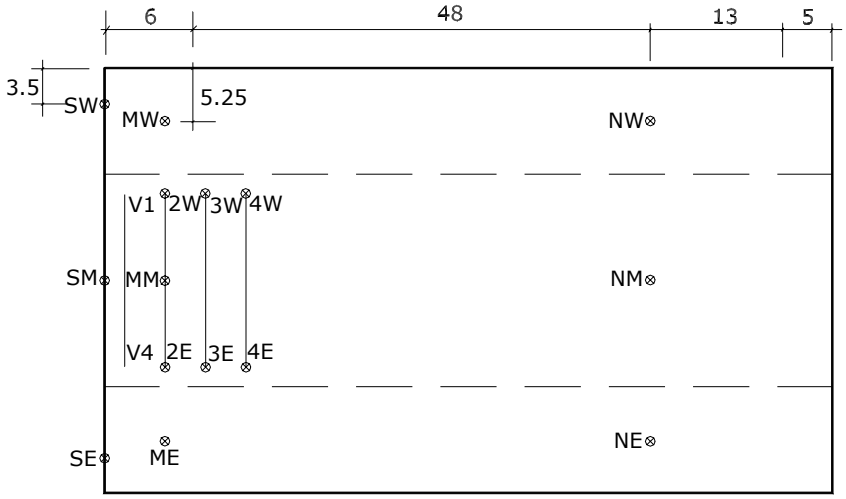

Top view of LVDT arrangement

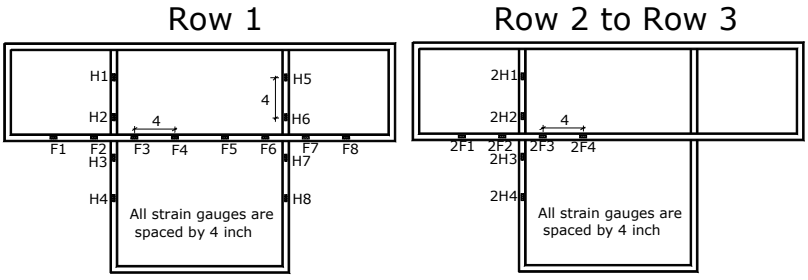

Strain Gauge arrangement

Fig. A1 LVDT and Strain Gauge Arrangement for Specimen E-0-6

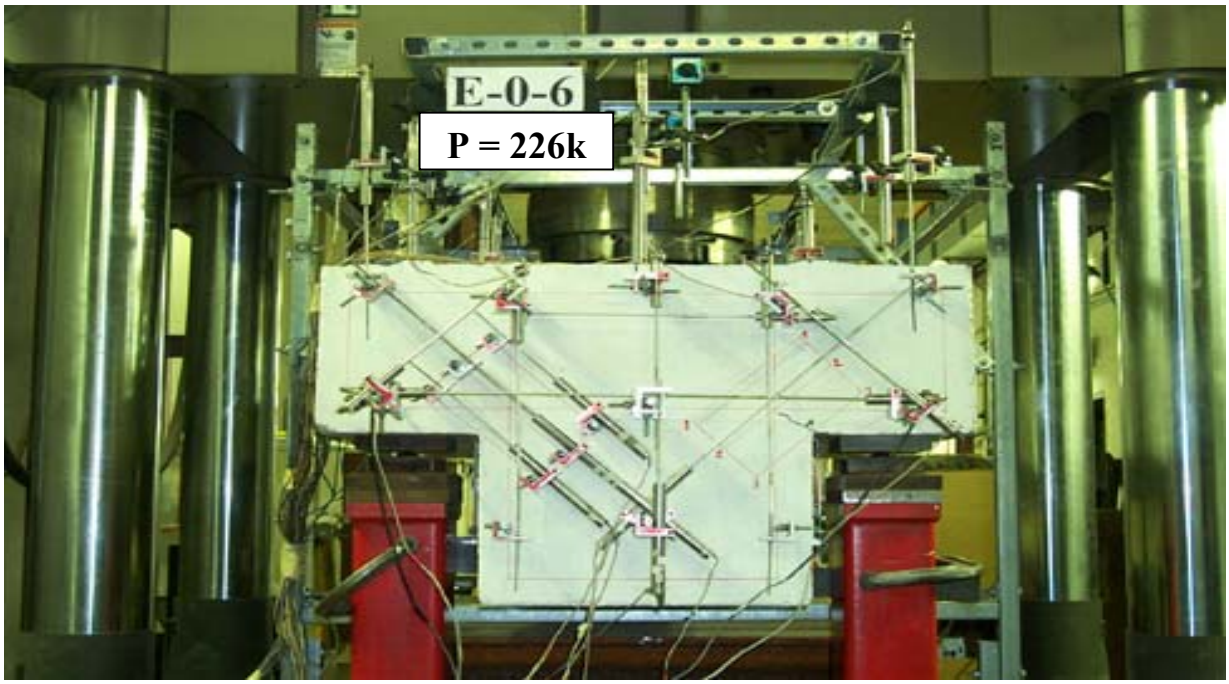

Fig. A2 Crack Pattern Before Nominal Shear Resistance for the Service Limit State (V_n = 262 K)

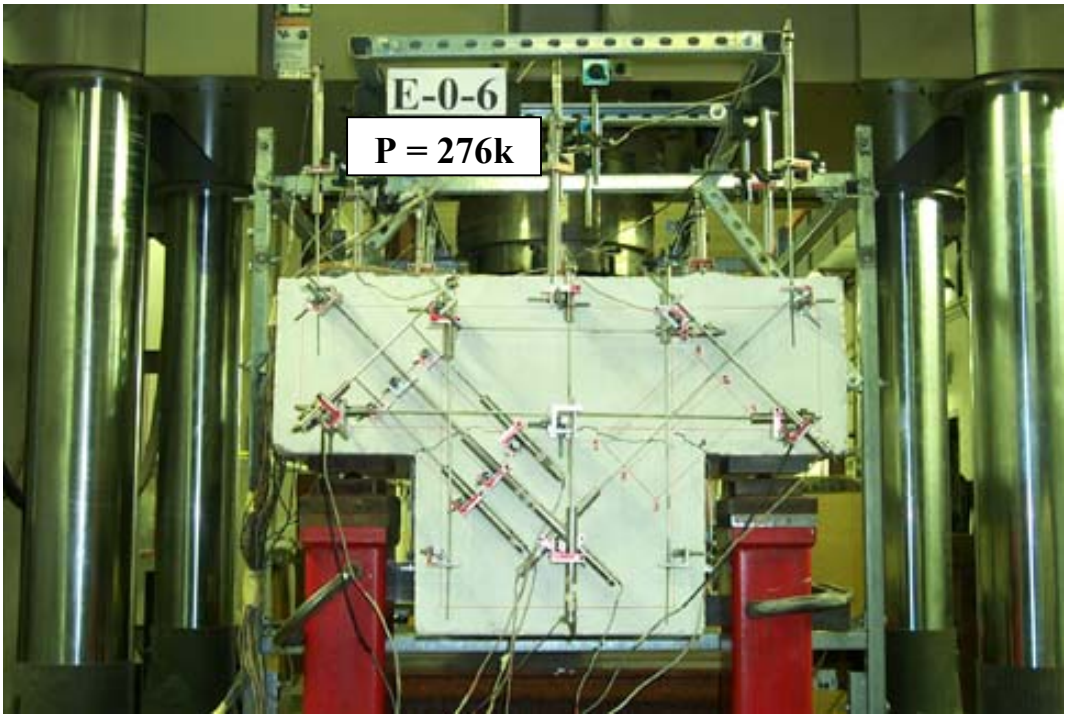

Fig. A3 Crack Pattern after Nominal Shear Resistance for the Service Limit State (V_n = 262 K)

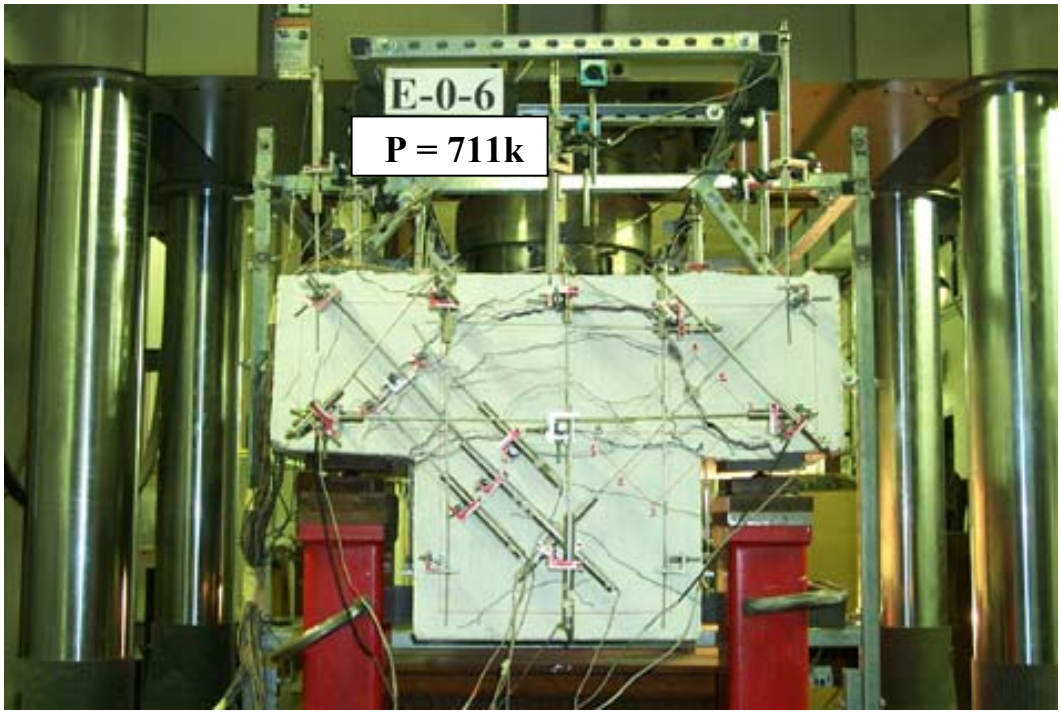

Fig. A4 Specimen at Failure

Table A1, Deflection of E-0-6 (inch)

V (k)	SW	SM	SE	MW	MM	ME	NW	NM	NE
3.5	0.0000	0.0034	-0.0001	0.0092	0.0084	0.0068	0.0265	0.0265	0.0254
6.0	0.0038	0.0096	0.0029	0.0186	0.0180	0.0203	0.0428	0.0420	0.0410
9.0	0.0142	0.0192	0.0124	0.0306	0.0298	0.0310	0.0566	0.0562	0.0548
12.1	0.0280	0.0289	0.0215	0.0424	0.0411	0.0407	0.0677	0.0676	0.0656
15.1	0.0367	0.0360	0.0286	0.0514	0.0501	0.0484	0.0776	0.0770	0.0746
18.1	0.0436	0.0424	0.0345	0.0590	0.0580	0.0554	0.0867	0.0858	0.0830
21.0	0.0495	0.0479	0.0397	0.0659	0.0648	0.0613	0.0948	0.0936	0.0904
24.1	0.0569	0.0541	0.0446	0.0733	0.0721	0.0675	0.1039	0.1024	0.0988
27.0	0.0598	0.0584	0.0493	0.0780	0.0779	0.0729	0.1120	0.1105	0.1065
30.1	0.0661	0.0661	0.0581	0.0840	0.0862	0.0789	0.1215	0.1205	0.1156
33.1	0.0662	0.0686	0.0581	0.0873	0.0922	0.0830	0.1323	0.1316	0.1257
36.1	0.0662	0.0731	0.0581	0.0916	0.1004	0.0882	0.1430	0.1419	0.1374
39.1	0.0662	0.0761	0.0587	0.0953	0.1059	0.0922	0.1524	0.1515	0.1469
42.1	0.0665	0.0809	0.0615	0.0994	0.1131	0.0973	0.1618	0.1611	0.1561
45.1	0.0684	0.0865	0.0627	0.1044	0.1206	0.1020	0.1731	0.1717	0.1666
48.1	0.0683	0.0885	0.0628	0.1071	0.1259	0.1051	0.1820	0.1803	0.1757
51.1	0.0683	0.0924	0.0635	0.1082	0.1312	0.1080	0.1892	0.1884	0.1828
54.1	0.0683	0.0960	0.0656	0.1128	0.1395	0.1129	0.1982	0.1966	0.1911
57.2	0.0684	0.1055	0.0659	0.1184	0.1511	0.1156	0.2151	0.2087	0.2028
60.1	0.0683	0.1089	0.0656	0.1223	0.1581	0.1186	0.2242	0.2177	0.2116
63.5	0.0683	0.1166	0.0655	0.1278	0.1700	0.1235	0.2384	0.2318	0.2255
66.7	0.0684	0.1204	0.0655	0.1316	0.1774	0.1271	0.2489	0.2423	0.2357
69.1	0.0684	0.1235	0.0655	0.1347	0.1844	0.1302	0.2587	0.2520	0.2454
72.2	0.0684	0.1309	0.0652	0.1403	0.1941	0.1352	0.2739	0.2670	0.2601
75.8	0.0631	0.1481	0.0487	0.1460	0.2077	0.1396	0.2988	0.2910	0.2848

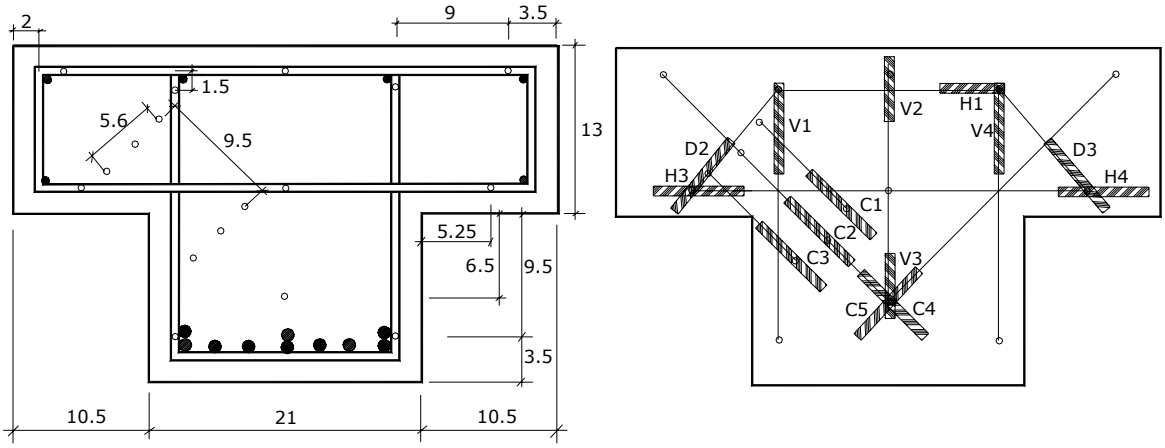

End view of LVDT arrangement

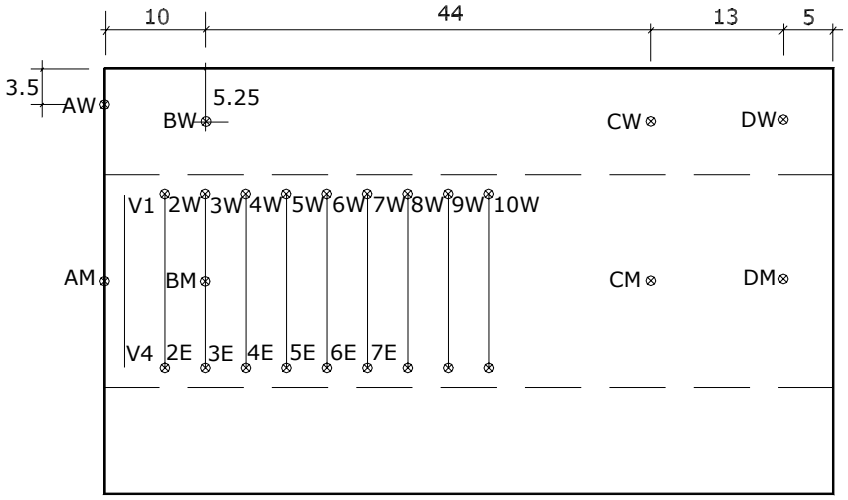

Top view of LVDT arrangement

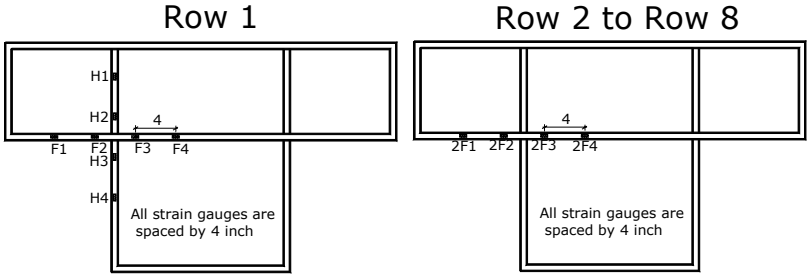

Strain Gauge arrangement

Fig. A5 LVDT and Strain Gauge Arrangement for Specimen E-0-10

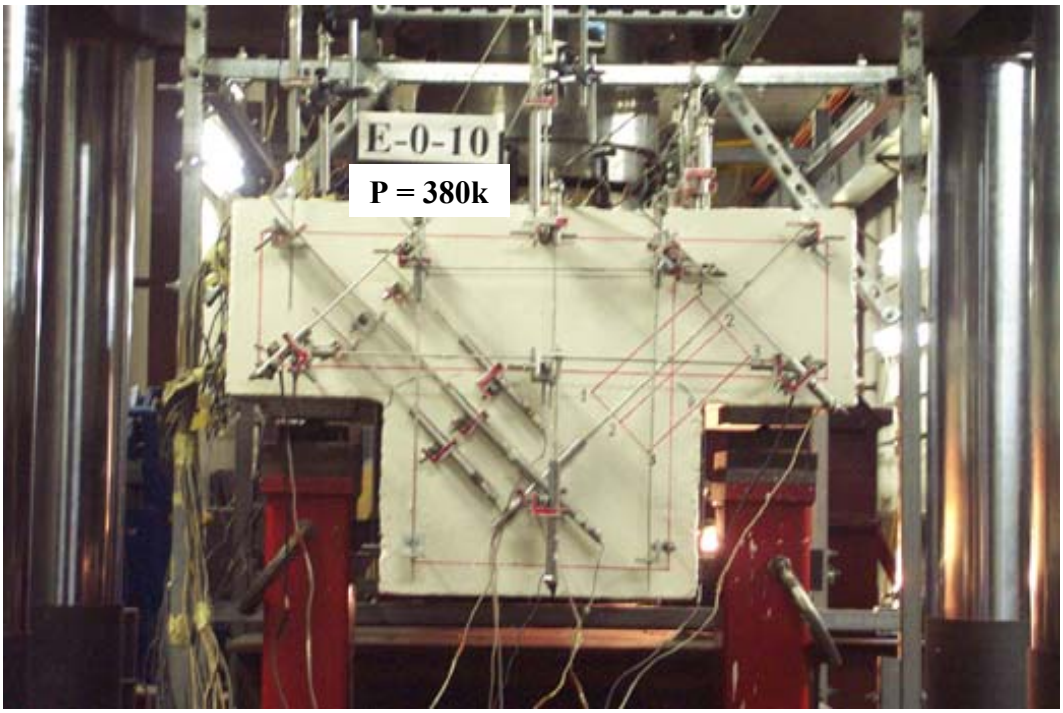

Fig. A6 Crack Pattern before Nominal Shear Resistance for the Service Limit State (V_n = 408 k)

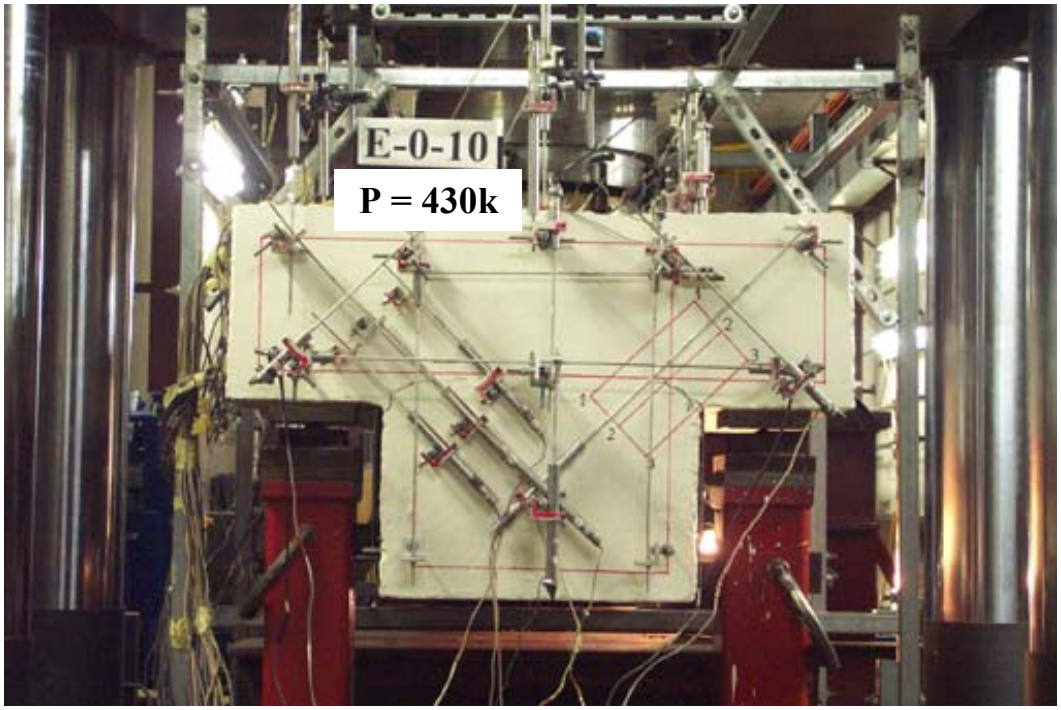

Fig. A7 Crack Pattern after Nominal Shear Resistance for the Service Limit State (V_n = 408 k)

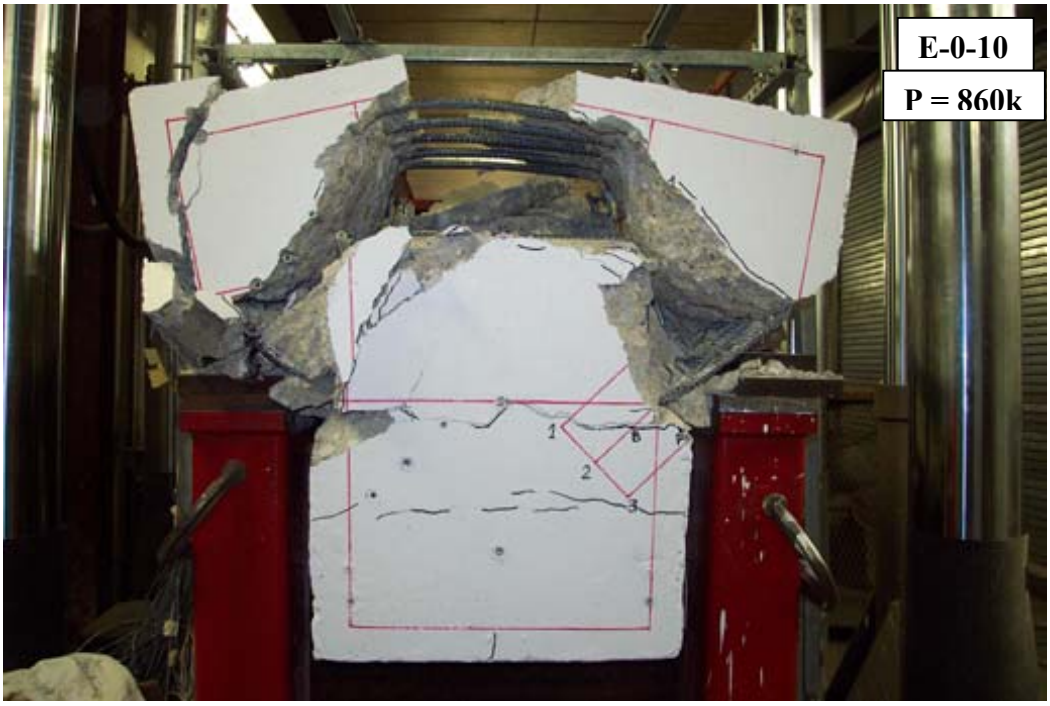

Fig. A8 Specimen at Failure

Fig. A9 Punching Shear Failure

Deflection measurement for Specimen E-0-10 was lost due to freezing of computer

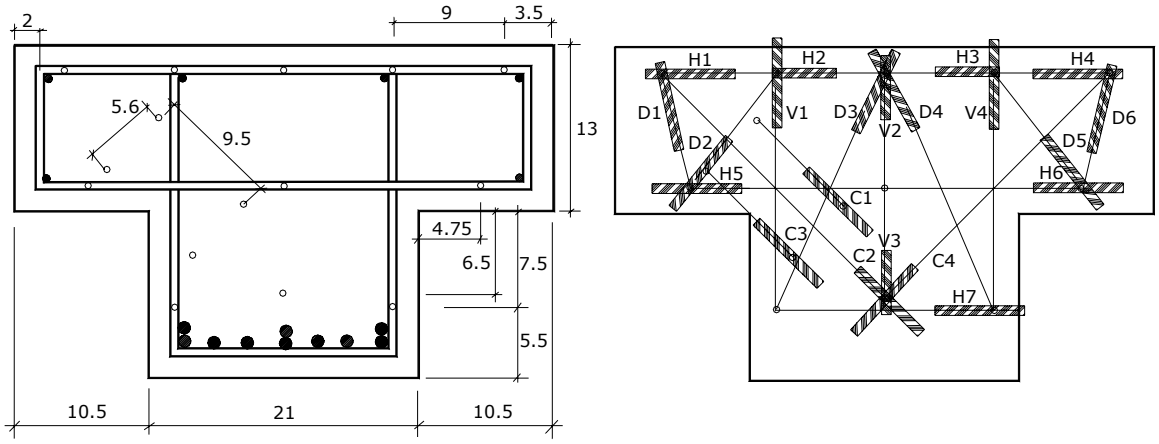

End view of LVDT arrangement

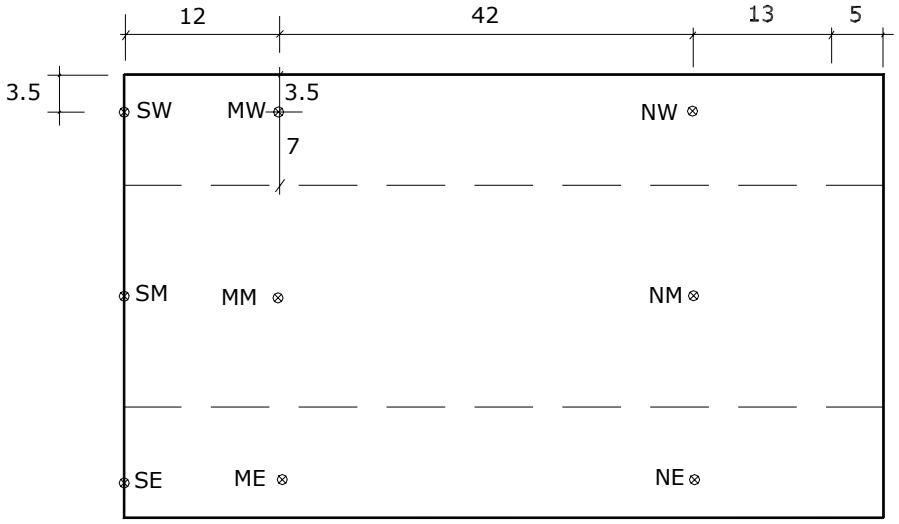

Top view of LVDT arrangement

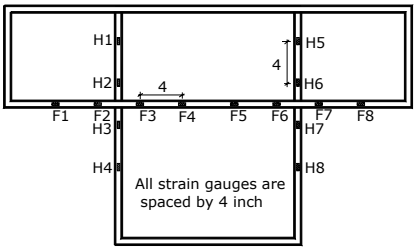

Strain Gauge arrangement

Fig. A10 LVDT and Strain Gauge Arrangement for Specimen E-0-12

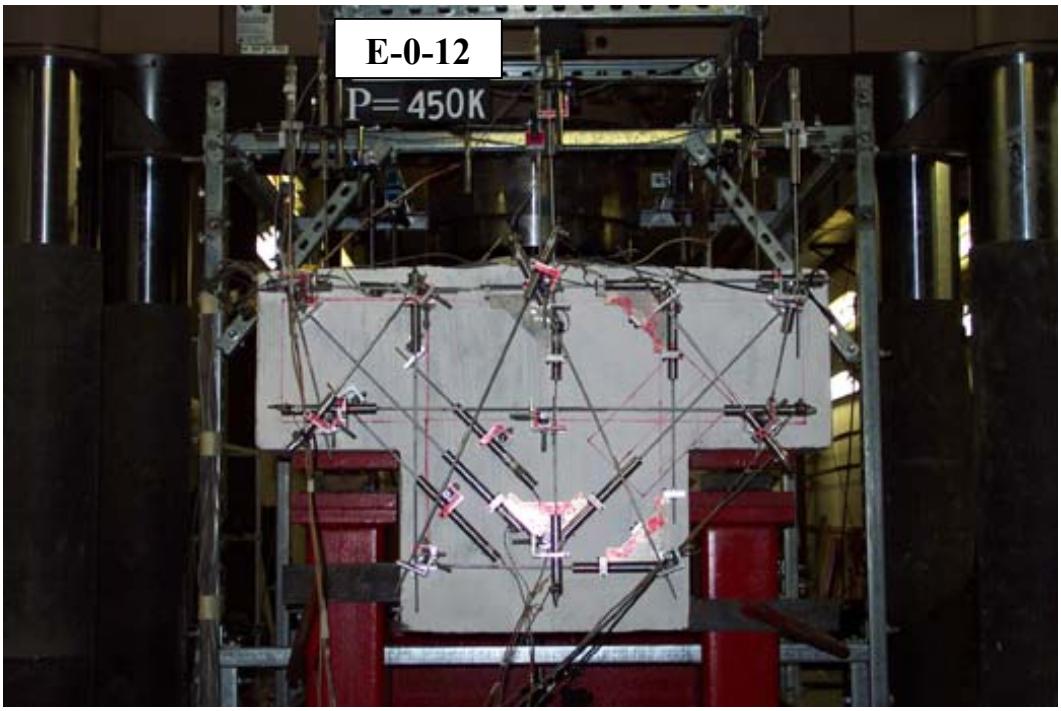

Fig. A11 Crack Pattern before Nominal Shear Resistance for the Service Limit State (V_n = 472 k)

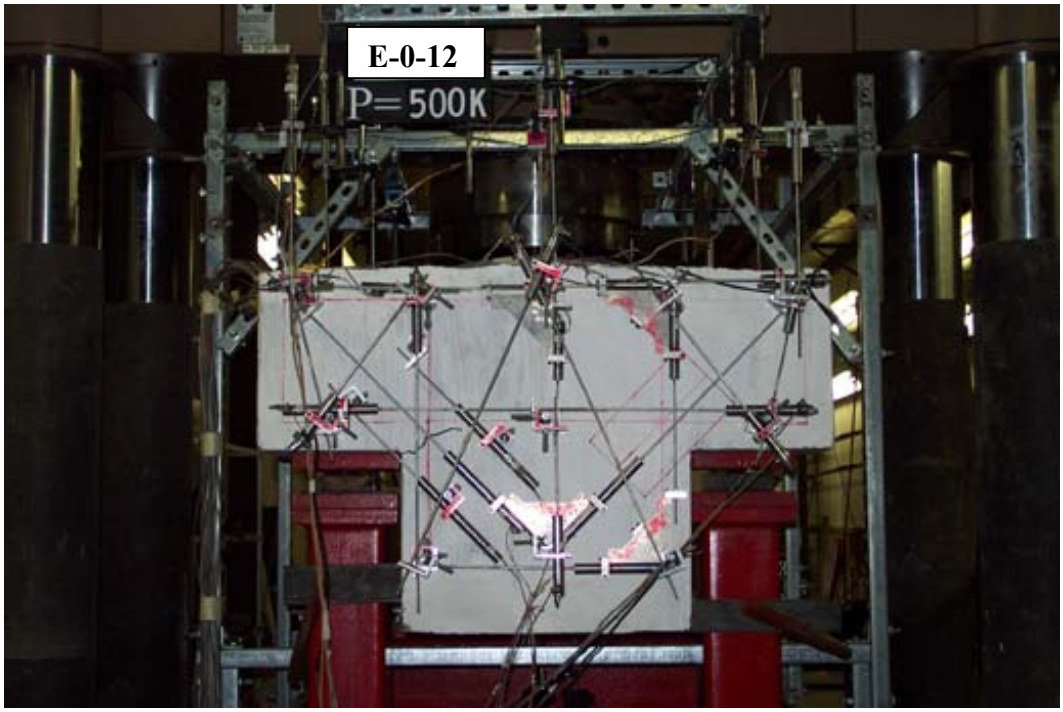

Fig. A12 Crack Pattern after Nominal Shear Resistance for the Service Limit State (V_n = 472 k)

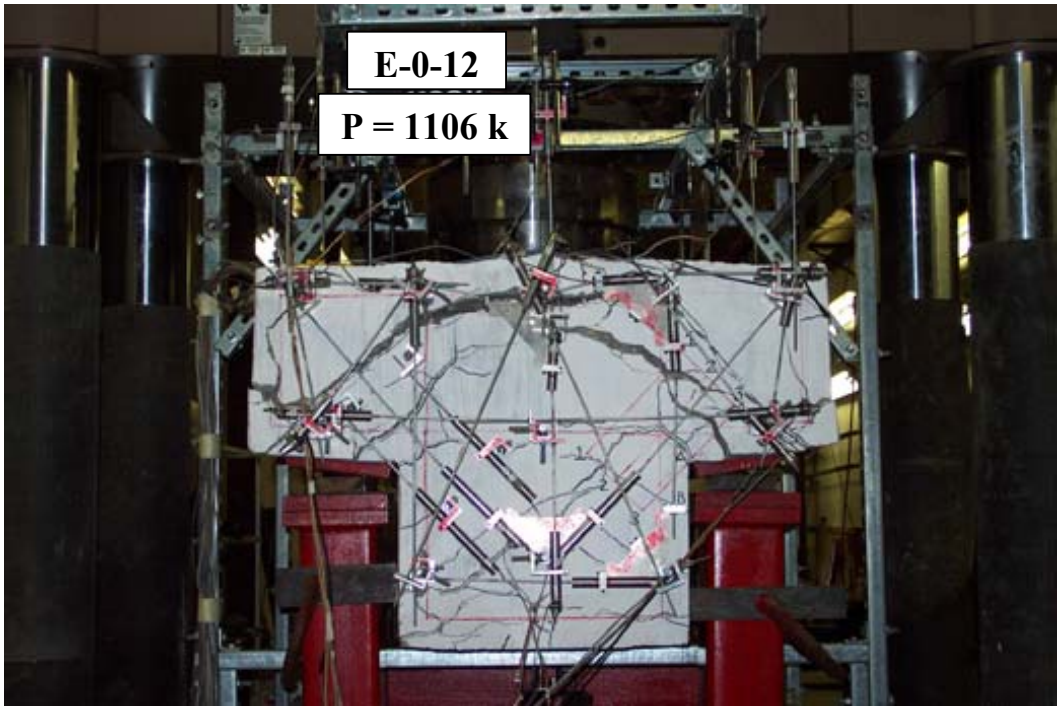

Fig. A13 Specimen at Failure

Table A2, Deflection of E-0-12 (inch)

V (k)	SW	SM	SE	MW	MM	ME	NW	NM	NE
5.3	0.0002	-0.0040	-0.0023	0.0232	0.0110	0.0000	0.0480	0.0430	0.0300
10.3	0.0192	0.0090	-0.0013	0.0501	0.0300	0.0110	0.0740	0.0730	0.0530
15.2	0.0290	0.0210	0.0008	0.0688	0.0450	0.0230	0.0840	0.0920	0.0690
20.2	0.0438	0.0330	0.0028	0.0856	0.0580	0.0330	0.0990	0.1080	0.0810
25.2	0.0581	0.0450	0.0045	0.1014	0.0700	0.0430	0.1150	0.1210	0.0920
30.1	0.0697	0.0550	0.0061	0.1146	0.0820	0.0530	0.1310	0.1360	0.1050
35.1	0.0796	0.0650	0.0081	0.1272	0.0940	0.0640	0.1470	0.1510	0.1170
40.1	0.0897	0.0750	0.0094	0.1394	0.1050	0.0740	0.1620	0.1650	0.1290
45.0	0.1001	0.0860	0.0116	0.1513	0.1160	0.0840	0.1750	0.1780	0.1400
50.3	0.1092	0.0950	0.0129	0.1631	0.1280	0.0940	0.1890	0.1930	0.1540
55.3	0.1184	0.1060	0.0149	0.1741	0.1390	0.1040	0.2010	0.2060	0.1660
60.3	0.1273	0.1160	0.0170	0.1844	0.1500	0.1150	0.2140	0.2180	0.1780
65.3	0.1306	0.1250	0.0181	0.1939	0.1630	0.1250	0.2280	0.2340	0.1930
70.2	0.1376	0.1330	0.0196	0.2039	0.1740	0.1360	0.2410	0.2470	0.2060
75.2	0.1422	0.1430	0.0205	0.2139	0.1870	0.1460	0.2540	0.2610	0.2200
80.2	0.1485	0.1520	0.0221	0.2224	0.2010	0.1570	0.2670	0.2750	0.2330
85.1	0.1511	0.1630	0.0236	0.2304	0.2140	0.1680	0.2820	0.2890	0.2470
90.5	0.1518	0.1790	0.0251	0.2403	0.2330	0.1780	0.2990	0.3070	0.2640
95.1	0.1575	0.1870	0.0251	0.2496	0.2440	0.1870	0.3130	0.3220	0.2780
100.3	0.1649	0.1970	0.0267	0.2592	0.2580	0.1970	0.3320	0.3340	0.2930
105.2	0.1674	0.2090	0.0277	0.2664	0.2720	0.2080	0.3490	0.3470	0.3070
110.1	0.1724	0.2270	0.0279	0.2756	0.2890	0.2180	0.3700	0.3690	0.3270
115.1	0.1754	0.2380	0.0280	0.2865	0.3030	0.2270	0.3880	0.3870	0.3450
120.1	0.1755	0.2470	0.0280	0.2973	0.3200	0.2370	0.4110	0.4110	0.3670
125.2	0.1733	0.2560	0.0280	0.3079	0.3360	0.2460	0.4350	0.4340	0.3900
130.7	0.1352	0.2580	0.0209	0.3215	0.3550	0.2530	0.4890	0.4930	0.4450

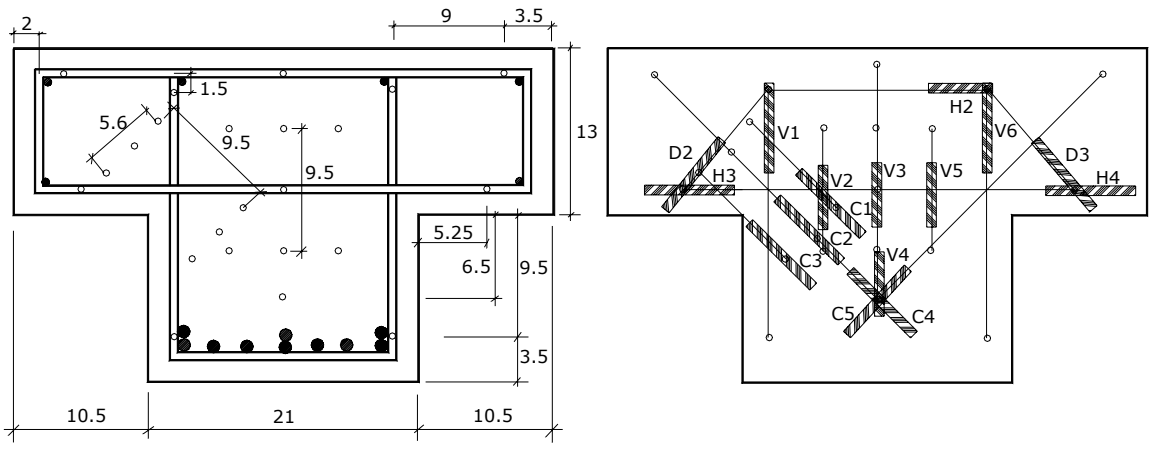

End view of LVDT arrangement

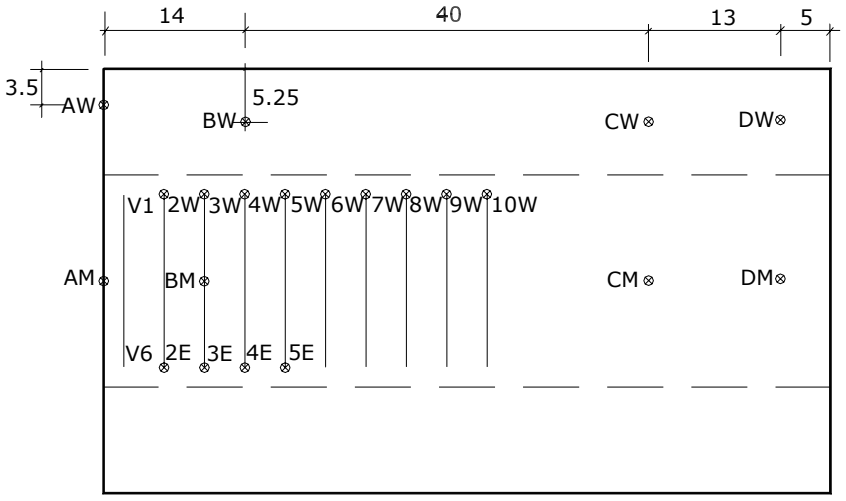

Top view of LVDT arrangement

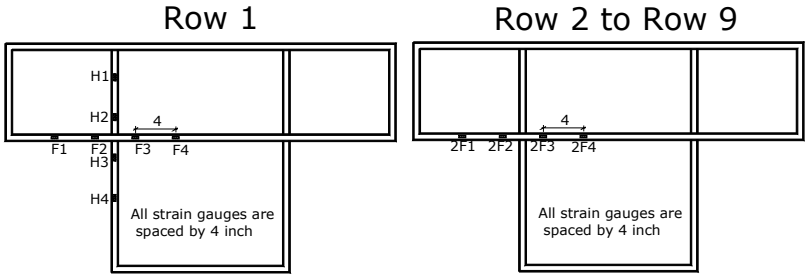

Strain Gauge arrangement

Fig. A14 LVDT and Strain Gauge Arrangement for Specimen E-0-14

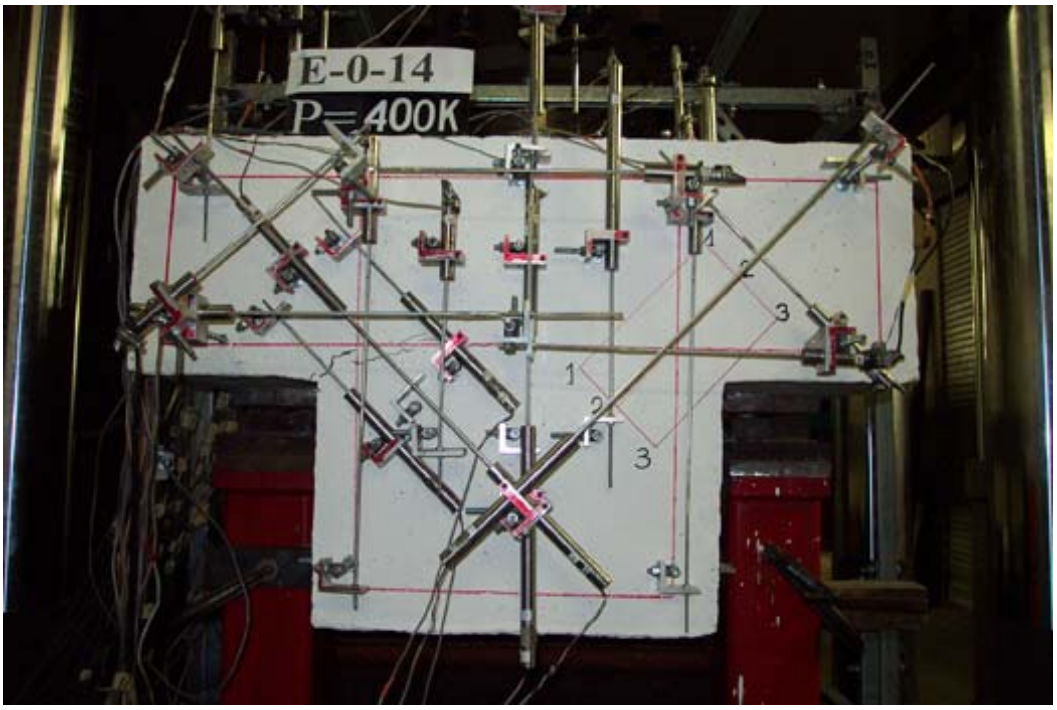

Fig. A15 Crack Pattern before Nominal Shear Resistance for the Service Limit State (V_n = 412 k)

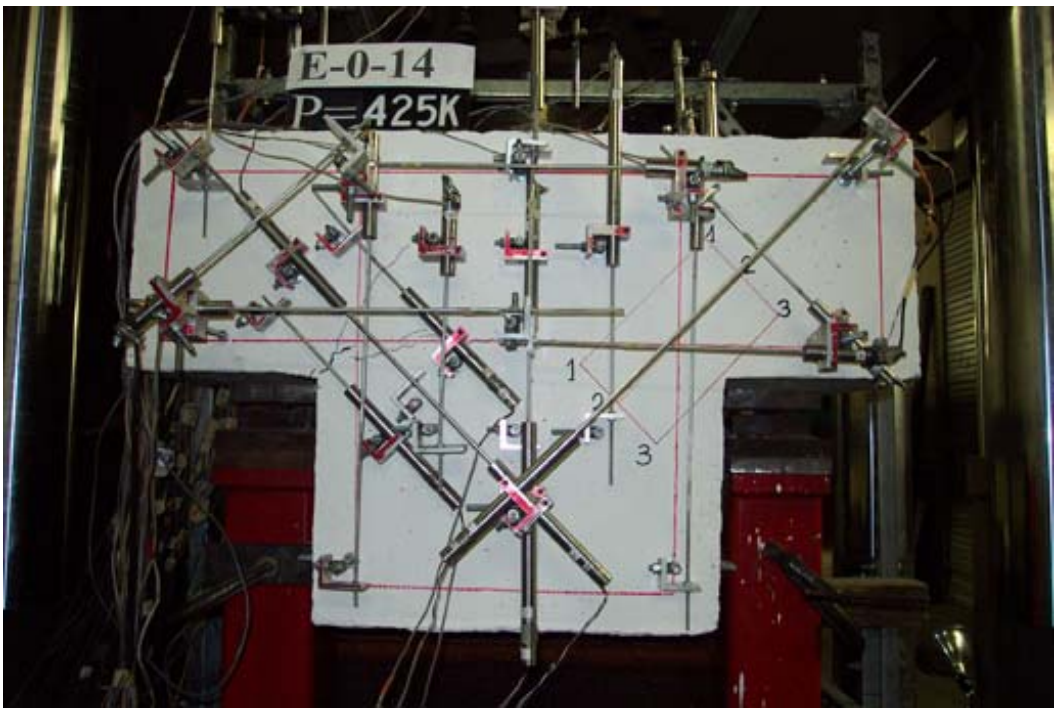

Fig. A16 Crack Pattern after Nominal Shear Resistance for the Service Limit State (V_n = 412 k)

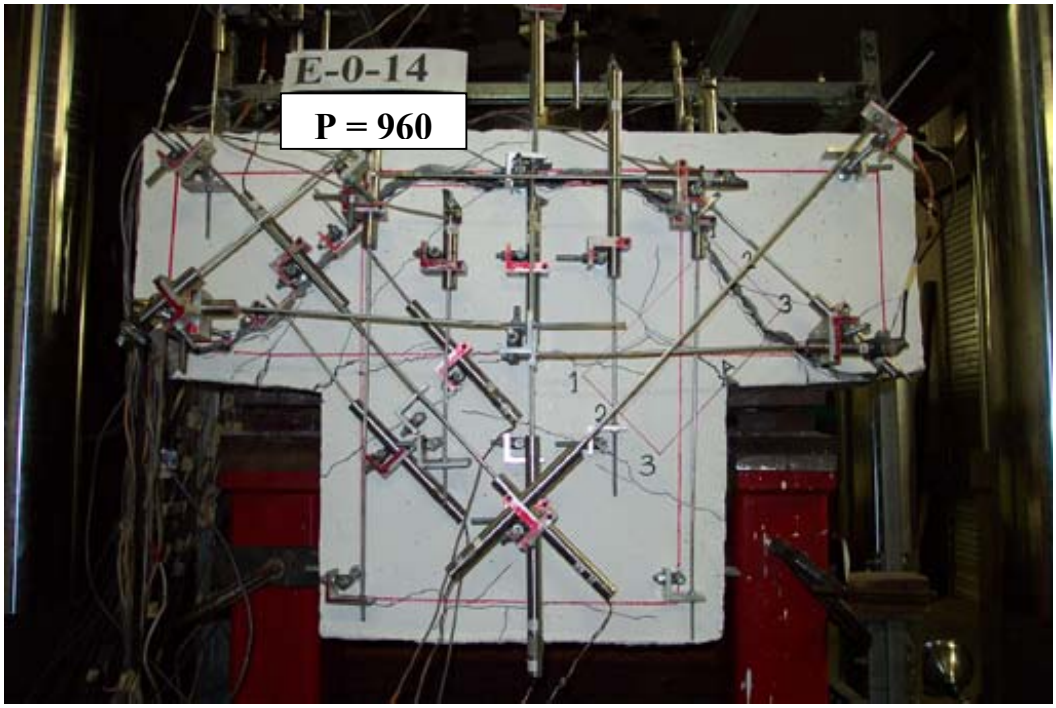

Fig. A17 Specimen at Failure

Table A3, Deflection of E-0-14 (inch)

V (k)	AW	BW	BM	CW	CM	DW	DM
5.0	0.0190	0.0183	0.0170	0.0350	0.0299	0.0391	0.0306
10.0	0.0450	0.0382	0.0363	0.0571	0.0510	0.0616	0.0485
15.0	0.0623	0.0518	0.0501	0.0734	0.0663	0.0773	0.0610
20.0	0.0762	0.0629	0.0611	0.0867	0.0786	0.0899	0.0709
25.0	0.0864	0.0712	0.0697	0.0985	0.0898	0.1002	0.0795
30.0	0.0959	0.0785	0.0785	0.1092	0.0977	0.1097	0.0875
35.0	0.1013	0.0836	0.0849	0.1205	0.1089	0.1192	0.0950
40.0	0.1072	0.0888	0.0916	0.1315	0.1204	0.1281	0.1026
45.0	0.1101	0.0925	0.0966	0.1429	0.1321	0.1365	0.1087
50.0	0.1136	0.0966	0.1022	0.1534	0.1430	0.1446	0.1156
55.0	0.1161	0.0987	0.1101	0.1649	0.1536	0.1536	0.1221
60.0	0.1203	0.1024	0.1158	0.1757	0.1649	0.1621	0.1293
65.0	0.1229	0.1056	0.1214	0.1861	0.1764	0.1701	0.1364
70.0	0.1240	0.1085	0.1271	0.1978	0.1873	0.1781	0.1429
75.0	0.1272	0.1120	0.1326	0.2085	0.1991	0.1848	0.1502
80.1	0.1280	0.1147	0.1372	0.2201	0.2115	0.1925	0.1568
85.0	0.1298	0.1176	0.1423	0.2305	0.2225	0.1999	0.1635
90.1	0.1384	0.1224	0.1490	0.2415	0.2345	0.2066	0.1704
95.2	0.1419	0.1258	0.1542	0.2523	0.2456	0.2134	0.1767
100.0	0.1460	0.1296	0.1616	0.2657	0.2601	0.2210	0.1840
105.0	0.1440	0.1312	0.1740	0.2807	0.2760	0.2294	0.1913
110.0	0.1440	0.1335	0.1811	0.2930	0.2884	0.2375	0.1986
115.1	0.1400	0.1348	0.1865	0.3099	0.3066	0.2473	0.2071
117.8	0.1287	0.1320	0.1856	0.3244	0.3214	0.2543	0.2128

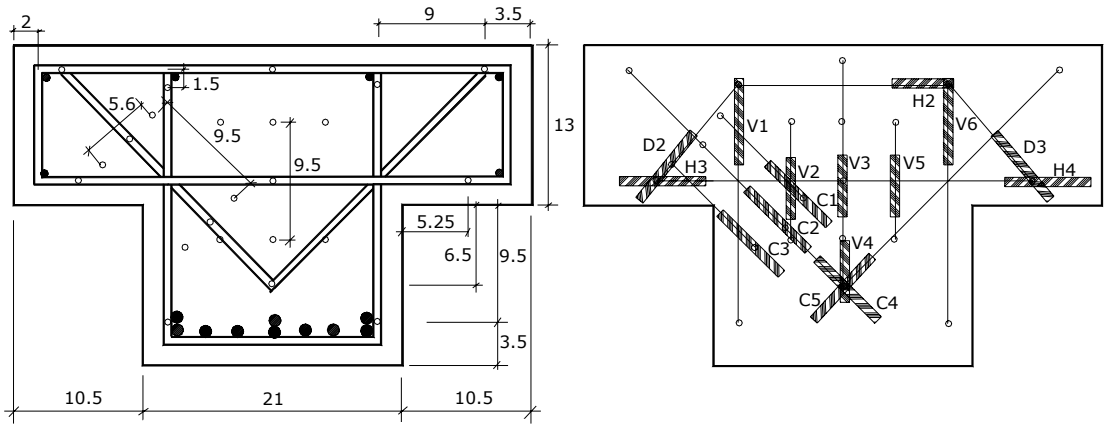

End view of LVDT arrangement

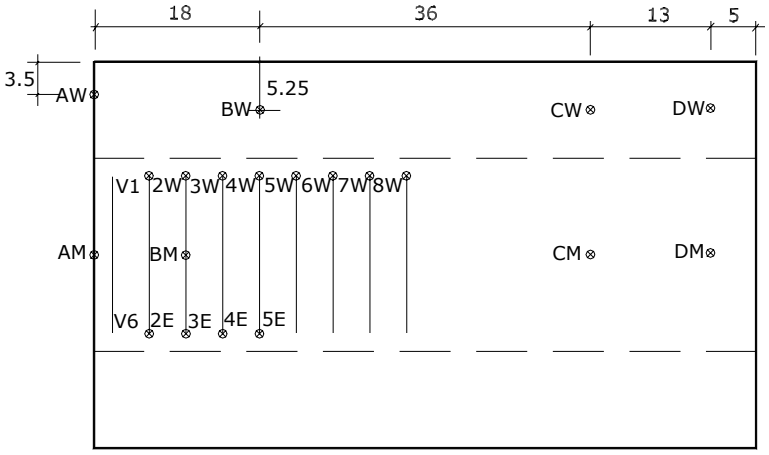

Top view of LVDT arrangement

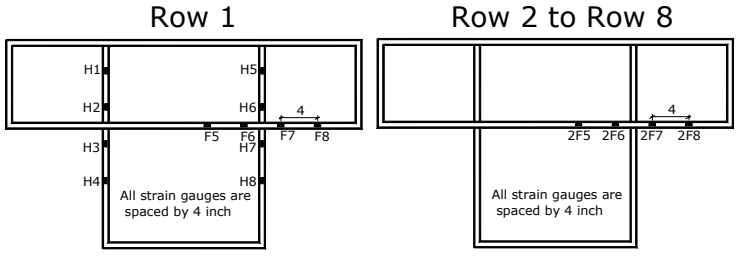

Strain Gauge arrangement

Fig. A18 LVDT and Strain Gauge Arrangement for Specimen E-0-18

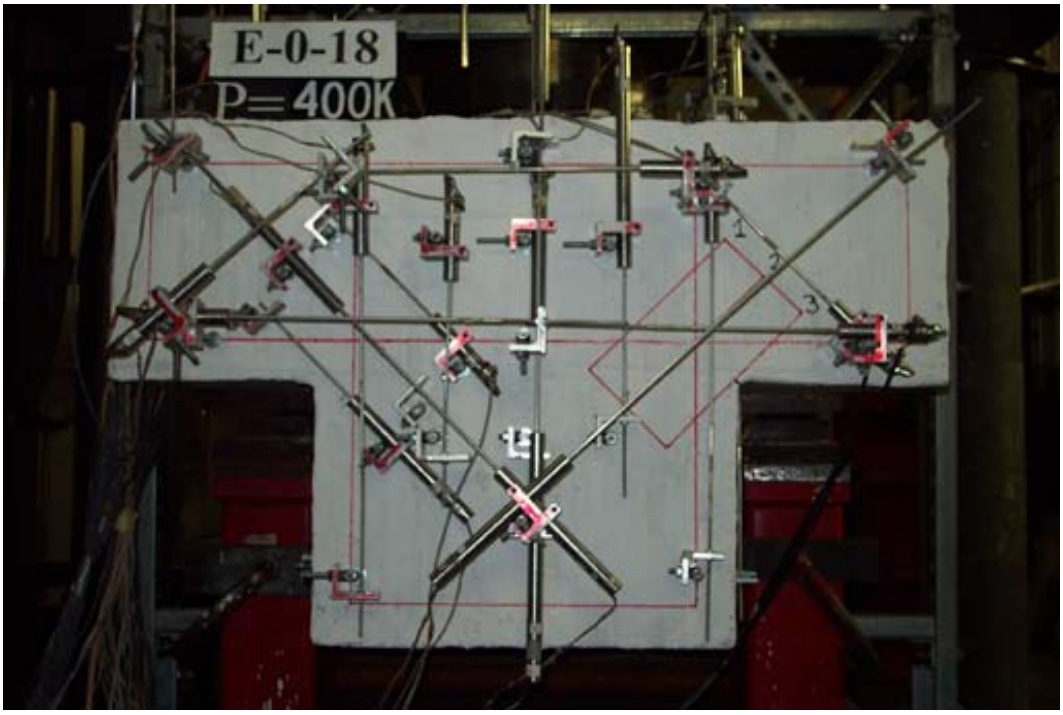

Fig. A19 Crack Pattern after Nominal Shear Resistance for the Service Limit State (V_n = 382 K)

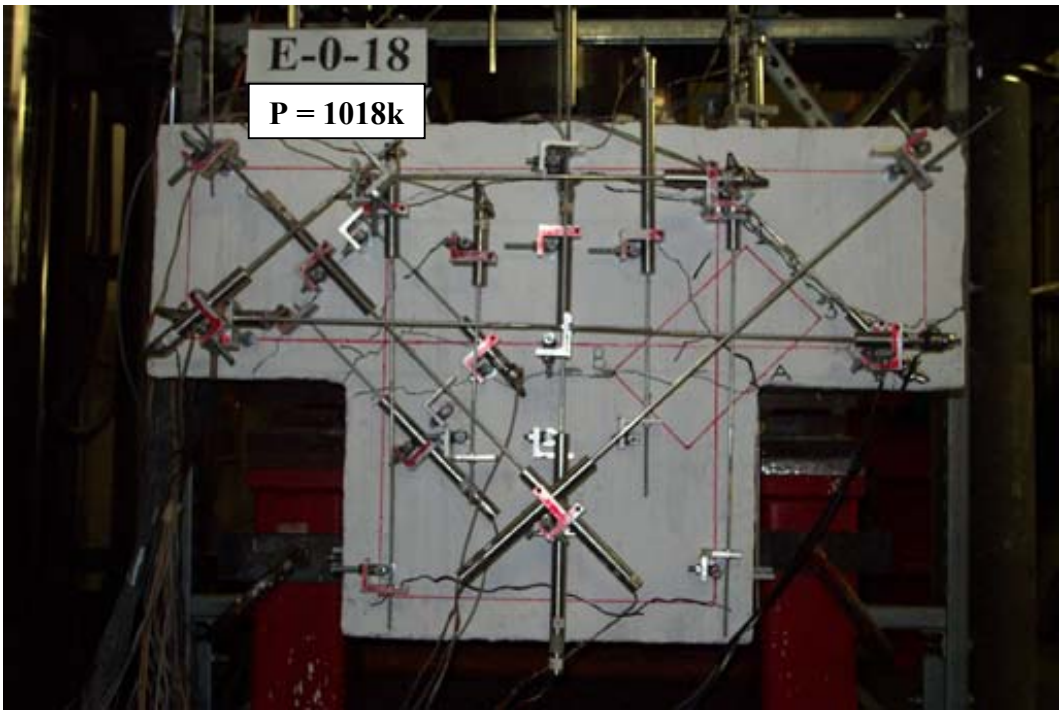

Fig. A20 Specimen at Failure

Table A4, Deflection of E-0-18 (inch)

V (k)	AW	AM	BW	BM	CW	CM	DW	DM
5.0	0.0078	0.0044	0.0092	0.0116	0.0275	0.0126	0.0319	0.0285
10.0	0.0299	0.0218	0.0253	0.0293	0.0501	0.0278	0.0546	0.0469
15.0	0.0478	0.0354	0.0381	0.0433	0.0673	0.0394	0.0713	0.0603
20.0	0.0629	0.0480	0.0485	0.0547	0.0799	0.0475	0.0829	0.0694
25.0	0.0747	0.0577	0.0568	0.0639	0.0901	0.0541	0.0918	0.0763
30.0	0.0846	0.0652	0.0637	0.0715	0.0993	0.0597	0.1000	0.0827
35.1	0.0921	0.0711	0.0696	0.0780	0.1089	0.0661	0.1078	0.0888
40.0	0.0995	0.0774	0.0751	0.0841	0.1179	0.0727	0.1151	0.0946
45.0	0.1053	0.0820	0.0800	0.0895	0.1276	0.0801	0.1223	0.1003
50.1	0.1101	0.0860	0.0840	0.0945	0.1384	0.0900	0.1290	0.1057
55.1	0.1155	0.0909	0.0884	0.0996	0.1476	0.0973	0.1358	0.1113
60.0	0.1214	0.0956	0.0924	0.1047	0.1564	0.1045	0.1423	0.1166
65.0	0.1282	0.1020	0.0969	0.1106	0.1658	0.1123	0.1490	0.1221
70.0	0.1367	0.1095	0.1016	0.1172	0.1759	0.1209	0.1558	0.1277
75.0	0.1442	0.1166	0.1062	0.1237	0.1859	0.1296	0.1628	0.1336
80.0	0.1504	0.1224	0.1100	0.1293	0.1957	0.1386	0.1694	0.1392
85.0	0.1537	0.1267	0.1132	0.1346	0.2057	0.1480	0.1763	0.1450
90.0	0.1577	0.1308	0.1160	0.1396	0.2164	0.1584	0.1828	0.1507
95.0	0.1636	0.1385	0.1199	0.1457	0.2278	0.1685	0.1889	0.1562
100.2	0.1668	0.1416	0.1225	0.1511	0.2417	0.1822	0.1964	0.1625
105.1	0.1715	0.1464	0.1258	0.1560	0.2520	0.1922	0.2033	0.1682
110.0	0.1766	0.1508	0.1294	0.1614	0.2639	0.2039	0.2112	0.1746
115.0	0.1873	0.1615	0.1357	0.1701	0.2766	0.2175	0.2187	0.1809
120.1	0.1914	0.1645	0.1387	0.1750	0.2888	0.2296	0.2267	0.1872
125.0	0.1968	0.1690	0.1423	0.1808	0.3029	0.2448	0.2357	0.1939
130.0	0.2006	0.1780	0.1454	0.1901	0.3193	0.2623	0.2454	0.2008
133.1	0.2072	0.1851	0.1482	0.1968	0.3287	0.2731	0.2507	0.2101
135.1	0.2537	0.2192	0.1651	0.2217	0.3454	0.2945	0.2549	0.2139

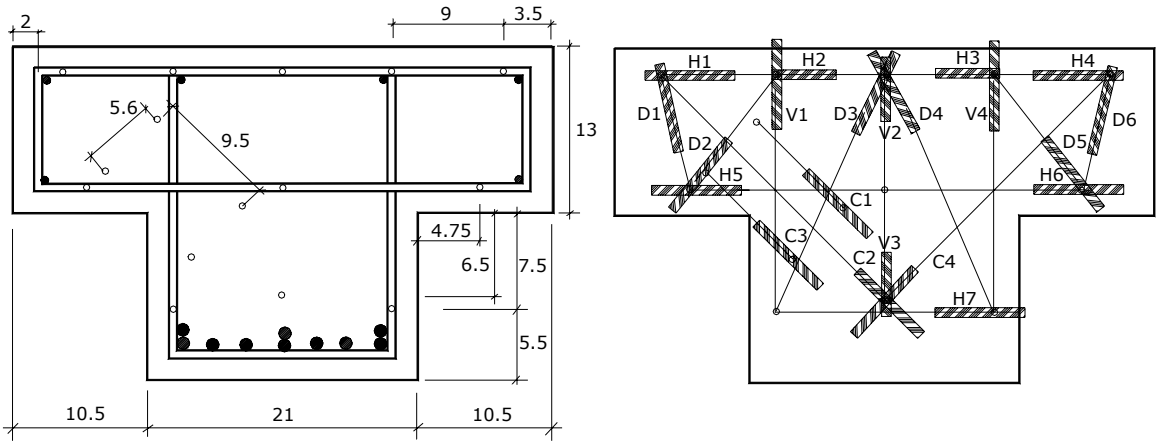

End view of LVDT arrangement

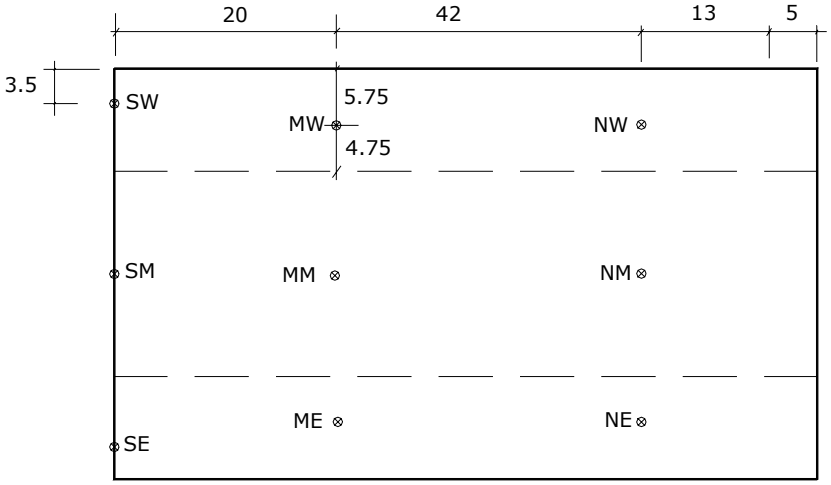

Top view of LVDT arrangement

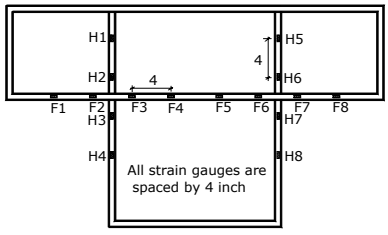

E-0-20

Strain Gauge arrangement

Fig. A21 LVDT and Strain Gauge Arrangement for Specimen E-0-20

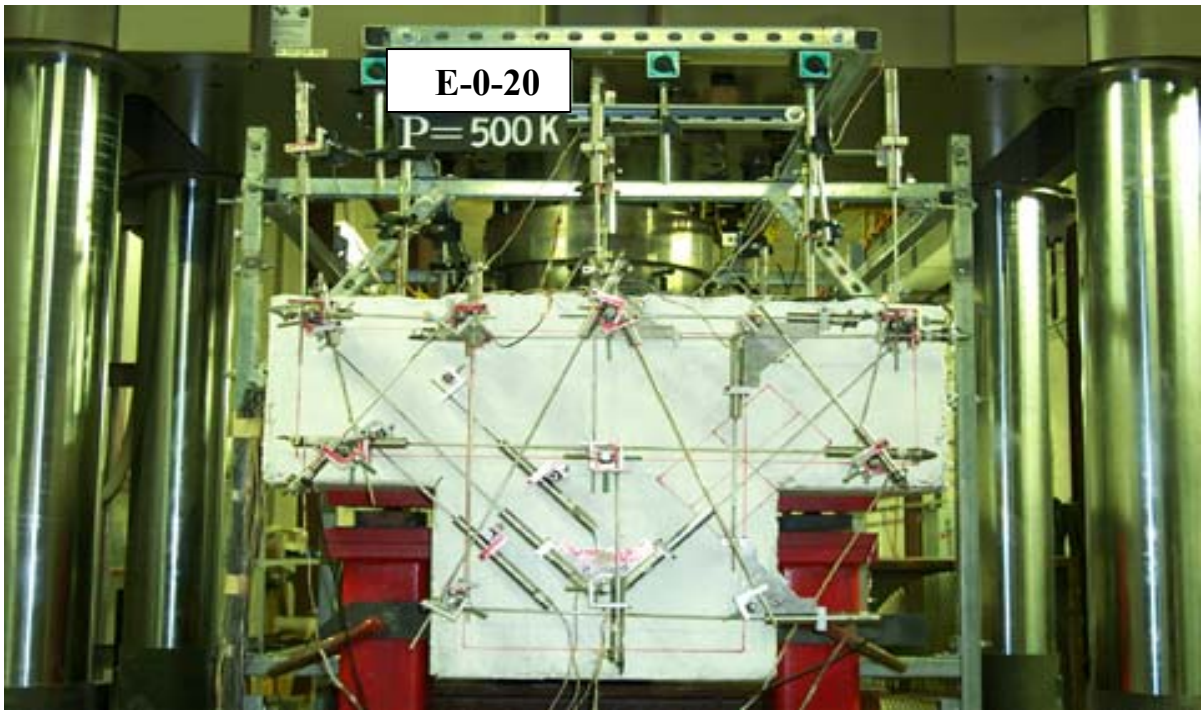

Fig. A22 Crack Pattern after Nominal Shear Resistance for the Service Limit State
(V_n = 408 K)

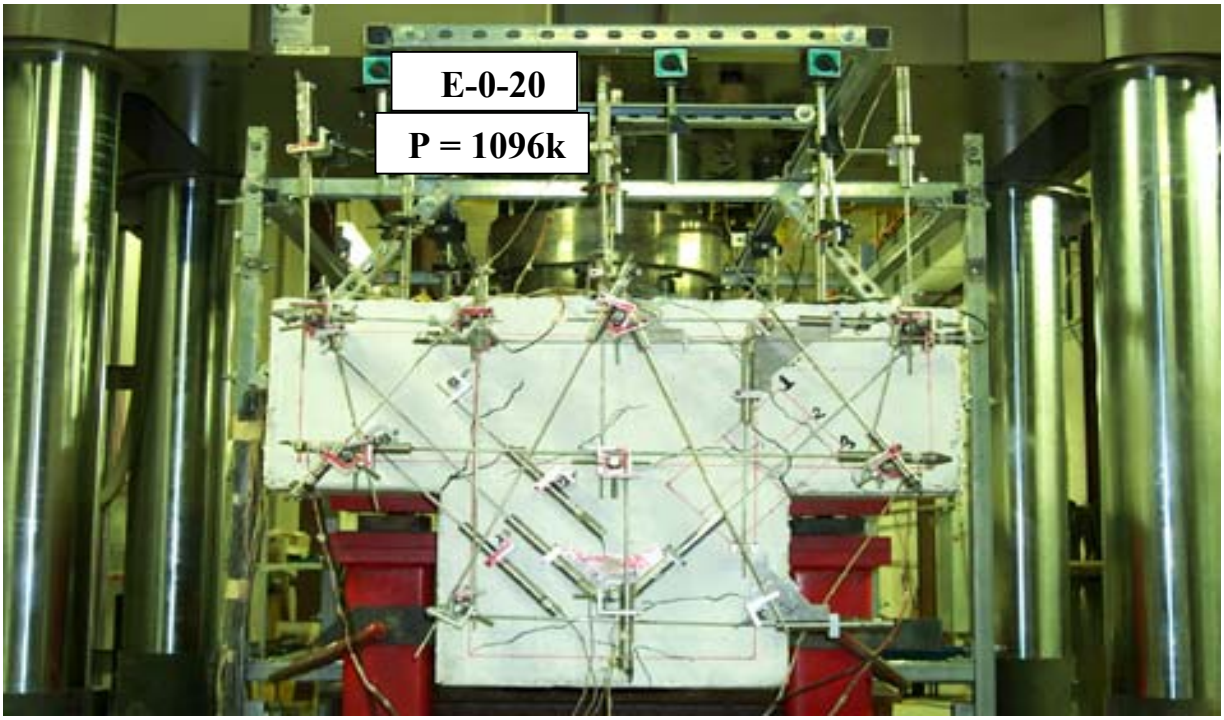

Fig. A23 Specimen at Failure

Table A5, Deflection of E-0-20 (inch)

V (k)	SW	SM	SE	MW	MM	ME	NW	NM	NE
5.0	-0.0005	0.0000	-0.0002	0.0105	0.0100	0.0010	0.0230	0.0220	0.0200
10.1	0.0022	0.0040	0.0004	0.0208	0.0190	0.0140	0.0370	0.0370	0.0330
15.1	0.0041	0.0060	-0.0002	0.0281	0.0260	0.0140	0.0480	0.0480	0.0420
20.0	0.0054	0.0090	-0.0002	0.0352	0.0320	0.0140	0.0570	0.0570	0.0500
25.0	0.0192	0.0220	0.0072	0.0434	0.0380	0.0020	0.0630	0.0660	0.0560
30.1	0.0192	0.0220	0.0072	0.0495	0.0440	0.0020	0.0700	0.0730	0.0630
35.0	0.0194	0.0230	0.0087	0.0550	0.0500	0.0020	0.0790	0.0840	0.0730
40.0	0.0195	0.0230	0.0116	0.0595	0.0550	0.0010	0.0870	0.0920	0.0800
45.1	0.0195	0.0270	0.0135	0.0649	0.0600	0.0010	0.0940	0.1000	0.0870
50.0	0.0195	0.0310	0.0156	0.0700	0.0660	0.0010	0.1010	0.1080	0.0940
55.0	0.0195	0.0330	0.0171	0.0747	0.0710	0.0010	0.1090	0.1170	0.1010
60.1	0.0202	0.0360	0.0191	0.0787	0.0760	0.0010	0.1150	0.1250	0.1090
65.0	0.0208	0.0380	0.0211	0.0820	0.0780	-0.0040	0.1210	0.1320	0.1140
70.0	0.0208	0.0410	0.0232	0.0858	0.0810	-0.0050	0.1280	0.1400	0.1210
75.1	0.0226	0.0480	0.0286	0.0886	0.0860	-0.0040	0.1350	0.1490	0.1280
80.0	0.0279	0.0570	0.0359	0.0923	0.0910	0.0000	0.1420	0.1570	0.1360
85.0	0.0255	0.0660	0.0433	0.0956	0.0950	0.0040	0.1500	0.1650	0.1440
90.1	0.0280	0.0740	0.0509	0.0990	0.1000	0.0080	0.1570	0.1740	0.1530
95.1	0.0307	0.0800	0.0566	0.1021	0.1050	0.0110	0.1650	0.1830	0.1610
100.0	0.0357	0.0920	0.0655	0.1054	0.1120	0.0130	0.1730	0.1930	0.1700
105.0	0.0399	0.1010	0.0715	0.1093	0.1180	0.0160	0.1810	0.2020	0.1790
110.0	0.0437	0.1070	0.0759	0.1065	0.1250	0.0180	0.1910	0.2170	0.1910
115.1	0.0473	0.1130	0.0799	0.1100	0.1290	0.0200	0.1960	0.2240	0.1970
120.1	0.0535	0.1210	0.0865	0.1127	0.1360	0.0230	0.2040	0.2340	0.2070
125.1	0.0624	0.1310	0.0922	0.1185	0.1430	0.0270	0.2130	0.2440	0.2160
130.1	0.0686	0.1380	0.0980	0.1238	0.1440	0.0310	0.2220	0.2550	0.2270
135.1	0.0784	0.1500	0.1082	0.1315	0.1520	0.0360	0.2320	0.2690	0.2410
140.1	0.0914	0.1640	0.1146	0.1401	0.1640	0.0430	0.2450	0.2870	0.2580
145.0	0.1073	0.1800	0.1293	0.1467	0.1730	0.0490	0.2570	0.3020	0.2730
150.1	0.1237	0.2000	0.1470	0.1542	0.1850	0.0570	0.2740	0.3240	0.2940
151.5	0.1310	0.2080	0.1526	0.1590	0.1910	0.0610	0.2820	0.3370	0.3060
151.5	0.1311	0.2080	0.1526	0.1621	0.1950	0.0630	0.2950	0.3560	0.3220

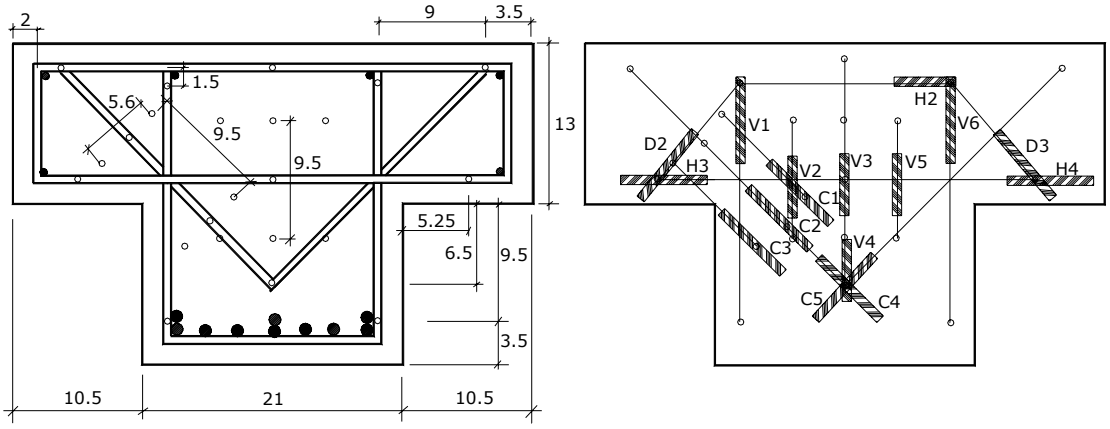

End view of LVDT arrangement

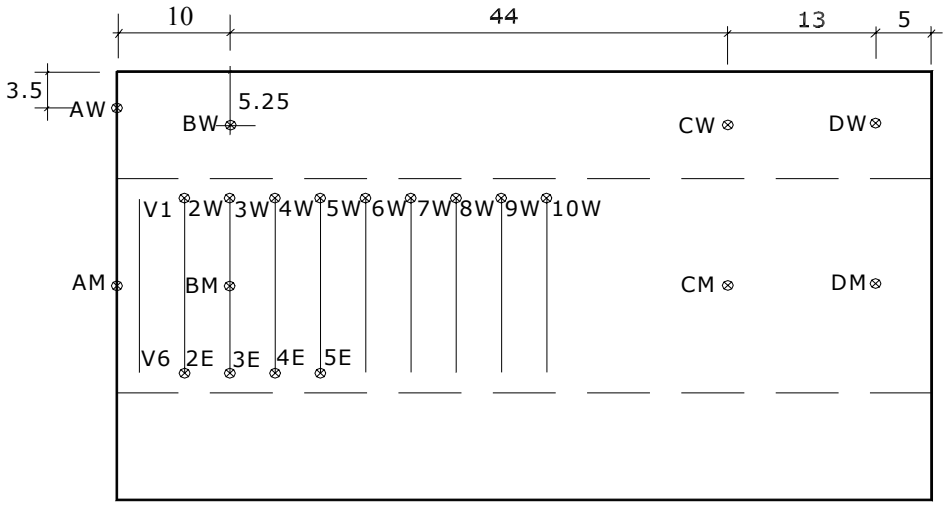

Top view of LVDT arrangement

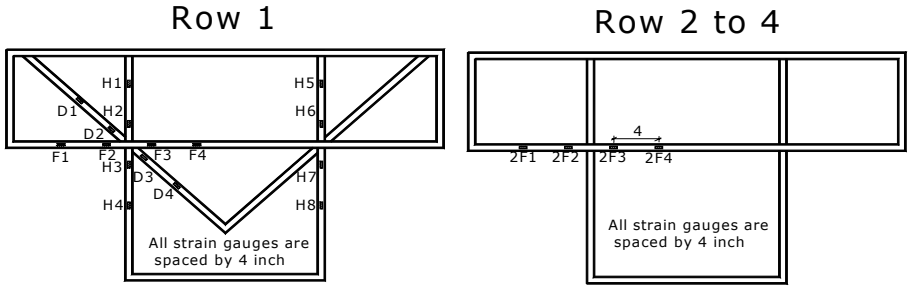

Strain Gauge arrangement

Fig. A24 LVDT and Strain Gauge Arrangement for Specimen E-1-10

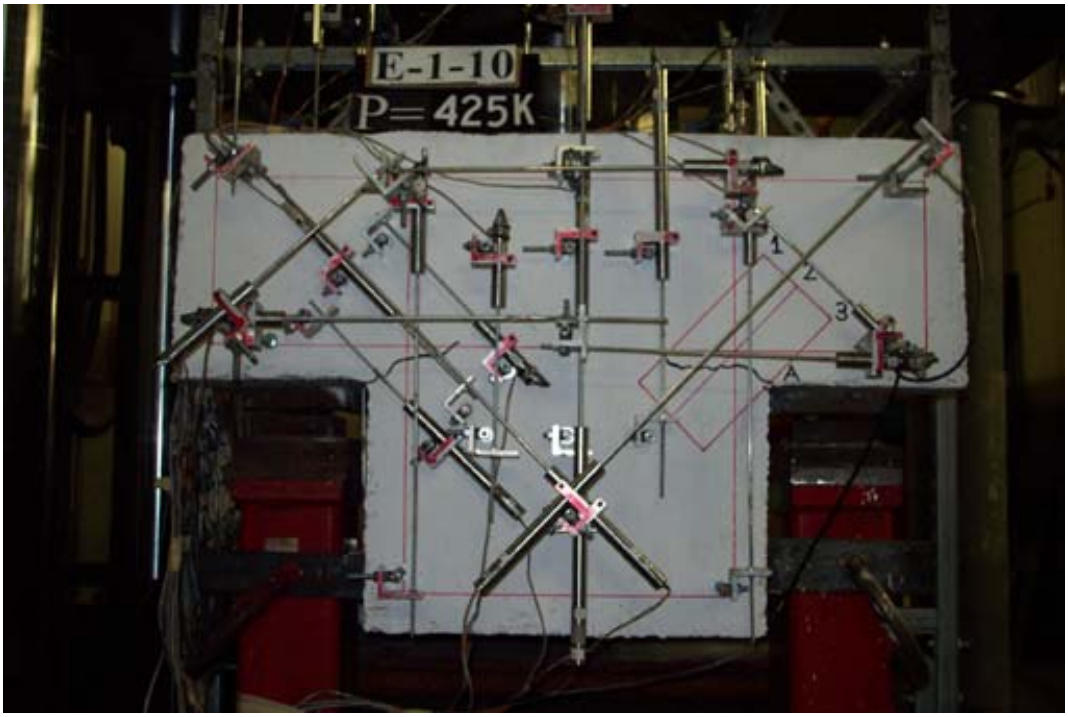

Fig. A25 Crack Pattern Before Nominal Shear Resistance for the Service Limit State (V_n = 408 K)

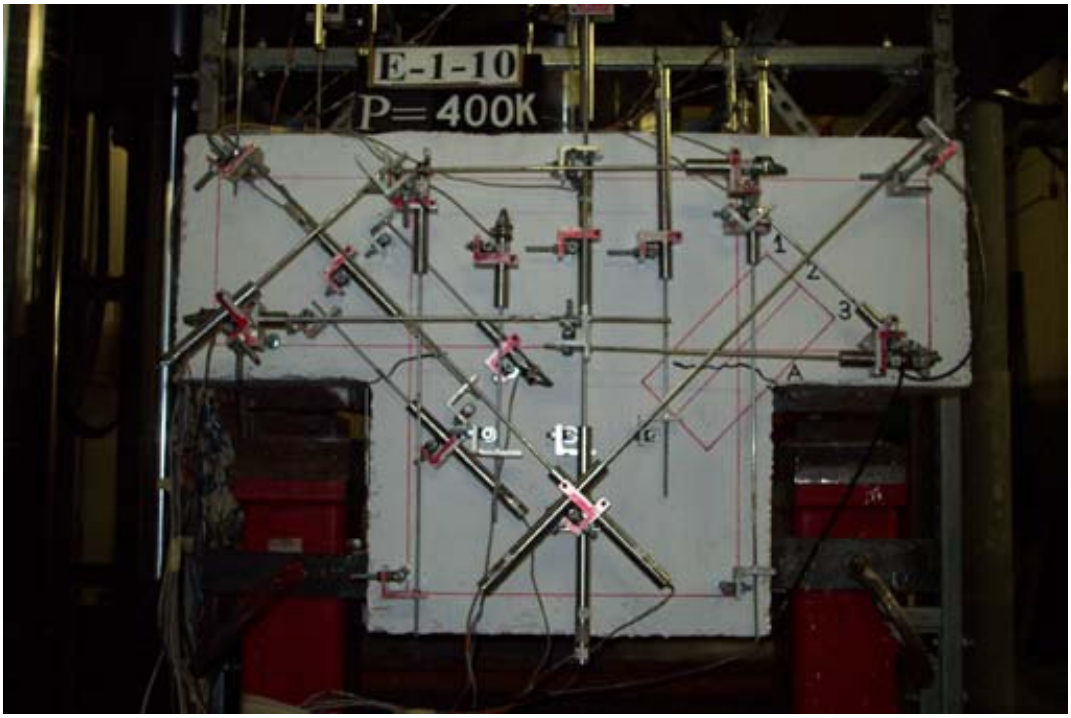

Fig. A26 Crack Pattern after Nominal Shear Resistance for the Service Limit State (V_n = 408 K)

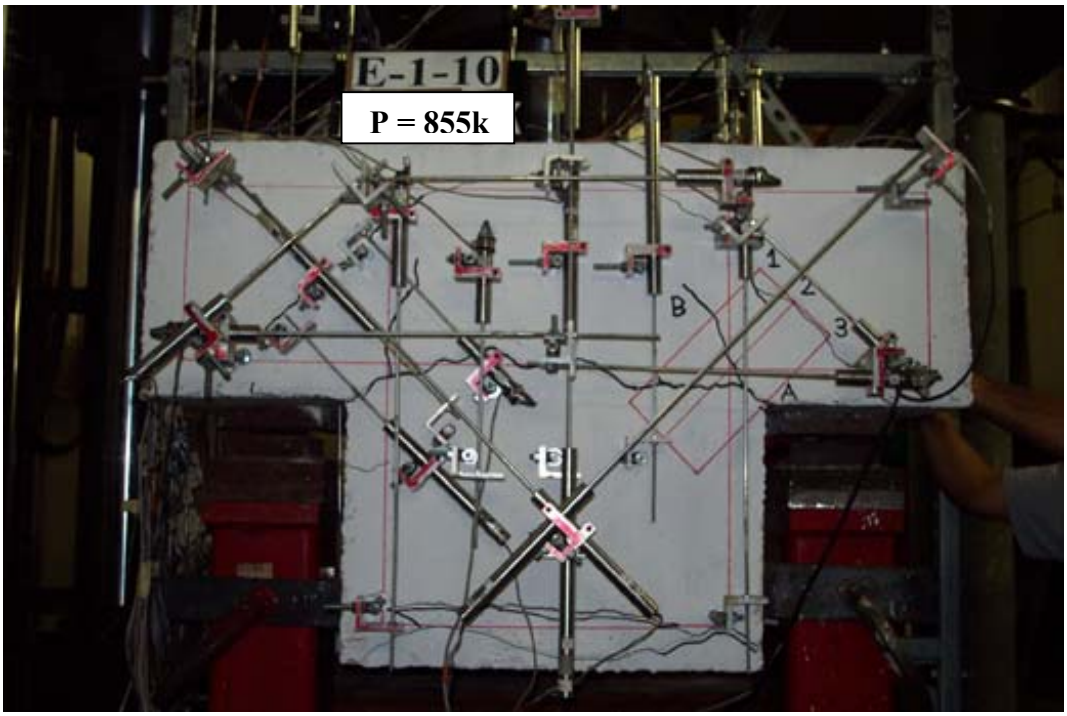

Fig. A27 Specimen at Failure

Table A6, Deflection of E-1-10 (inch)

V (k)	AW	AM	BW	BM	CW	CM	DW	DM
4.0	0.0004	0.0106	0.0060	0.0157	0.0266	0.0348	0.0314	0.0352
8.0	0.0159	0.0258	0.0190	0.0304	0.0425	0.0523	0.0474	0.0499
12.0	0.0305	0.0384	0.0300	0.0438	0.0575	0.0682	0.0620	0.0627
16.0	0.0438	0.0502	0.0401	0.0555	0.0706	0.0811	0.0740	0.0734
20.0	0.0558	0.0607	0.0490	0.0657	0.0811	0.0913	0.0829	0.0808
24.0	0.0655	0.0688	0.0563	0.0740	0.0903	0.1001	0.0906	0.0872
28.0	0.0728	0.0749	0.0625	0.0809	0.1001	0.1103	0.0974	0.0934
32.0	0.0796	0.0810	0.0683	0.0874	0.1094	0.1200	0.1039	0.0992
36.0	0.0859	0.0870	0.0738	0.0935	0.1181	0.1287	0.1103	0.1057
40.0	0.0915	0.0916	0.0792	0.0997	0.1270	0.1382	0.1166	0.1111
44.0	0.0966	0.0969	0.0840	0.1054	0.1353	0.1461	0.1229	0.1165
48.0	0.1013	0.1014	0.0886	0.1109	0.1436	0.1547	0.1290	0.1216
52.0	0.1042	0.1038	0.0935	0.1175	0.1541	0.1658	0.1350	0.1268
56.0	0.1079	0.1057	0.0984	0.1236	0.1643	0.1768	0.1414	0.1325
60.0	0.1113	0.1101	0.1024	0.1287	0.1730	0.1858	0.1473	0.1378
64.0	0.1136	0.1125	0.1062	0.1339	0.1824	0.1956	0.1540	0.1436
68.0	0.1172	0.1165	0.1104	0.1395	0.1919	0.2055	0.1605	0.1493
72.0	0.1173	0.1204	0.1135	0.1453	0.2022	0.2161	0.1672	0.1548
76.0	0.1176	0.1234	0.1167	0.1509	0.2130	0.2280	0.1740	0.1606
80.3	0.1177	0.1272	0.1208	0.1585	0.2275	0.2432	0.1823	0.1675
84.1	0.1178	0.1285	0.1250	0.1669	0.2459	0.2627	0.1918	0.1758
88.0	0.1178	0.1293	0.1263	0.1689	0.2502	0.2672	0.1945	0.1782
92.1	0.1182	0.1328	0.1322	0.1779	0.2694	0.2887	0.2057	0.1884
97.6	0.1149	0.1311	0.1363	0.1848	0.2844	0.3042	0.2116	0.1939

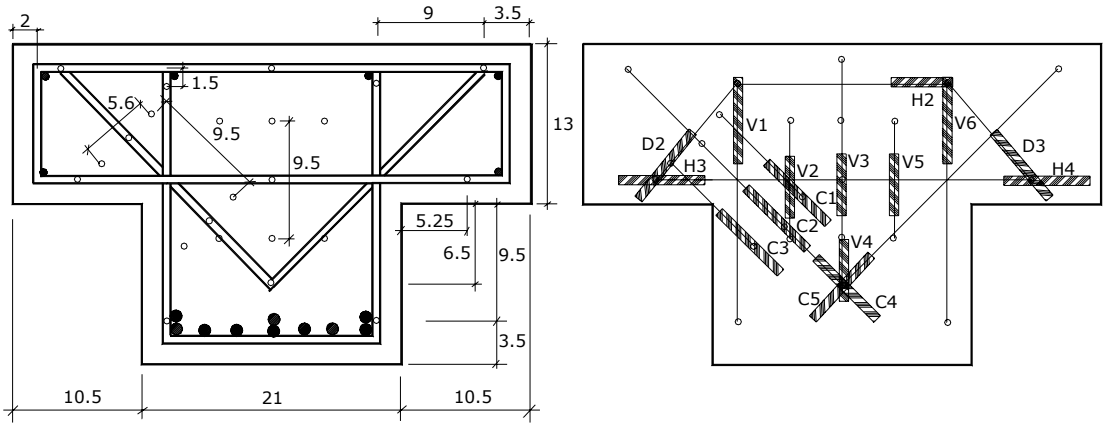

End view of LVDT arrangement

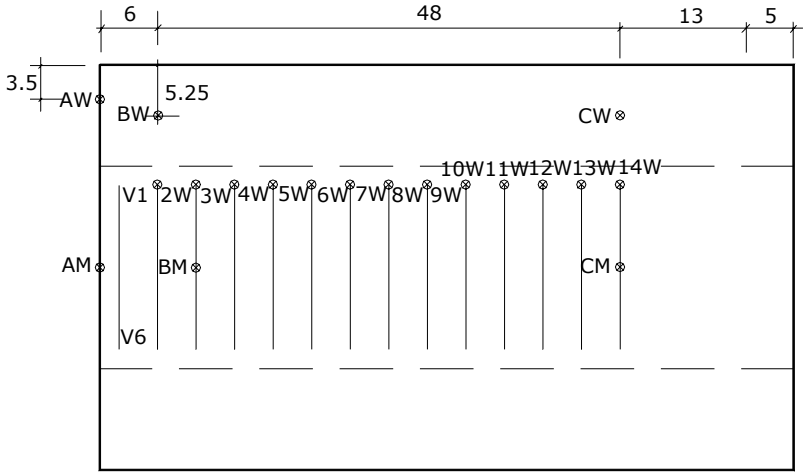

Top view of LVDT arrangement

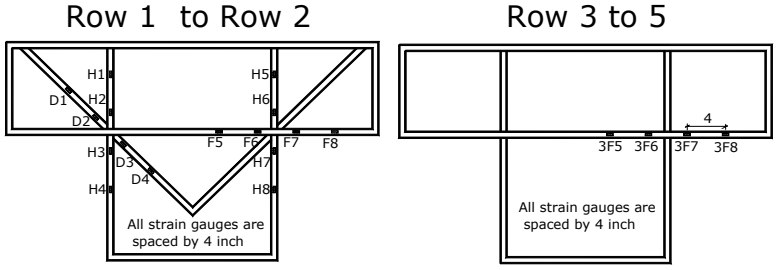

Strain Gauge arrangement

Fig. A28 LVDT and Strain Gauge Arrangement for Specimen E-2-6

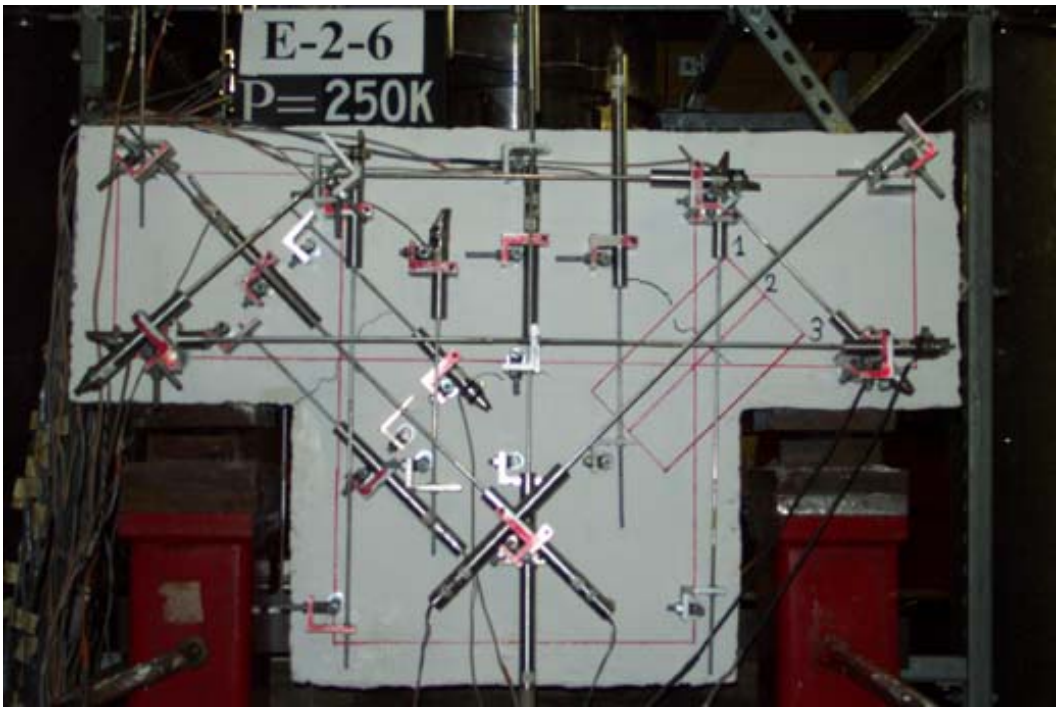

Fig. A29 Crack Pattern Before Nominal Shear Resistance for the Service Limit State (V_n = 262 K)

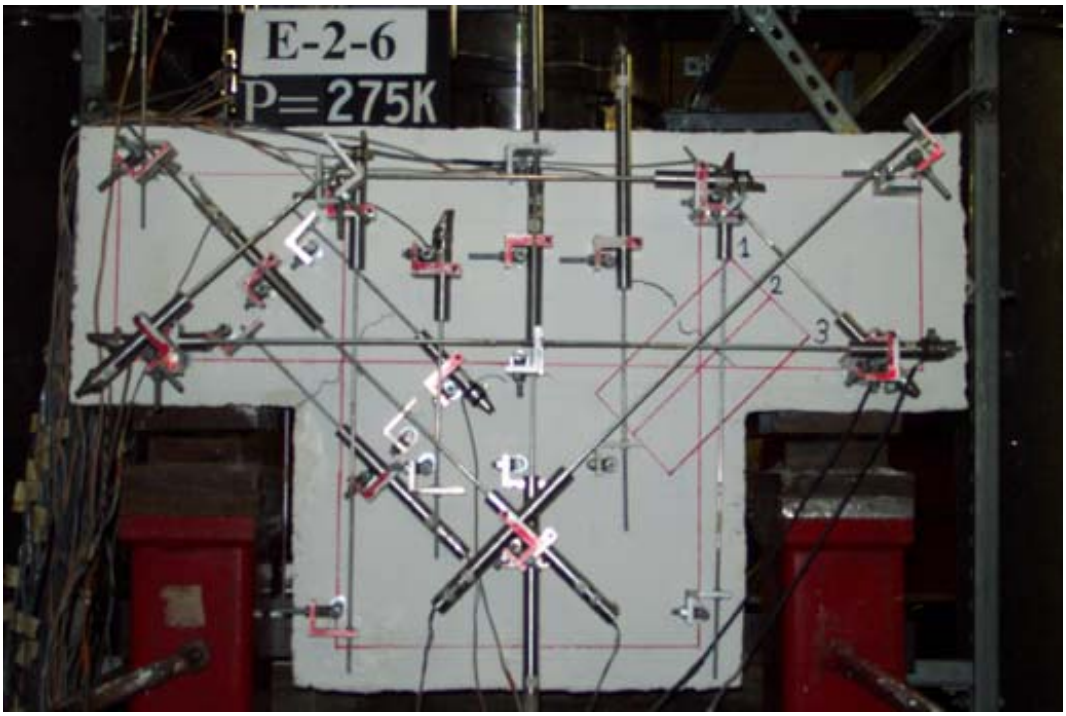

Fig. A30 Crack Pattern after Nominal Shear Resistance for the Service Limit State (V_n = 262 K)

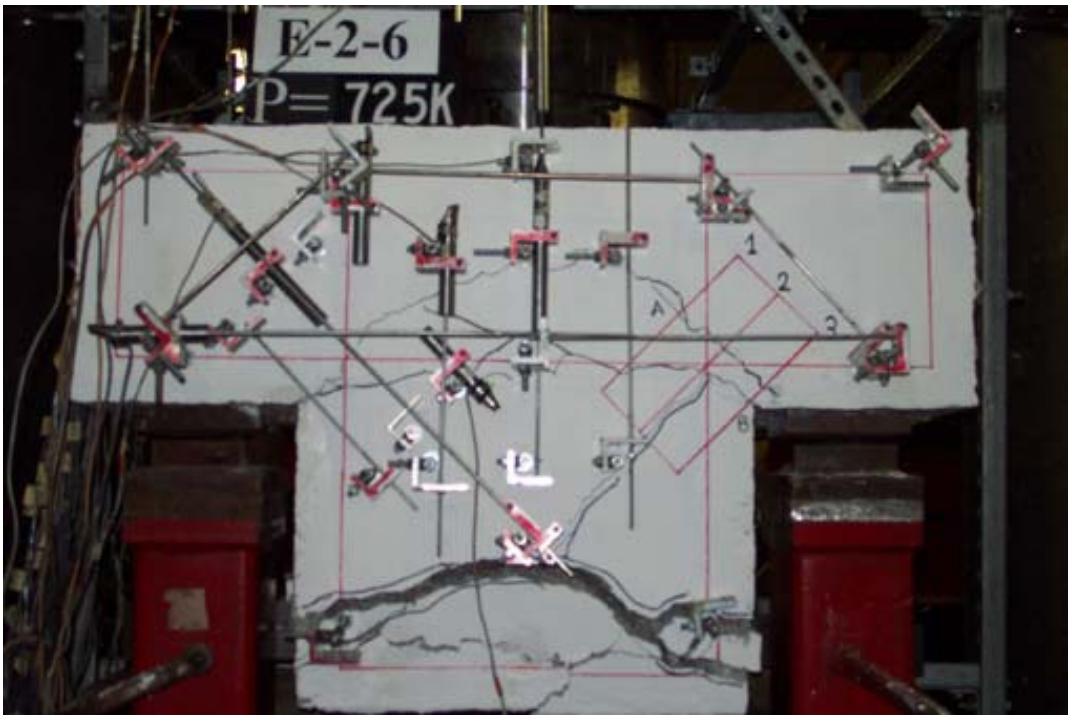

Fig. A31 Specimen at Failure

Table A7, Deflection of E-2-6 (inch)

V (k)	AW	AM	BW	BM	CW	CM
3.0	-0.0002	0.0068	0.0056	0.0111	0.0260	0.0276
6.0	0.0127	0.0191	0.0175	0.0248	0.0486	0.0505
9.0	0.0251	0.0298	0.0272	0.0361	0.0618	0.0643
12.0	0.0356	0.0385	0.0377	0.0453	0.0713	0.0751
15.0	0.0453	0.0469	0.0452	0.0534	0.0797	0.0844
18.0	0.0531	0.0544	0.0517	0.0608	0.0877	0.0923
21.0	0.0600	0.0608	0.0576	0.0673	0.0955	0.0992
24.0	0.0660	0.0661	0.0630	0.0731	0.1036	0.1065
27.0	0.0718	0.0714	0.0682	0.0793	0.1136	0.1161
30.0	0.0748	0.0751	0.0721	0.0841	0.1210	0.1241
33.0	0.0789	0.0795	0.0765	0.0892	0.1286	0.1329
36.0	0.0841	0.0841	0.0810	0.0938	0.1356	0.1413
39.0	0.0865	0.0866	0.0848	0.0991	0.1430	0.1483
42.0	0.0892	0.0911	0.0894	0.1057	0.1507	0.1577
45.0	0.0906	0.0936	0.0934	0.1110	0.1586	0.1654
48.0	0.0954	0.0978	0.0984	0.1152	0.1655	0.1719
51.0	0.0963	0.1003	0.1017	0.1214	0.1727	0.1797
54.0	0.0999	0.1039	0.1065	0.1269	0.1799	0.1881
57.0	0.0999	0.1061	0.1099	0.1318	0.1877	0.1977
60.0	0.1010	0.1086	0.1136	0.1370	0.1961	0.2064
63.0	0.1010	0.1108	0.1173	0.1420	0.2047	0.2154
66.1	0.1036	0.1133	0.1224	0.1475	0.2146	0.2263
69.0	0.1046	0.1151	0.1256	0.1516	0.2222	0.2334
69.1	0.1005	0.1115	0.1334	0.1607	0.2339	0.2447
70.0	0.1005	0.1115	0.1350	0.1631	0.2370	0.2480
71.0	0.1001	0.1114	0.1367	0.1654	0.2404	0.2514
72.0	0.0994	0.1112	0.1387	0.1681	0.2444	0.2553
73.0	0.0979	0.1109	0.1416	0.1720	0.2494	0.2608
70.0	0.0843	0.1001	0.1460	0.1772	0.2518	0.2624
71.0	0.0620	0.0804	0.1596	0.1926	0.2669	0.2777
72.0	0.0267	0.0489	0.1790	0.2135	0.2940	0.3019
74.0	0.0049	0.0331	0.1894	0.2251	0.3100	0.3171
73.0	-0.0200	0.0069	0.2027	0.2370	0.3333	0.3352

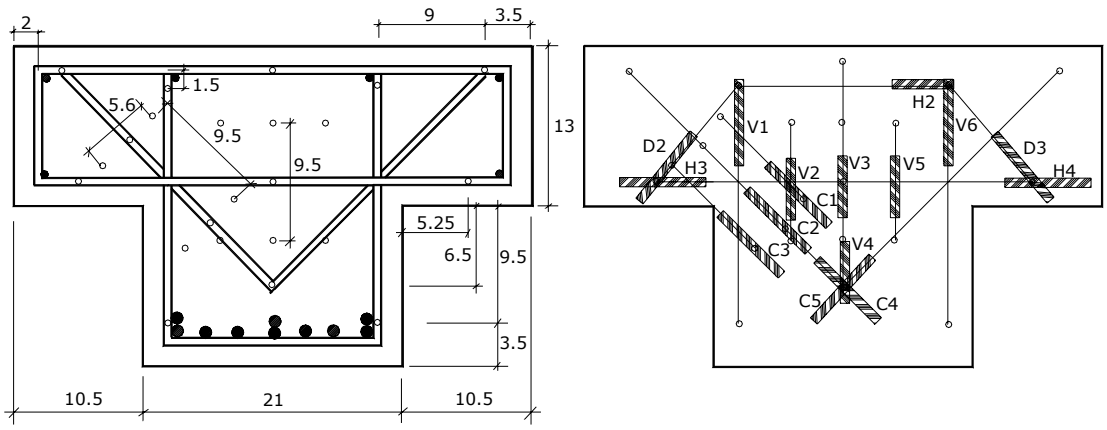

End view of LVDT arrangement

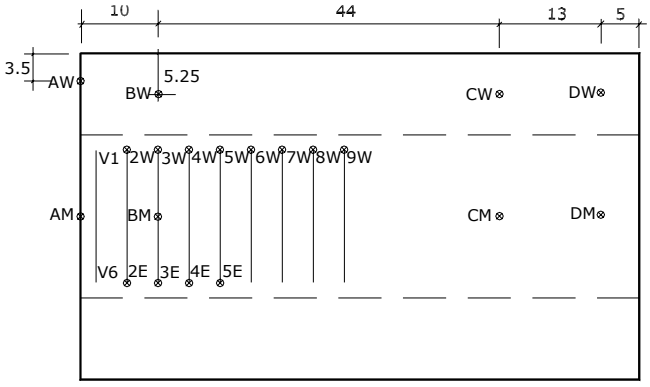

Top view of LVDT arrangement

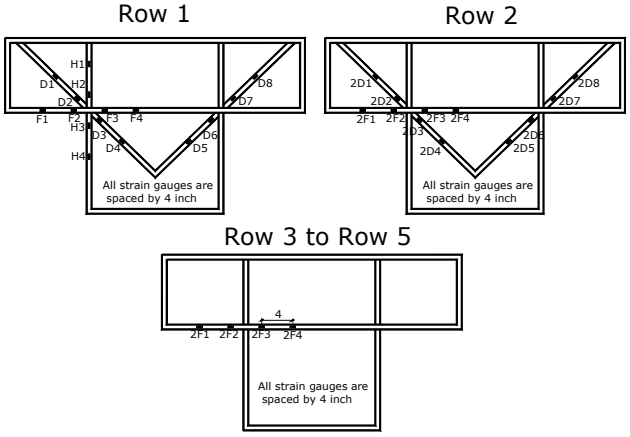

Strain Gauge arrangement

Fig. A32 LVDT and Strain Gauge Arrangement for Specimen E-2-10

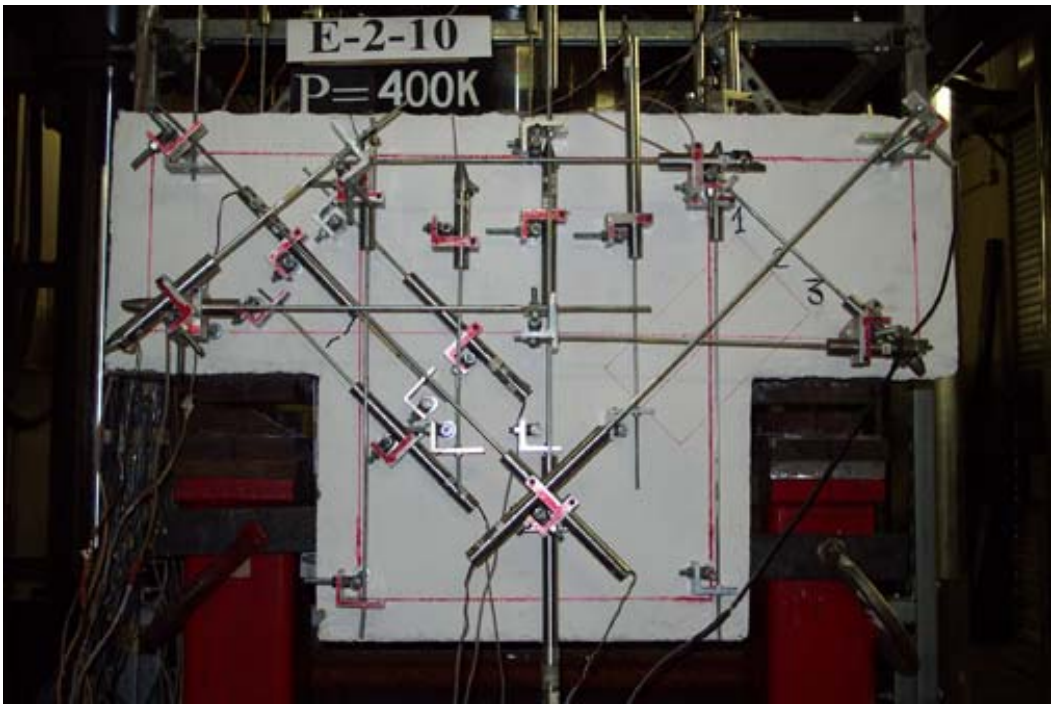

Fig. A33 Crack Pattern Before Nominal Shear Resistance for the Service Limit State (V_n = 408 K)

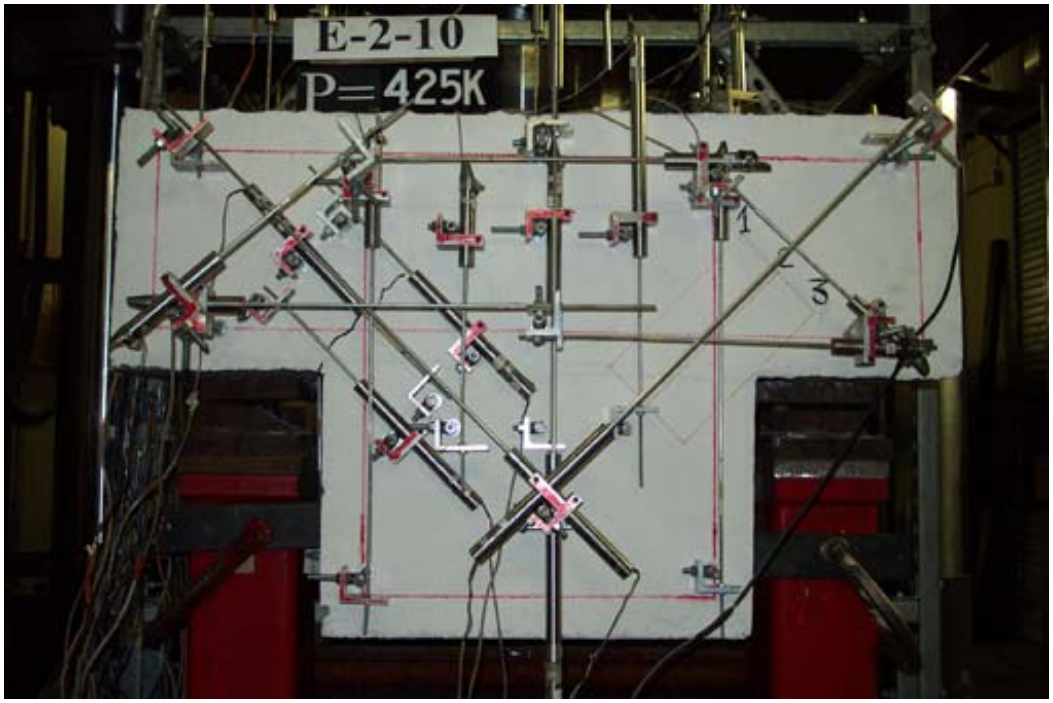

Fig. A34 Crack Pattern after Nominal Shear Resistance for the Service Limit State (V_n = 408 K)

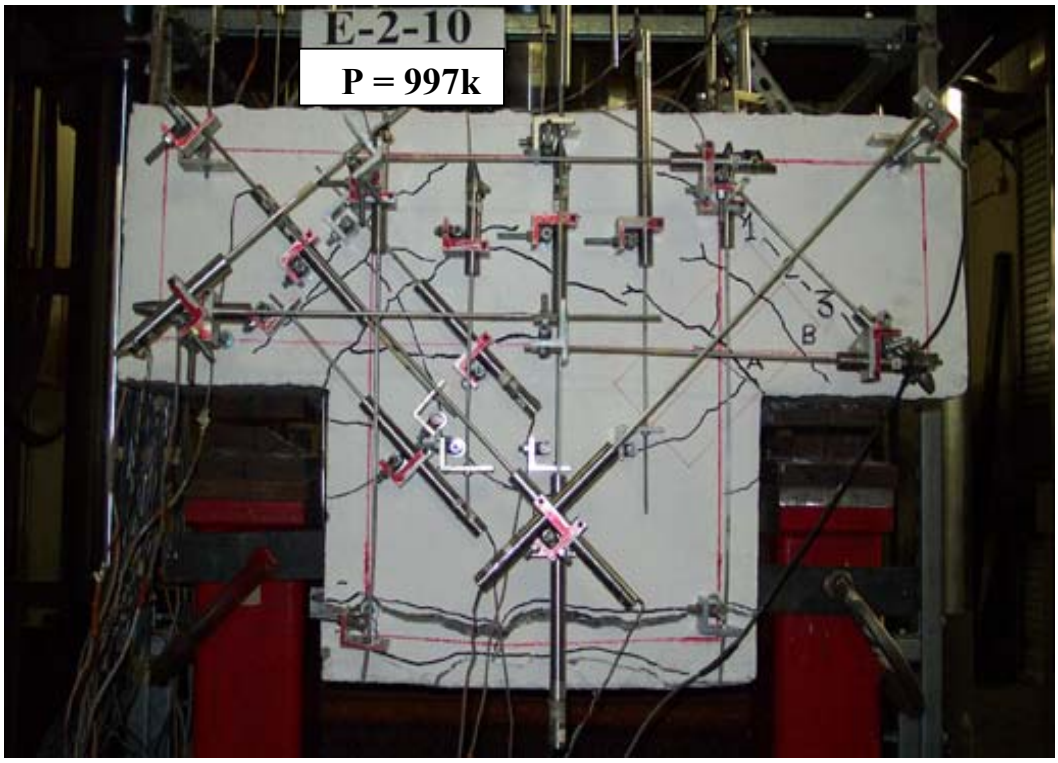

Fig. A35 Specimen at Failure

Table A8, Deflection of E-2-10 (inch)

V	AW	AM	BW	BM	CW	CM	DW	DM
5.1	0.0179	0.0161	0.0167	0.0218	0.0408	0.0391	0.0478	0.0404
10.0	0.0365	0.0339	0.0305	0.0409	0.0596	0.0600	0.0669	0.0598
15.0	0.0520	0.0473	0.0422	0.0555	0.0755	0.0791	0.0826	0.0747
20.0	0.0643	0.0578	0.0514	0.0668	0.0882	0.0910	0.0948	0.0855
25.0	0.0744	0.0666	0.0591	0.0764	0.0988	0.1011	0.1053	0.0943
30.0	0.0821	0.0738	0.0653	0.0847	0.1089	0.1126	0.1143	0.1026
35.0	0.0893	0.0804	0.0715	0.0929	0.1204	0.1246	0.1226	0.1100
40.0	0.0954	0.0863	0.0770	0.1004	0.1318	0.1363	0.1311	0.1177
45.0	0.1011	0.0927	0.0819	0.1075	0.1412	0.1464	0.1380	0.1242
50.0	0.1060	0.0976	0.0865	0.1140	0.1507	0.1570	0.1448	0.1309
55.0	0.1098	0.1024	0.0907	0.1205	0.1612	0.1685	0.1516	0.1378
60.0	0.1140	0.1073	0.0949	0.1275	0.1712	0.1794	0.1583	0.1447
65.0	0.1162	0.1119	0.0984	0.1348	0.1815	0.1904	0.1655	0.1518
70.0	0.1201	0.1169	0.1017	0.1419	0.1922	0.2016	0.1728	0.1588
75.0	0.1242	0.1214	0.1053	0.1481	0.2029	0.2128	0.1805	0.1658
80.1	0.1270	0.1250	0.1090	0.1542	0.2136	0.2242	0.1880	0.1728
85.2	0.1300	0.1285	0.1128	0.1603	0.2254	0.2363	0.1962	0.1803
90.1	0.1303	0.1305	0.1173	0.1673	0.2423	0.2535	0.2057	0.1879
95.0	0.1290	0.1312	0.1202	0.1739	0.2571	0.2685	0.2148	0.1956
100.1	0.1308	0.1344	0.1239	0.1800	0.2704	0.2826	0.2239	0.2032
105.0	0.1245	0.1333	0.1291	0.1910	0.2917	0.3040	0.2349	0.2125
110.0	0.1151	0.1291	0.1327	0.2003	0.3120	0.3240	0.2458	0.2217
111.1	0.1092	0.1255	0.1334	0.2034	0.3189	0.3308	0.2489	0.2246
112.2	0.0985	0.1198	0.1345	0.2088	0.3288	0.3398	0.2522	0.2272
113.0	0.0912	0.1146	0.1354	0.2115	0.3362	0.3465	0.2547	0.2295
113.5	0.0840	0.1094	0.1359	0.2135	0.3423	0.3518	0.2567	0.2312
113.7	0.0151	0.0554	0.1357	0.2235	0.3852	0.3842	0.2640	0.2375

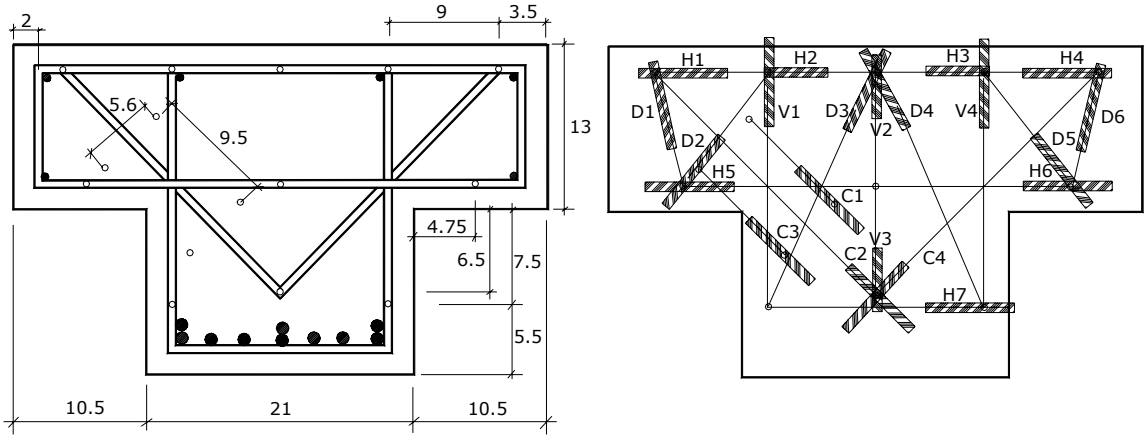

End view of LVDT arrangement

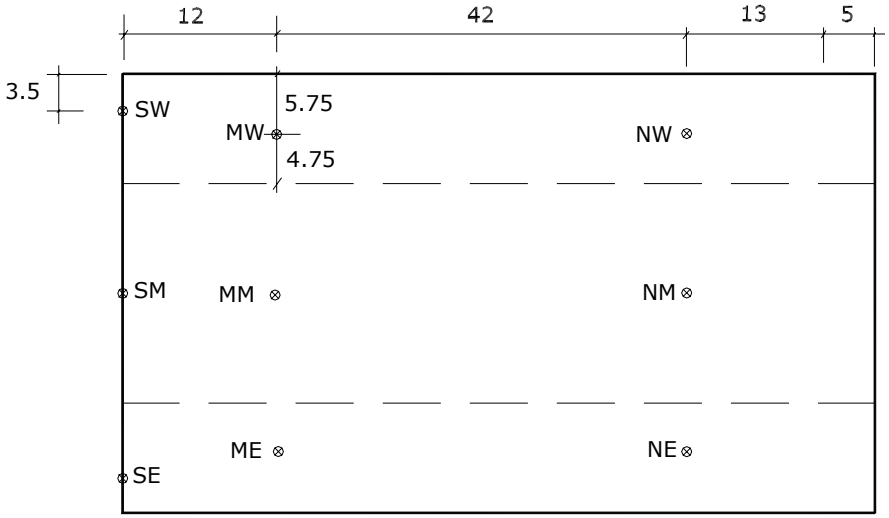

Top view of LVDT arrangement

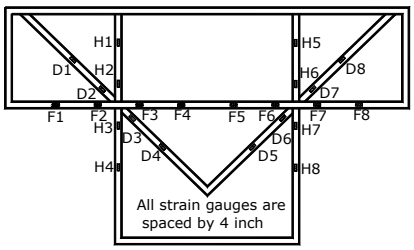

Strain Gauge arrangement

Fig. A36 LVDT and Strain Gauge Arrangement for Specimen E-5-12

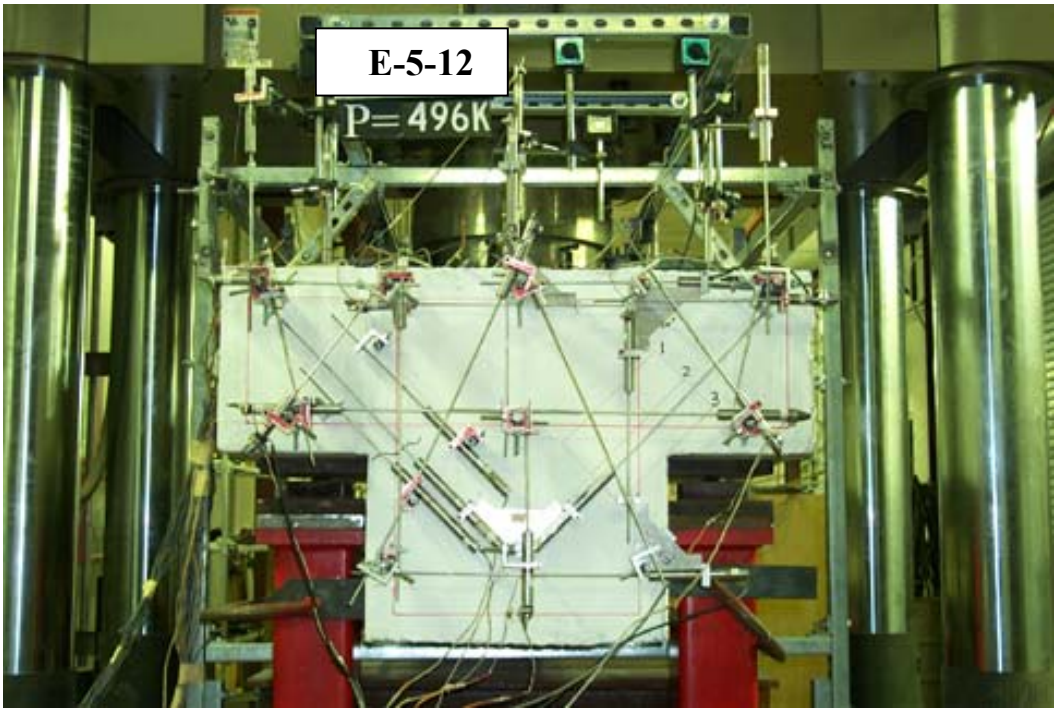

Fig. A37 Crack Pattern after Nominal Shear Resistance for the Service Limit State (V_n = 472 k)

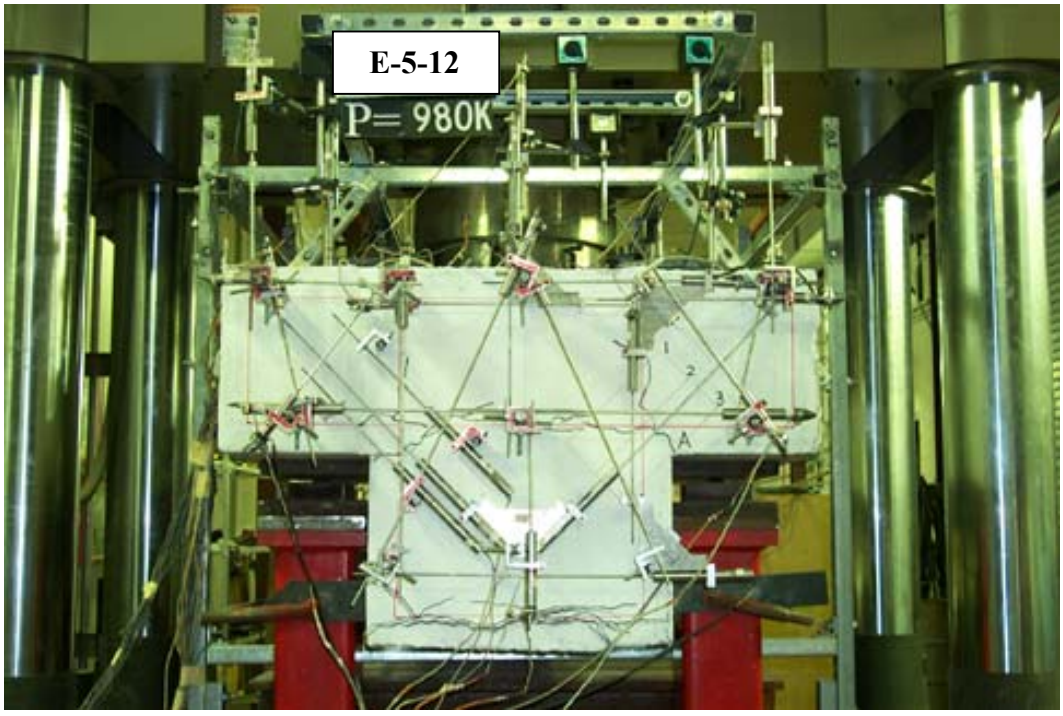

Fig. A38 Specimen at Failure

Table A9, Deflection of E-5-12 (inch)

V	SW	SM	SE	MW	MM	ME	NW	NM	NE
5.1	0.0192	0.0170	0.0069	0.0291	0.0210	0.0140	0.0420	0.0360	0.0280
10.1	0.0332	0.0320	0.0181	0.0486	0.0360	0.0250	0.0610	0.0530	0.0400
15.1	0.0453	0.0460	0.0309	0.0647	0.0490	0.0350	0.0760	0.0650	0.0500
20.0	0.0552	0.0580	0.0406	0.0776	0.0610	0.0440	0.0870	0.0750	0.0580
25.1	0.0654	0.0700	0.0536	0.0906	0.0740	0.0550	0.0970	0.0840	0.0710
30.0	0.0721	0.0780	0.0588	0.0999	0.0830	0.0630	0.1070	0.0910	0.0800
35.1	0.0773	0.0870	0.0670	0.1086	0.0920	0.0720	0.1180	0.1020	0.0900
40.1	0.0827	0.0940	0.0748	0.1168	0.1000	0.0790	0.1260	0.1110	0.0980
45.0	0.0881	0.1020	0.0821	0.1248	0.1100	0.0860	0.1350	0.1200	0.1060
50.1	0.0924	0.1080	0.0884	0.1322	0.1170	0.0920	0.1440	0.1280	0.1140
55.1	0.0970	0.1150	0.0941	0.1393	0.1240	0.0980	0.1520	0.1360	0.1220
60.0	0.1026	0.1220	0.1009	0.1463	0.1310	0.1050	0.1600	0.1450	0.1290
65.1	0.1047	0.1260	0.1039	0.1526	0.1370	0.1100	0.1690	0.1530	0.1380
70.0	0.1086	0.1330	0.1083	0.1598	0.1440	0.1170	0.1760	0.1610	0.1470
75.0	0.1115	0.1380	0.1138	0.1659	0.1500	0.1220	0.1850	0.1700	0.1550
80.1	0.1151	0.1430	0.1171	0.1721	0.1570	0.1280	0.1930	0.1790	0.1630
85.3	0.1182	0.1480	0.1208	0.1782	0.1630	0.1330	0.2020	0.1880	0.1730
90.0	0.1204	0.1520	0.1240	0.1838	0.1690	0.1380	0.2100	0.1970	0.1820
95.1	0.1204	0.1530	0.1251	0.1891	0.1750	0.1440	0.2200	0.2080	0.1920
100.1	0.1208	0.1530	0.1258	0.1950	0.1820	0.1500	0.2330	0.2210	0.2070
105.0	0.1208	0.1500	0.1199	0.2008	0.1890	0.1550	0.2440	0.2340	0.2210
110.4	0.1145	0.1440	0.1109	0.2070	0.1960	0.1610	0.2580	0.2490	0.2380
115.2	0.1038	0.1320	0.0948	0.2119	0.2020	0.1650	0.2740	0.2680	0.2590
115.7	0.0978	0.1250	0.0871	0.2138	0.2030	0.1660	0.2800	0.2730	0.2650
115.0	0.0826	0.1070	0.0679	0.2127	0.2020	0.1660	0.2880	0.2810	0.2740
114.6	0.0775	0.1000	0.0606	0.2120	0.2010	0.1650	0.2900	0.2830	0.2760
113.3	0.0697	0.0900	0.0493	0.2109	0.2000	0.1640	0.2930	0.2860	0.2800
112.1	0.0681	0.0880	0.0468	0.2106	0.2000	0.1640	0.2940	0.2860	0.2800
111.5	0.0663	0.0860	0.0450	0.2105	0.2000	0.1640	0.2950	0.2870	0.2810
110.2	0.0615	0.0810	0.0397	0.2087	0.1990	0.1630	0.2950	0.2870	0.2820